Challenging the stress

A single-cell study of the Dps response

De Martino, Michela

DOI
10.4233/uuid:8f3046ac-2fa3-494e-b6fb-4c6b78ac1783

Publication date
2016

Document Version
Final published version

Citation (APA)
De Martino, M. (2016). *Challenging the stress: A single-cell study of the Dps response*. [Dissertation (TU Delft), Delft University of Technology]. https://doi.org/10.4233/uuid:8f3046ac-2fa3-494e-b6fb-4c6b78ac1783

Challenging the stress

A single-cell study of the Dps response

Michela De Martino

Challenging the stress

A single-cell study of the Dps response

Proefschrift

ter verkrijging van de graad van doctor
aan de Technische Universiteit Delft,
op gezag van de Rector Magnificus prof.ir. K.C.A.M. Luyben;
voorzitter van het College voor Promoties,
in het openbaar te verdedigen op
27 Mei 2016 om 10:00 uur

door

Michela De Martino

Master of Science in de Biotechnology for Agro-industry,
Universitá di Napoli “Federico II”, Italië
geboren te Salerno, Italië

This dissertation has been approved by the
Promotor
Prof. dr. S. J. Tans TU Delft

Copromotor
Dr. A. S .Meyer TU Delft

Composition of the doctoral committee:
Rector Magnificus chairman

Independent members
Prof. dr. M. Dogterom TU Delft
Prof. dr. L.W. Hamoen U-Amsterdam
Prof. dr. R.A.L. Bovenberg RU Groningen
Dr. W.K. Smits LUMC Leiden
Dr. P.A.S. Daran-Lapujade TU Delft

Reserve member
Prof. dr. A.H. Engel TU Delft

Keywords: Bacterial stress response, Dps response, single cell analysis, time-lapse fluorescence microscopy, agarose pad, microfluidics

Printed by: Gildeprint

Cover by: Stanley Dinesh Chandradoss

Casimir PhD series, Delft-Leiden 2016-13

ISBN 978.90.8593.255.0

An electronic copy of this dissertation is available at http://repository.tudelft.nl/

Contents

Chapter 1

Introduction

1.1 Bacteria and stress response

Bacteria live in a dynamic environment and are exposed to constant variation in nutrient availability, temperature, pH and chemical composition. A quick adaptation to these changes is the key for survival in a hostile background. Many bacterial response mechanisms involve specific sets of genes activated to help the cell to adapt to the stress. To initiate transcription, RNA polymerase (RNAP) binds to dissociable sigma factors (σ) that are responsible for the promoter recognition [1]. Alternative sigma factors act as transcription initiators to control the activation of specialized regulons during specific growth or stress conditions [2]. In *Escherichia coli*, alternative sigma factors of the σ^{70} family, are frequent regulatory mechanisms [2]. They compete for the same RNAP under specific conditions. The transcription factor σ^{70} (or σ^{D}) controls housekeeping genes during the exponential growth [1, 3]. In addition to σ^{70}, other four different alternative sigma factors are found in *E. coli*: σ^{E}, σ^{H}, FecI, and σ^{S}, each responds to different stress conditions and drive different transcriptional programs.

σ^{E} (or σ^{24}) is a minor sigma factor, and it is specialized in the response to extreme heat and stresses on membrane and periplasmic proteins. This protein regulates the expression of genes for the restoration of cell envelope integrity [4], and it is controlled by a protease system that is responsible for the perception of the damages in the unfolded proteins in the cell envelope. During induction, the RseA protein, an anti-σ factor that suppresses σ^{E}, transduces the stress signal is into the cytoplasm. The two proteases DegS and YaeL release σ^{E} by cleaving RseA [5].

One of the target genes of σ^{E} regulation is another sigma factor, σ^{H} (or σ^{32}) [6]. σ^{H} controls the heat shock response during exponential phase, and it is induced by unfolded protein as a result of heat stress [7]. Following a heat shock, σ^{H} levels rise, plateau and then drop, causing a subsequent induction with similar kinetics in its dependent genes [8]. The regulation of σ^{H} occurs at several different levels. Translational control is exerted via mRNA secondary structure. The *rpoH* mRNA, coding for σ^{H}, forms secondary structures that are disrupted by higher temperatures [9]. The σ^{H} protein is very unstable, but it is transiently stabilized during heat shock [10] by the lowered levels of the chaperone protein GroES and by the increased levels of misfolded proteins [11, 12].

A third sigma factor is FecI (or σ^{19}). Upon iron starvation, FecI controls the *fecABCDE* operon, for the translocation of iron citrate into the cell [13]. FecI initiates transcription of genes involved in the ferric citrate transport in response to the presence of periplasmic iron (III) dicitrate [14]. The FecI response involves different proteins. The Fur protein, which senses iron starvation, represses FecI during optimal iron concentration and dissociates when the levels decrease. FecA is a receptor in the outer membrane that binds to citrate and transmits the stress signal into the cytoplasm. FecI is bound to the anti-sigma FecR that undergoes conformational changes with the interaction with FecA,

with consequent release of FecI. FecI is able to interact with RNAP and transcribe the *fec* genes [15].

In addition to the aforementioned sigma factors involved in the stress response, bacteria have also other sigma factors. σ^F (or σ^{28}), is involved in the transcription of a number of genes for motility and flagellar assembly [15]. It is required, for example, for flagellin production, the principal substituent of bacterial flagellum [15].

Many bacteria carry another family of σ factors, called σ^N (or σ^{54}). The gene encoding for σ^N does not share homology in sequence with the σ^{70} family and uses a different method of assembly with RNAP [16]. This transcription factor controls expression of nitrogen-related genes [15].

1.2 The σ^S - mediated response in *E. coli*

The main regulatory protein of the stress response genes is the general stress response sigma factor σ^S (or σ^{38}). It is involved in the transcription of over 70 genes, conferring resistance to carbon/phosphate/nitrogen starvation, heat shock, high/low pH, UV-radiation, and oxidative stress, among others [17, 18]. Its protein level under optimal growth condition is low and increases during stationary phase or unfavorable growth conditions. The expression of the *rpoS* gene, encoding for σ^S, is regulated at different levels: transcription, translation and protein stability. Transcription of the σ^S gene is promoted by (p)ppGpp (guanosine 3',5'- bispyrophosphate), a molecule for the signaling of many stress conditions. Moreover, this molecule stimulates the σ^S translation, prevents the σ^S degradation, and enhances the σ^S regulatory activity [19-21]. Two additional molecules instead have an antagonistic effect on σ^S: cAMP (cyclic AMP) and CRP (catabolite response protein) [22]. The σ^S mRNA includes secondary structures that impede the access to ribosomes. Its translation is assisted by sRNAs (small RNAs) and Hfq, an RNA chaperone protein that is able to penetrate the hairpin loops [23-25]. Regulatory sRNAs can also inhibit the translation of proteins, such as OxyS sRNA that negatively regulates the translation of OxyR [26]. Cellular levels of σ^S are further influenced by degradation. In fact, the σ^S protein is highly unstable. It is rapidly degraded during exponential phase, but this process stops during stress exposure and in stationary phase [22, 27]. σ^S degradation is determined by the general ATP-dependent ClpXP protease [28]. The proteolysis requires an adaptor protein RssB to deliver σ^S to the hexameric ClpX unit, that is the binding and unfolding component of the proteolytic protein [29]. Under adverse growth conditions, three antiadaptor proteins modulate the binding of RssB: the Ira (inhibitors of RssB activity) proteins named IraM, IraP and IraD. Binding of one of the Ira proteins to the adaptor limits σ^S protein degradation during stress conditions [30, 31].

Sigma factors compete for binding to the RNAP core. The amount of RNAP remains largely constant during various physiological states [32, 33]. During exponential

phase, σ^S levels are almost undetectable, whereas the σ^{70} amount is the highest among the sigma factors. When the bacteria reach the stationary phase, the cellular amount of σ^S reaches the maximum concentration of one third of the levels of the vegetative sigma factor σ^{70} [34]. Moreover, the σ^S has a weaker binding affinity to the RNAP compare to σ^{70} [35, 36]. Despite this, under stress condition σ^S is able to efficiently bind the RNAP core and recognize its promoters. Bacteria developed efficient strategies to overcome the dominance of the σ^{70} and to allow a more effective competition of the other sigma factors for the binding to the polymerase. For example during stationary phase, Rsd, an anti-σ^{70} factor, binds to σ^{70} to allow its dissociation with RNAP, promoting binding of σ^S [37]. The protein Crl triggers the formation of the σ^S holoenzyme and is necessary for the expression of σ^S-dependent genes [38]. Another example of the mechanisms adopted by the cells to support σ^S binding to RNAP is accumulation of the 6S regulatory RNA during stationary phase and its binding to the σ^{70} holoenzyme, which stalls it in an inactive form [39]. Moreover, during stationary phase the Rds protein binds to the σ^{70} and interferes with its interaction with RNAP, promoting the binding of σ^S [40].

1.2.1 Interdependency between the σ^S regulon and other defense systems

The regulatory cascade of the general stress response pathway, including the control of both σ^S and the members of its regulon, is quite complex. Many signaling molecules and proteins are implicated in the reaction to distinct stresses. However it is now clear that some specific stress pathways share some regulatory proteins or molecule with the σ^S mechanism, while some others are negative regulators. In *E. coli* cells, the above-mentioned (p)ppGpp is the principal effector of the starvation response. (p)ppGpp is also responsible for the so-called stringent response, in which it modulates the transcription of several genes during stress conditions as iron or amino acids limitation or heat shock [41]. (p)ppGpp favors the binding of σ^S to RNAP, activating the expression of the anti-σ factor Rsd [42, 43]. (p)ppGpp also positively regulates the antiadaptors Ira P and IraD, stabilizing the σ^S protein [44, 45].

The induction of σ^S in some cases is linked to the expression of regulatory sRNAs. The accumulation of σ^S during low temperatures depends on its increased translation level due to the activity of sRNA DsrA [46]. DsrA promotes the efficient translation of σ^S and downregulates the translation of a global gene expression regulator, H-NS [47]. H-NS represses transcription of the σ^{70} - and σ^S - dependent genes, in general increasing the σ^S-dependency of many promoters [48]. During oxidative stress, another sRNA negatively regulates the general stress response. When during exponential phase cells are subjected to hydrogen peroxide, the sRNA OxyS is transcribed, under the control of the OxyR

regulon, which downregulates σ^S translation [49]. Another sRNA activator of σ^S is ArcZ, which is expressed under aerobic conditions. In anaerobic environments, the two-component system ArcAB represses the activity of ArcZ, with a consequent halt of σ^S translation [25]. It was also shown that the proteins ArcA and ArcB can themselves carry out repression of σ^S transcription and σ^S protein degradation [50]. The σ^S general stress response system is also implicated in biofilm formation, by the activity of a sRNA. Some biofilm development genes are in fact σ^S-dependent [51]. The positive regulation of σ^S in a biofilm is attributed to the sRNA RprA, which ensures proper timing of σ^S production during biofilm formation. RprA is in turn activated by the RcsBCD phosphorelay system [52]. This regulatory mechanism is responsible, for example, for the downregulation of cell motility and for activating the synthesis of colonic acid, a matrix component of the biofilm [53, 54]. The Rcs system is also induced when cells are exposed to high osmolarity, with consequent RprA activation of σ^S [55, 56].

The effect of the σ^S -dependent response during one stress condition may be perceived by the cell similar to another stress exposure. The genes regulated by σ^S during one stress condition, in fact, may overlap with the genes upregulated in response to other conditions. For example, during cold shock σ^S induces *otsAB* genes, necessary for the synthesis of the osmoprotectant trehalose [57]. The *otsAB* genes are also important for survival during high osmolarity in stationary phase [58]. Thus, a high level of trehalose may enhance the protection of proteins from denaturation, during either extreme temperature or osmolarity. *E. coli* cells in stationary phase are resistant to pH 2.5 [59]. In fact, during acid stress, several genes regulated by σ^S are activated, for example *cfa.* This gene encodes for a cyclopropane fatty acyl phospholipid synthase necessary for the alteration of phospholipid composition to tolerate low pH [60]. At low pH, also the *hdeA* gene is transcribed. The resultant protein has a chaperone-like activity, binding to damaged or misfolded proteins to prevent their aggregation, releasing them when the pH returns to normal [61]. The PhoPQ system is activated at low Mg^{2+} levels in the cells, but it was also shown to be involved in the stabilization of σ^S during acidic pH exposure. In fact, the synthesis of the IraP antiadaptor, responsible for the halt of the σ^S degradation during phosphate starvation, is connected to this two-component system [62].

These are some examples of the interconnections between the general stress response and some specific response mechanisms, but the complete list is much longer. The increasing number of factors that contribute to the control of σ^S at different levels makes it one of the most complex regulation pathway in *E. coli*. All these controls do not work independently from each other, but their action is coordinated. One of the example of the connection between the σ^S response and other regulatory network is the above-mentioned link with oxidative stress, via the OxyS sRNA. Oxidative stress among the most frequent stresses experienced by bacteria, and in *E. coli* the response to this stress is one of the most studied.

1.3 Oxidative stress response

1.3.1 Defense against internal oxidating agents

Microorganisms living in an aerobic environment unavoidably experience oxidative stress as a byproduct of their aerobic metabolism [63]. Oxygen and hydrogen peroxide are the main chemical agents responsible for the production of intracellular reactive oxygen species (ROS), according to the following reaction [64]:

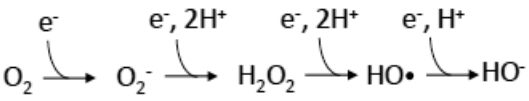

The rate of endogenous superoxide (O_2^-) formation inside *E. coli* cells is estimated to be about 5 µM/s [15], and hydrogen peroxide (H_2O_2) is thought to form at a rate of 10-15 µM/s in aerobic conditions in *E. coli* based on *in vitro* studies [65]. The resultant formation of ROS can is responsible for the damages to biological components including membranes, DNA, and proteins [64]. As an adaptation to these conditions, bacterial cells induce the production of enzymes including superoxide, dismutases, and reductases enzymes to remove these toxic components [66]. *E. coli* contains three superoxide dismutase (SOD) enzymes: two cytoplasmic (FeSOD and MnSOD) and one periplasmic (CuZnSOD). The cytoplasmic SODs keep the intracellular level of superoxide to approximately 0.1 nM [15]. Their high activity is necessary to protect vulnerable enzymes and ensure growth. In fact, exposure to 0.1 nM of O_2^- inactivates [4Fe-4S] enzymes with a half-life of around 30 minutes [67].

The regulation of FeSOD and MnSOD is linked to iron levels. Whenever the iron amount is high inside the cell, Fur blocks the synthesis of MnSOD. When the iron level decreases, Fur is deactivated, leading to the induction of MnSOD synthesis and the transcription of sRNA RyhB, which catalyzes the degradation of FeSOD mRNA [68, 69]. CuZnSOD serves to protect periplasmic molecules from the superoxide that leaks out of the cytoplasmic membrane [70]. In pathogens such as *S. typhimurium*, it serves as a defense against the oxidative burst produced by macrophages during phagocytosis as part of the immune response [71].

The scavenging of hydrogen peroxide is more complex than that of superoxide. Contrary to O_2^-, H_2O_2 is an uncharged molecule that can passively diffuse across bacterial membranes [72]. *E. coli* has three main enzymes to protect against hydrogen peroxide: alkyl hydroperoxide reductase (Ahp), catalase G (KatG) and catalase E (KatE). When H_2O_2 levels are low inside the cell, the heme group of the two catalase enzymes can stall in the

ferryl/radical form, an intermediate oxidant form, with consequent damages to the local polypeptides [73]. The Ahp system, in contrast, during its own catalytic activity does not form an intermediate oxidative species being more efficient to scavenge low amount of H_2O_2, but when levels of H_2O_2 in the cytoplasm exceed 20 μM, it is saturated [74]. Therefore, bacteria depend on the Ahp system when the amount of H_2O_2 is low and on the catalases when the H_2O_2 amount is high or the cells are in stationary phase [75]. The two-component system AhpCF is the principal scavenging enzyme during no-stress growth. It transfers electrons from NADH to H_2O_2, converting it to H_2O [74]. KatG is only weakly expressed in exponential phase and KatE is expressed in stationary phase [64]. The *ahpCF* and *katG* regulation is OxyR-dependent when bacteria are exposed to exogenous hydrogen peroxide [76]. KatE is controlled by the σ^S system [77].

1.3.2 Defense against external oxidating agents

The scavenging mechanisms previously illustrated are only enough to defend bacterial cells from endogenous production of H_2O_2 and O_2^-. However, cells also face external sources of ROS that can contribute to oxidative damage. Some bacteria secrete ROS to prevent the growth of their competitors [78]; plants can generate organic peroxides in the presence of pathogens [79]; redox cycling compounds can cause intracellular redox reactions with consequent damage to cellular compartments [80]; and macrophages can produce nitric oxide and superoxide to neutralize bacteria [81].

When the external concentration of H_2O_2 overcomes 200 nM, the rate of H_2O_2 uptake in the cell exceeds the endogenous production [72]. The higher dose of H_2O_2 saturates the Ahp, after which the concentration of H_2O_2 rises to 100 nM inside the cell, leading to OxyR activation. OxyR belongs to the transcriptional regulators protein family LysR [82]. It is a key regulator of adaptive response to oxidative stress [76, 83]. Transcriptional activation of OxyR-dependent genes occurs when OxyR is converted into the oxidized form [84]. The reduced and oxidized form have different structures [85], such that oxidized OxyR positively regulates the transcription of its dependent promoters [86], while the reduced form inhibits the transcription of other genes, such as *stiA* gene involved in the starvation-stress response (SSR) in *S. typhimurium* [87] and the *agn43* gene encoding for an protein of the outer membrane named antigen 43 in *E. coli* [88]. In *E. coli* , the OxyR regulon contains over 20 genes, such as genes involved in H_2O_2 scavenging (e.g. *katG* and *ahpF*), heme biosynthesis, Fe-S centre proteins, iron scavenging, repression of iron import, and disulphide reduction [89]. OxyR also activates the transcription of glutaredoxines and thioredoxins for its own deactivation [90]. Besides protecting bacteria from oxidative stress, it is additionally involved in defense from heat stress [91], UV radiation [92], and damages due to lipid peroxidation [93].

The principal regulator of superoxide defense against excess superoxide in *E. coli* is the SoxRS system. Although O_2^- is charged and cannot penetrate cellular membranes [94], plants and bacteria can induce the production of superoxide inside targeted bacteria with the secretion of redox-cycling compounds (e.g. quinones or phenazine) that can passively penetrate the cell [95]. SoxR is a homodimer accomodating two [2Fe-2S] clusters that are oxidized during exposure to redox-active compounds [96, 97]. Oxidized SoxR binds to the *soxS* promoter, that is involved in the activation of over 100 genes [98, 99]. When redox-cycling compounds are eliminated from the media, SoxR restores the reduced state, and SoxS is quickly degraded [100, 101]. Previous *in vivo* studies have demonstrated that the main effector of the SoxRS systems, which most efficiently oxidizes SoxR, is not O_2^-, but redox-cycling compounds [102]. Many of the proteins produced via the SoxRS response act to eliminate redox-cycling compounds from inner compartments, pumping them outside the cell or modifying them chemically [103-105]. Other members of the SoxRS response serve to reduce cell damage, for example by protecting from oxidation the iron-sulfate proteins [106] or the induction of mechanisms to repair the DNA, as endonuclease IV [107].

Another critical type of ROS in bacteria is hydroxyl radicals that is formed during the Fenton reaction. However, no protein-based response to detoxify these compounds has been identified. The importance of hydroxyl radicals during stress exposure is related to their use by cells to commit suicide when stress is too severe [108].

1.4 The Dps response to oxidative stress

The combined actions of the previously described oxidative response systems trigger many diverse mechanisms during response to oxidation conditions: production of scavenging superoxide enzymes, repression of iron import and DNA repair to list only a few [66]. One of the main players among the oxidative stress response mechanisms is the DNA binding protein from starved cells (Dps) [109, 110]. *E. coli dps* mutants experience a severe reduction in survival when exposed to several stresses including oxidative stress, heat shock, metal exposure, UV and gamma irradiation, or extreme pH [111-113]. Furthermore, Dps was shown to protect the DNA from strand breakage [114]. The protective ability of Dps is attributed its dual biochemical functions. The ability of Dps to bind DNA and form Dps-DNA crystals is thought to provide mechanical shielding against damaging agents [111, 115, 116]. The ferroxidase activity also contributes significantly to its protective role. The binding to DNA and ferroxidase activitiy of Dps are biochemically dissociable, but they both contribute to maintain DNA stability and bacterial viability [117].

One of the mechanisms of intracellular formation of hydroxyl radicals is the reaction between H_2O_2 and ferrous iron, as shown with the Fenton reaction:

$$Fe^{2+} + H_2O_2 \rightarrow Fe^{3+} + OH^- + OH\cdot$$

Dps catalyzes the oxidation of ferrous iron through its ferroxidase activity, preferring H_2O_2 as a reactant rather than O_2, thereby competing with the formation of hydroxyl radicals [118]. The following chemical reaction is catalyzed by the Dps ferroxidase centers:

$$2Fe^{2+} + 1H_2O_2 + 2H_2O \rightarrow 2FeOOH\text{-}P + 4H^+$$

Dps has also a role in iron storage. It can store up to 500 atoms of Fe(III) oxyhydroxide, which can be released following subsequent reduction [119].

1.4.1 Dps structure

E. coli Dps has many structural features in common with bacterial ferritins. It is a highly symmetrical protein, which forms a very compact and stable complex [120]. A Dps oligomer consists of consists of 12 identical Dps subunits each folded into a compact four-helix bundle, with an external dodecamer diameter of ~ 9 nm (90 Å) and a central spherical cavity of ~ 4.5 nm (45 Å) that serves as room for iron storage [118, 121]. Protruding out away from the complex are the flexible N-terminal regions of each monomer (Fig. 1.1). These regions are positively charged, each containing 3 lysine residues [121]. They are crucial for co-crystallization of Dps and the DNA and self-aggregation of the Dps monomer [122]. Self-aggregation of purified Dps molecules in solution leads to the formation of two-dimensional hexagonal Dps crystals. The ability to self-aggregate is also responsible for the creation of multilayered Dps-DNA crystals both *in vivo* and *in vitro* [122, 123]. The binding of Dps to DNA occurs without apparent sequence specificity [111]. Highly ordered Dps-DNA structures can be formed between Dps and linear double-stranded DNA, closed supercoiled plasmids or single-stranded RNA [123]. During prolonged starvation, *E. coli* can reorganize its nucleoid into a so-called bio-crystal. This structure consists of alternating stacked layers of Dps proteins hexagonally packed and layers of parallel DNA strands [123, 124]. This structure may serve as a physical barrier protecting the DNA from damaging agents [125].

The ferroxidase activity of Dps is its second major protective feature. Within each dodecamer, the catalytic sites are present at the interface formed by two Dps subunits that relate to each other with two-fold symmetry. Each interface between two monomers contains two ferroxidase active sites, with a total of 12 for each Dps dodecamer [126].

Each active site of Dps in *E. coli* accommodates two iron-binding sites: site A with strong affinity and site B with reduced affinity [126, 127]. In the site A, one iron atom is coordinated by histidine, aspartate and glutamate residues, while the site B often contains water.

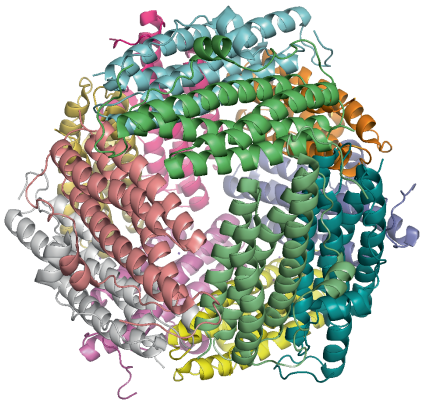

Fig. 1.1 *E. coli* Dps structure (PDB 1L8H, Luo, J., Liu, D., White, M.A., Fox, R.O. DNA Protection and Binding by *E. coli* Dps Protein). Dps oligomer consists of consists of 12 identical subunits (represented in different colors) that form a central spherical cavity that serves for iron storage. Protruding out are the flexible N-terminal regions of each monomer.

1.4.2 Dps regulation

The Dps regulation of in *E. coli* is a complicated network, including controls at the transcription, translation, and protein stability. During the exponential phase, each cell contains around 6000 molecules. During starvation and in stationary phase, number of Dps molecules increases up to around 180000, and it becomes the most abundant DNA-binding protein [128]. *dps* gene is transcribed from one single promoter identified by both the σ^{70} or σ^{S} sigma factors in response to different growth and environmental conditions [129-131]. In exponential growth, treatment of the cells with a low dose of H_2O_2 affects the redox activation of the OxyR protein, with consequent recruitment of σ^{70} to initiate *dps* gene transcription. During stationary phase or starvation, σ^{S} controls the expression of the *dps* gene, with the cooperation of the heterodimeric IHF protein [129, 132] (Fig. 1.2). When bacteria are growing exponentially and not exposed to stress, the *dps* promoter is downregulated by two nucleoid-binding proteins: Fis and H-NS [130, 133] (Fig. 1.3). Both of these proteins repress transcription by binding near the core of the *dps* promoter,

preventing the binding of σ^{70}, using different mechanisms of action. H-NS binds to the *dps* promoter, preventing σ^{70} binding [130], allowing however the binding of σ^{S} in stationary phase. Fis downregulates the *dps* transcription by interaction with σ^{70} and trapping it at the promoter, forming a tightly bound complex. In this case, the promoter is inaccessible also for σ^{S} [130].

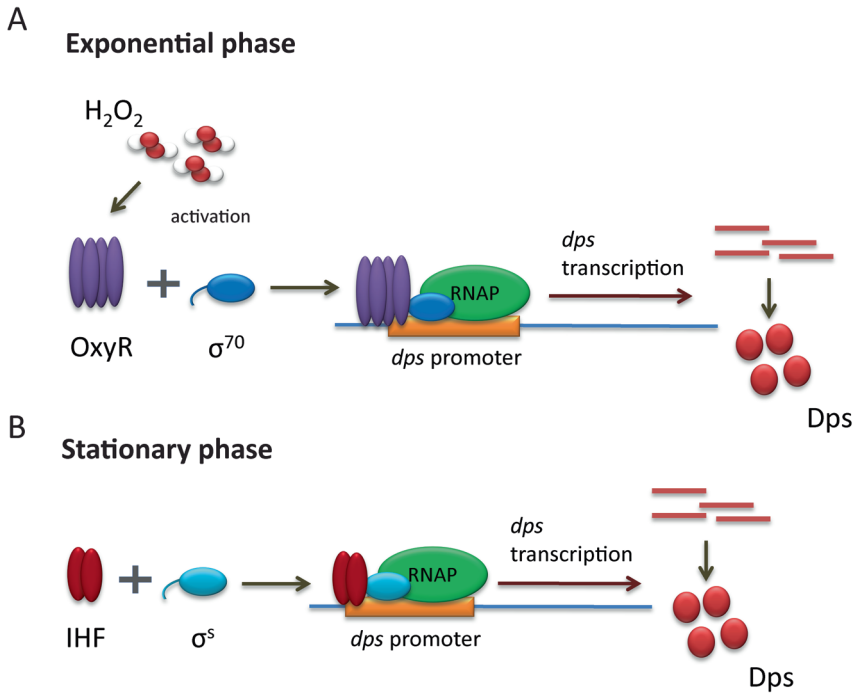

Fig 1.2. Upregulation of *dps* gene in *E. coli*. A) During exponential growth, exposure to low dose of H_2O_2 determines the redox activation of the OxyR protein. σ^{70}-RNAP is recruited to the promoter to initiate *dps* gene transcription. B) In stationary phase or starvation, the transcription of the *dps* gene is under the controls of σ^{S} which cooperates with the IHF protein.

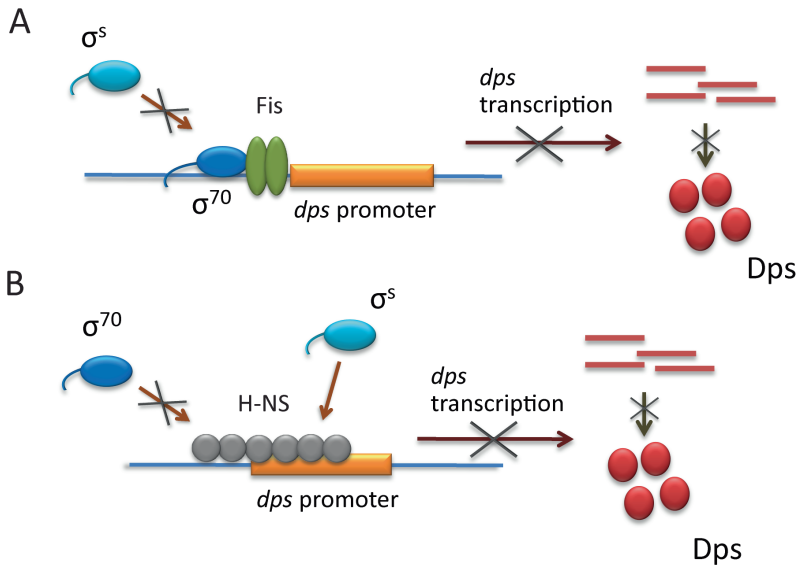

Fig 1.3. Downregulation of *dps* gene during exponential growth in *E. coli*. When bacteria are not exposed to stress during exponential growth *dps* transcription is downregulated by two nucleoid-binding proteins: Fis and H-NS. A) Fis interact with σ^{70} and traps it at the promoter, forming a tightly bound complex. The promoter is unavailable for σ^{S}. B) H-NS binds to the *dps* promoter, preventing the binding of σ^{70}, allowing however of σ^{S} binding during stationary phase.

The regulation at post-translational level of the Dps protein involves the ClpXP and ClpAP proteases, which directly degrade Dps during exponential growth [134], although the detailed mechanisms are still not completely clarified. Dps degradation is growth phase dependent. It is degraded in exponential phase, keeping protein levels low. The degradation stops during stress exposure or when the cells reach the stationary phase, but it is resumed after the stress is concluded. Both ClpXP and ClpAP regulate Dps concentration. ClpXP controls the protein stability in exponential growth and ClpAP the synthesis during stationary phase. ClpXP degradation of Dps also occurs when the cells re-enter exponential phase [135]. The ClpXP-mediated degradation does not require the RssB adaptor protein to allow the recognition of the Dps substrate [136]. The two proteases both utilize the N-terminal region of Dps as a recognition tag, although they identify different motifs. The residues 2-5 are essential for ClpXP proteolysis [135, 137]. Dps strongly accumulates during stationary phase, during which ClpAP plays an important role by facilitating the translation of Dps protein [134]. During exponential growth, ClpAP-

mediated degradation requires an adaptor protein, ClpS. It recognizes the N-terminal residue, Leu6, in a truncated version of the Dps protein (6-167 residues) [137].

Despite the extensive knowledge acquired in recent years, many of the aspects of Dps regulation, in particular the transcriptional regulation in presence of different stress conditions, are still unknown. For example, the temporal dynamics of the Dps response is still unexplored. Little is known also about how the dynamics of *dps* expression are affected when the cells are exposed to various stressor concentrations. In this thesis, we tried to answer some questions related to the regulation of Dps transcription during hydrogen peroxide exposure and extreme pH. In particular, we investigated the transcriptional *dps* regulation at the single-cell level, revealing the high-resolution transcriptional dynamics, and their correlation with stressor concentrations. We also investigated the variability of the Dps response in individual cells and its effect on cellular growth rate.

1.5 Novel approaches for gene expression studies: single-cell analysis and microfluidics

Traditionally, microbiology studies have being concentrated at population level. The technical progresses that are taking place in the recent years and the recognition of the presence of cellular heterogeneity have brought to the development of more complex methods of investigation of individual microbial cell. The possibility to gain very detailed information allows to dissect the complexity of a population, and in general of an organism. New insight on biochemical and genetic pathways can now be studied with a detailed precision not possible so far.

Investigations performed at single-cell level are not subjected to averaging effects characteristic of the bulk analysis at population level. This feature allows to identify and to quantify the variability among different cells [138]. Non-genetic cell-to-cell heterogeneity within a clonal population is, in fact, common to many biological processes [139]. It can arise from a broad range of phenomena including stochastic biochemical interactions, noise in gene expression, difference in the intracellular protein concentration, non-synchronicity in cell cycle stage, fluctuation in molecule synthesis and degradation [140-143]. All these processes together or only some of them can contribute simultaneously to the observed variability. In most single-cell studies, stochastic models are applied to explain the experimental observations. They take into account only one or few parameters of cellular stochasticity to simplify the analysis [144-146].

Analysis of single-cell gene expression showed that there are two kind of noise involved in the expression process: intrinsic and extrinsic. The noise is defined as standard

deviation divided by the mean [141]. The intrinsic noise is the linked to the gene sequence and the protein that it encodes; the extrinsic noise is related to the transcription and translation machinery (number of polymerases and ribosomes), to the cell cycle stage and cell age [147]. Both source of noise contribute to the gene expression mechanism [148].

In parallel with the spread of the single-cell approach to analyze cellular processes, technical development arose to allow the accurately observation and quantification of the dynamic events in living cells. The use of fluorescent reporter has become a well-established technique for gene expression studies. Fluorescence-based assays include *in-situ* hybridization (FISH), immunofluorescence, flow cytometry and microscopy [138, 149]. This last technique showed the strongest potential for the single-cell analysis, allowing *in vivo* imaging. The combination of fluorescence and microscopy, together with more sensitive cameras, automated stages and faster computers, has allowed to capture gene expression dynamics with increased precision. Fluorescence microscopes resolve the fluorescence of microscopic objects as a function of spatial coordinates in two or three dimensions. The extraction of single-cell expression levels require time-lapse movies, segmentation of the image into individual cell and quantification of the fluorescence within the cell boundary. The possibility to perform lineage tracking, to identify protein distribution during cell division and to specify protein localization are some of the possible applications [145, 150, 151].

To perform live-cell imaging with time-lapse fluorescence microscopy requires the growth of bacteria during the imaging. Two main approach can be identified: the use of agarose pads [152] and microfluidic chambers [153]. The agar pad technique consists in the growth of the cell between an agar pad, containing the growth nutrient and eventual inducing molecules, and a coverglass. This technique is simple and inexpensive, and allow an extensive growth of the cells in a monolayer. However, there are some limitations. It is not possible to change the environmental conditions and the pads can be subjected to desiccation during long-term experiments [154, 155]. Microfluidic devises overcome some of these disadvantages, although they need very sophisticated components. They gave the possibility to precisely control the environmental condition of the cell culture, they allow a continuous and regulated perfusion of nutrients and chemical agents, and to create chemical gradients. The combination with automated stages and powerful computers increases drastically the amount of parallel data acquisition with high temporal and spatial resolution. Another important advantage of microfluidic devices is the use of miniaturized components. Using smaller volume of fluids reduces the consumption of reagents, reducing the costs and the waste production [156-158]. By combining fluorescence microscopy and microfluidic devices, the potential of single cell study expands considerably.

The combination of the advantages of the single-cell gene expression analysis and the microfluidic device represented a novel approach to investigate *dps* expression. This

thesis represents the first step towards the understanding of the global regulatory transcriptional mechanism of *dps* gene in response to diverse environmental stress conditions. Further studies will clarify the network of regulators involved during the Dps response activation.

1.6 This thesis

This thesis contains five chapters. Each of them deals with a particular aspect of the bacterial stress response. In particular, our attention was focused on the *E. coli* Dps response to different stresses. In the chapter 2 the basis of the principal experiments is described. It was fundamental to identify the optimal conditions, both experimental and microbiological, to allow the detection of *dps* expression, without the influence of external factors that could have led to misleading results.

Chapter 3 is the core of the thesis. It deals with the analysis of *dps* expression in single cells using time-lapse fluorescence microscopy. For the first time we detected and characterized the kinetics of the induction of *dps* expression in individual cells exposed to hydrogen peroxide. We observed a single pulse of activation of the *dps* operon, with variable intensity and duration based on the H_2O_2 concentrations applied to the cells. Lower H_2O_2 concentrations strongly activated the *dps* promoter with little effect on growth rate, while higher concentrations led to a slower and highly variable cellular growth. Comparison of cells exposed to the same stressor concentration showed that increased levels of *dps* expression did not confer a growth advantage. This aspect showed that healing from oxidative stress may largely depend upon the amount of damage in each individual cell.

In the chapter 4 the Dps response to alkaline pH stress is described. With time-lapse fluorescence microscopy, we were able to identify *dps* expression at single cell level for the first time. We observed a single pulse of transcription induction in all the cells exposed, with an intensity and a duration of the response proportional to the increasing pH value. The analysis of the variability within and between the microcolonies, showed a strong homogeneity in the *dps* promoter activation. The increase in the alkalinity of the growth media did not correspond to a proportional decrease in the cellular growth. As observed during oxidative stress exposure, the comparison of cells exposed to the same stressor environment showed that a stronger and longer *dps* induction do not improve the growth. This aspect confirm the hypothesis that the intensity of the damages in each individual cell may be responsible for the recovery more than the induction of a specific stress response protein.

In the chapter 5 we investigated the Dps response to oxidative stress using another experimental technique, a microfluidics device. The possibility of a precise

regulate the timing of the stress exposure and the continuous perfusion of fresh H_2O_2 solution to the cells allowed a more accurate control of the stressor delivery, compared to the agarose pads. The PDMS-based microfluidic device allowed the study of the *dps* promoter activity at single cell level in response to oxidative stress. As observed in the cells exposed to the stressor onto the agarose pads, a single pulse of transcription was identified in bacteria exposed to concentrations of H_2O_2 between 0 and 500 μM. The intensity of the *dps* induction was correlated to the amount of the applied stress, but no correlation was identified between the duration of the induction and the stress concentration. Concentrations of H_2O_2 up to 30 μM did not affect cellular growth although initiated the *dps* transcription. Correlation analysis of cells exposed to the same stressor concentration, revealed that cells with more intense *dps* induction did not receive a growth advantage. A similar behavior was observed also in microcolonies grown on agarose pads. Overall, these results support the thesis that the defense mechanism depends more on the amount of damage experienced by individual cells than on the expression of specific proteins.

1.7 References

1. Gross, C.A., et al., *The functional and regulatory roles of sigma factors in transcription.* Cold Spring Harb Symp Quant Biol, 1998. **63**: p. 141-55.
2. Gruber, T.M. and C.A. Gross, *Multiple sigma subunits and the partitioning of bacterial transcription space.* Annu Rev Microbiol, 2003. **57**: p. 441-66.
3. Paget, M.S. and J.D. Helmann, *The sigma70 family of sigma factors.* Genome Biol, 2003. **4**(1): p. 203.
4. Alba, B.M. and C.A. Gross, *Regulation of the Escherichia coli sigma-dependent envelope stress response.* Mol Microbiol, 2004. **52**(3): p. 613-9.
5. Alba, B.M., et al., *DegS and YaeL participate sequentially in the cleavage of RseA to activate the sigma(E)-dependent extracytoplasmic stress response.* Genes Dev, 2002. **16**(16): p. 2156-68.
6. Ades, S.E., I.L. Grigorova, and C.A. Gross, *Regulation of the alternative sigma factor sigma(E) during initiation, adaptation, and shutoff of the extracytoplasmic heat shock response in Escherichia coli.* J Bacteriol, 2003. **185**(8): p. 2512-9.
7. Arsene, F., T. Tomoyasu, and B. Bukau, *The heat shock response of Escherichia coli.* Int J Food Microbiol, 2000. **55**(1-3): p. 3-9.
8. Zhao, K., M. Liu, and R.R. Burgess, *The global transcriptional response of Escherichia coli to induced sigma 32 protein involves sigma 32 regulon activation followed by inactivation and degradation of sigma 32 in vivo.* J Biol Chem, 2005. **280**(18): p. 17758-68.
9. Morita, M., et al., *Heat-induced synthesis of sigma32 in Escherichia coli: structural and functional dissection of rpoH mRNA secondary structure.* J Bacteriol, 1999. **181**(2): p. 401-10.
10. Straus, D.B., W.A. Walter, and C.A. Gross, *The heat shock response of E. coli is regulated by changes in the concentration of sigma 32.* Nature, 1987. **329**(6137): p. 348-51.
11. Kanemori, M., H. Mori, and T. Yura, *Induction of heat shock proteins by abnormal proteins results from stabilization and not increased synthesis of sigma 32 in Escherichia coli.* J Bacteriol, 1994. **176**(18): p. 5648-53.
12. Kanemori, M., H. Mori, and T. Yura, *Effects of reduced levels of GroE chaperones on protein metabolism: enhanced synthesis of heat shock proteins during steady-state growth of Escherichia coli.* J Bacteriol, 1994. **176**(14): p. 4235-42.
13. Visca, P., et al., *Iron transport and regulation, cell signalling and genomics: lessons from Escherichia coli and Pseudomonas.* Mol Microbiol, 2002. **45**(5): p. 1177-90.
14. Ochs, M., et al., *Regulation of citrate-dependent iron transport of Escherichia coli: fecR is required for transcription activation by FecI.* Mol Microbiol, 1995. **15**(1): p. 119-32.
15. Imlay, J.A. and I. Fridovich, *Assay of metabolic superoxide production in Escherichia coli.* J Biol Chem, 1991. **266**(11): p. 6957-65.
16. Buck, M., et al., *The bacterial enhancer-dependent sigma(54) (sigma(N)) transcription factor.* J Bacteriol, 2000. **182**(15): p. 4129-36.

17. Battesti, A., N. Majdalani, and S. Gottesman, *The RpoS-mediated general stress response in Escherichia coli.* Annu Rev Microbiol, 2011. **65**: p. 189-213.
18. Hengge-Aronis, R., *Signal transduction and regulatory mechanisms involved in control of the sigma(S) (RpoS) subunit of RNA polymerase.* Microbiol Mol Biol Rev, 2002. **66**(3): p. 373-95.
19. Hirsch, M. and T. Elliott, *Role of ppGpp in rpoS stationary-phase regulation in Escherichia coli.* J Bacteriol, 2002. **184**(18): p. 5077-87.
20. Shiba, T., et al., *Inorganic polyphosphate and the induction of rpoS expression.* Proc Natl Acad Sci U S A, 1997. **94**(21): p. 11210-5.
21. Traxler, M.F., et al., *The global, ppGpp-mediated stringent response to amino acid starvation in Escherichia coli.* Mol Microbiol, 2008. **68**(5): p. 1128-48.
22. Lange, R. and R. Hengge-Aronis, *The cellular concentration of the sigma S subunit of RNA polymerase in Escherichia coli is controlled at the levels of transcription, translation, and protein stability.* Genes Dev, 1994. **8**(13): p. 1600-12.
23. Brennan, R.G. and T.M. Link, *Hfq structure, function and ligand binding.* Curr Opin Microbiol, 2007. **10**(2): p. 125-33.
24. Majdalani, N., et al., *DsrA RNA regulates translation of RpoS message by an anti-antisense mechanism, independent of its action as an antisilencer of transcription.* Proc Natl Acad Sci U S A, 1998. **95**(21): p. 12462-7.
25. Mandin, P. and S. Gottesman, *Integrating anaerobic/aerobic sensing and the general stress response through the ArcZ small RNA.* EMBO J, 2010. **29**(18): p. 3094-107.
26. Hussein, R. and H.N. Lim, *Disruption of small RNA signaling caused by competition for Hfq.* Proc Natl Acad Sci U S A, 2011. **108**(3): p. 1110-5.
27. Mandel, M.J. and T.J. Silhavy, *Starvation for different nutrients in Escherichia coli results in differential modulation of RpoS levels and stability.* J Bacteriol, 2005. **187**(2): p. 434-42.
28. Schweder, T., et al., *Regulation of Escherichia coli starvation sigma factor (sigma s) by ClpXP protease.* J Bacteriol, 1996. **178**(2): p. 470-6.
29. Zhou, Y., et al., *The RssB response regulator directly targets sigma(S) for degradation by ClpXP.* Genes Dev, 2001. **15**(5): p. 627-37.
30. Bougdour, A., et al., *Multiple pathways for regulation of sigmaS (RpoS) stability in Escherichia coli via the action of multiple anti-adaptors.* Mol Microbiol, 2008. **68**(2): p. 298-313.
31. Bougdour, A., S. Wickner, and S. Gottesman, *Modulating RssB activity: IraP, a novel regulator of sigma(S) stability in Escherichia coli.* Genes Dev, 2006. **20**(7): p. 884-97.
32. Grigorova, I.L., et al., *Insights into transcriptional regulation and σ competition from an equilibrium model of RNA polymerase binding to DNA.* Proceedings of the National Academy of Sciences of the United States of America, 2006. **103**(14): p. 5332-5337.
33. Piper, S.E., et al., *A global view of Escherichia coli Rsd protein and its interactions.* Mol Biosyst, 2009. **5**(12): p. 1943-7.

34. Jishage, M., et al., *Regulation of RNA polymerase sigma subunit synthesis in Escherichia coli: intracellular levels of four species of sigma subunit under various growth conditions.* J Bacteriol, 1996. **178**(18): p. 5447-51.
35. Jishage, M. and A. Ishihama, *Regulation of RNA polymerase sigma subunit synthesis in Escherichia coli: intracellular levels of sigma 70 and sigma 38.* J Bacteriol, 1995. **177**(23): p. 6832-5.
36. Maeda, H., N. Fujita, and A. Ishihama, *Competition among seven Escherichia coli sigma subunits: relative binding affinities to the core RNA polymerase.* Nucleic Acids Res, 2000. **28**(18): p. 3497-503.
37. Jishage, M., D. Dasgupta, and A. Ishihama, *Mapping of the Rsd contact site on the sigma 70 subunit of Escherichia coli RNA polymerase.* J Bacteriol, 2001. **183**(9): p. 2952-6.
38. Pratt, L.A. and T.J. Silhavy, *Crl stimulates RpoS activity during stationary phase.* Mol Microbiol, 1998. **29**(5): p. 1225-36.
39. Cavanagh, A.T. and K.M. Wassarman, *6S RNA, a global regulator of transcription in Escherichia coli, Bacillus subtilis, and beyond.* Annu Rev Microbiol, 2014. **68**: p. 45-60.
40. Yuan, A.H., et al., *Rsd family proteins make simultaneous interactions with regions 2 and 4 of the primary sigma factor.* Mol Microbiol, 2008. **70**(5): p. 1136-51.
41. Potrykus, K. and M. Cashel, *(p)ppGpp: still magical?* Annu Rev Microbiol, 2008. **62**: p. 35-51.
42. Costanzo, A. and S.E. Ades, *Growth phase-dependent regulation of the extracytoplasmic stress factor, sigmaE, by guanosine 3',5'-bispyrophosphate (ppGpp).* J Bacteriol, 2006. **188**(13): p. 4627-34.
43. Durfee, T., et al., *Transcription profiling of the stringent response in Escherichia coli.* J Bacteriol, 2008. **190**(3): p. 1084-96.
44. Bougdour, A. and S. Gottesman, *ppGpp regulation of RpoS degradation via anti-adaptor protein IraP.* Proc Natl Acad Sci U S A, 2007. **104**(31): p. 12896-901.
45. Merrikh, H., A.E. Ferrazzoli, and S.T. Lovett, *Growth phase and (p)ppGpp control of IraD, a regulator of RpoS stability, in Escherichia coli.* J Bacteriol, 2009. **191**(24): p. 7436-46.
46. Soper, T., et al., *Positive regulation by small RNAs and the role of Hfq.* Proc Natl Acad Sci U S A, 2010. **107**(21): p. 9602-7.
47. Lease, R.A. and M. Belfort, *Riboregulation by DsrA RNA: trans-actions for global economy.* Mol Microbiol, 2000. **38**(4): p. 667-72.
48. Barth, M., et al., *Role for the histone-like protein H-NS in growth phase-dependent and osmotic regulation of sigma S and many sigma S-dependent genes in Escherichia coli.* J Bacteriol, 1995. **177**(12): p. 3455-64.
49. Zhang, A., et al., *The OxyS regulatory RNA represses rpoS translation and binds the Hfq (HF-I) protein.* EMBO J, 1998. **17**(20): p. 6061-8.
50. Mika, F. and R. Hengge, *A two-component phosphotransfer network involving ArcB, ArcA, and RssB coordinates synthesis and proteolysis of sigmaS (RpoS) in E. coli.* Genes Dev, 2005. **19**(22): p. 2770-81.

51. Adams, J.L. and R.J. McLean, *Impact of rpoS deletion on Escherichia coli biofilms.* Appl Environ Microbiol, 1999. **65**(9): p. 4285-7.
52. Majdalani, N., D. Hernandez, and S. Gottesman, *Regulation and mode of action of the second small RNA activator of RpoS translation, RprA.* Mol Microbiol, 2002. **46**(3): p. 813-26.
53. Francez-Charlot, A., et al., *RcsCDB His-Asp phosphorelay system negatively regulates the flhDC operon in Escherichia coli.* Mol Microbiol, 2003. **49**(3): p. 823-32.
54. Gottesman, S. and V. Stout, *Regulation of capsular polysaccharide synthesis in Escherichia coli K12.* Mol Microbiol, 1991. **5**(7): p. 1599-606.
55. Francez-Charlot, A., et al., *Osmotic regulation of the Escherichia coli bdm (biofilm-dependent modulation) gene by the RcsCDB His-Asp phosphorelay.* J Bacteriol, 2005. **187**(11): p. 3873-7.
56. Majdalani, N., et al., *Regulation of RpoS by a novel small RNA: the characterization of RprA.* Mol Microbiol, 2001. **39**(5): p. 1382-94.
57. Kandror, O., A. DeLeon, and A.L. Goldberg, *Trehalose synthesis is induced upon exposure of Escherichia coli to cold and is essential for viability at low temperatures.* Proc Natl Acad Sci U S A, 2002. **99**(15): p. 9727-32.
58. Stoebel, D.M., et al., *Compensatory evolution of gene regulation in response to stress by Escherichia coli lacking RpoS.* PLoS Genet, 2009. **5**(10): p. e1000671.
59. Zhao, B. and W.A. Houry, *Acid stress response in enteropathogenic gammaproteobacteria: an aptitude for survival.* Biochem Cell Biol, 2010. **88**(2): p. 301-14.
60. Chang, Y.Y. and J.E. Cronan, Jr., *Membrane cyclopropane fatty acid content is a major factor in acid resistance of Escherichia coli.* Mol Microbiol, 1999. **33**(2): p. 249-59.
61. Tapley, T.L., et al., *Protein refolding by pH-triggered chaperone binding and release.* Proc Natl Acad Sci U S A, 2010. **107**(3): p. 1071-6.
62. Eguchi, Y., et al., *Regulation of acid resistance by connectors of two-component signal transduction systems in Escherichia coli.* J Bacteriol, 2011. **193**(5): p. 1222-8.
63. Korshunov, S. and J.A. Imlay, *Two sources of endogenous hydrogen peroxide in Escherichia coli.* Mol Microbiol, 2010. **75**(6): p. 1389-401.
64. Imlay, J.A., *The molecular mechanisms and physiological consequences of oxidative stress: lessons from a model bacterium.* Nat Rev Microbiol, 2013. **11**(7): p. 443-54.
65. Seaver, L.C. and J.A. Imlay, *Are respiratory enzymes the primary sources of intracellular hydrogen peroxide?* J Biol Chem, 2004. **279**(47): p. 48742-50.
66. Imlay, J.A., *Cellular defenses against superoxide and hydrogen peroxide.* Annu Rev Biochem, 2008. **77**: p. 755-76.
67. Gort, A.S. and J.A. Imlay, *Balance between endogenous superoxide stress and antioxidant defenses.* J Bacteriol, 1998. **180**(6): p. 1402-10.
68. Masse, E. and S. Gottesman, *A small RNA regulates the expression of genes involved in iron metabolism in Escherichia coli.* Proc Natl Acad Sci U S A, 2002. **99**(7): p. 4620-5.

69. Tardat, B. and D. Touati, *Two global regulators repress the anaerobic expression of MnSOD in Escherichia coli::Fur (ferric uptake regulation) and Arc (aerobic respiration control).* Mol Microbiol, 1991. **5**(2): p. 455-65.
70. Korshunov, S. and J.A. Imlay, *Detection and quantification of superoxide formed within the periplasm of Escherichia coli.* J Bacteriol, 2006. **188**(17): p. 6326-34.
71. De Groote, M.A., et al., *Periplasmic superoxide dismutase protects Salmonella from products of phagocyte NADPH-oxidase and nitric oxide synthase.* Proc Natl Acad Sci U S A, 1997. **94**(25): p. 13997-4001.
72. Seaver, L.C. and J.A. Imlay, *Hydrogen peroxide fluxes and compartmentalization inside growing Escherichia coli.* J Bacteriol, 2001. **183**(24): p. 7182-9.
73. Putnam, C.D., et al., *Active and inhibited human catalase structures: ligand and NADPH binding and catalytic mechanism.* J Mol Biol, 2000. **296**(1): p. 295-309.
74. Seaver, L.C. and J.A. Imlay, *Alkyl hydroperoxide reductase is the primary scavenger of endogenous hydrogen peroxide in Escherichia coli.* J Bacteriol, 2001. **183**(24): p. 7173-81.
75. Poole, L.B., *Bacterial defenses against oxidants: mechanistic features of cysteine-based peroxidases and their flavoprotein reductases.* Arch Biochem Biophys, 2005. **433**(1): p. 240-54.
76. Christman, M.F., G. Storz, and B.N. Ames, *OxyR, a positive regulator of hydrogen peroxide-inducible genes in Escherichia coli and Salmonella typhimurium, is homologous to a family of bacterial regulatory proteins.* Proc Natl Acad Sci U S A, 1989. **86**(10): p. 3484-8.
77. Schellhorn, H.E. and H.M. Hassan, *Transcriptional regulation of katE in Escherichia coli K-12.* J Bacteriol, 1988. **170**(9): p. 4286-92.
78. He, X., et al., *Oral-derived bacterial flora defends its domain by recognizing and killing intruders--a molecular analysis using Escherichia coli as a model intestinal bacterium.* Microb Ecol, 2010. **60**(3): p. 655-64.
79. Lamb, C. and R.A. Dixon, *The Oxidative Burst in Plant Disease Resistance.* Annu Rev Plant Physiol Plant Mol Biol, 1997. **48**: p. 251-275.
80. Cohen, G.M. and M. d'Arcy Doherty, *Free radical mediated cell toxicity by redox cycling chemicals.* Br J Cancer Suppl, 1987. **8**: p. 46-52.
81. Robinson, J.M., *Phagocytic leukocytes and reactive oxygen species.* Histochem Cell Biol, 2009. **131**(4): p. 465-9.
82. Schell, M.A., *Molecular biology of the LysR family of transcriptional regulators.* Annu Rev Microbiol, 1993. **47**: p. 597-626.
83. Tao, K., et al., *Purification and characterization of the Escherichia coli OxyR protein, the positive regulator for a hydrogen peroxide-inducible regulon.* J Biochem, 1991. **109**(2): p. 262-6.
84. Storz, G., L.A. Tartaglia, and B.N. Ames, *Transcriptional regulator of oxidative stress-inducible genes: direct activation by oxidation.* Science, 1990. **248**(4952): p. 189-94.
85. Choi, H., et al., *Structural basis of the redox switch in the OxyR transcription factor.* Cell, 2001. **105**(1): p. 103-13.
86. Tao, K., et al., *Mapping of the OxyR protein contact site in the C-terminal region of RNA polymerase alpha subunit.* J Bacteriol, 1995. **177**(23): p. 6740-4.

87. Seymour, R.L., et al., *Essential roles of core starvation-stress response loci in carbon-starvation-inducible cross-resistance and hydrogen peroxide-inducible adaptive resistance to oxidative challenge in Salmonella typhimurium.* Mol Microbiol, 1996. **20**(3): p. 497-505.
88. Henderson, I.R. and P. Owen, *The major phase-variable outer membrane protein of Escherichia coli structurally resembles the immunoglobulin A1 protease class of exported protein and is regulated by a novel mechanism involving Dam and oxyR.* J Bacteriol, 1999. **181**(7): p. 2132-41.
89. Zheng, M., et al., *DNA microarray-mediated transcriptional profiling of the Escherichia coli response to hydrogen peroxide.* J Bacteriol, 2001. **183**(15): p. 4562-70.
90. Zheng, M., F. Aslund, and G. Storz, *Activation of the OxyR transcription factor by reversible disulfide bond formation.* Science, 1998. **279**(5357): p. 1718-21.
91. Christman, M.F., et al., *Positive control of a regulon for defenses against oxidative stress and some heat-shock proteins in Salmonella typhimurium.* Cell, 1985. **41**(3): p. 753-62.
92. Kramer, G.F. and B.N. Ames, *Oxidative mechanisms of toxicity of low-intensity near-UV light in Salmonella typhimurium.* J Bacteriol, 1987. **169**(5): p. 2259-66.
93. Yoon, S.J., et al., *OxyR regulon controls lipid peroxidation-mediated oxidative stress in Escherichia coli.* J Biochem Mol Biol, 2002. **35**(3): p. 297-301.
94. Lynch, R.E. and I. Fridovich, *Permeation of the erythrocyte stroma by superoxide radical.* J Biol Chem, 1978. **253**(13): p. 4697-9.
95. Hassan, H.M. and I. Fridovich, *Intracellular production of superoxide radical and of hydrogen peroxide by redox active compounds.* Arch Biochem Biophys, 1979. **196**(2): p. 385-95.
96. Greenberg, J.T., et al., *Positive control of a global antioxidant defense regulon activated by superoxide-generating agents in Escherichia coli.* Proc Natl Acad Sci U S A, 1990. **87**(16): p. 6181-5.
97. Tsaneva, I.R. and B. Weiss, *soxR, a locus governing a superoxide response regulon in Escherichia coli K-12.* J Bacteriol, 1990. **172**(8): p. 4197-205.
98. Blanchard, J.L., et al., *Rapid changes in gene expression dynamics in response to superoxide reveal SoxRS-dependent and independent transcriptional networks.* PLoS One, 2007. **2**(11): p. e1186.
99. Pomposiello, P.J., M.H. Bennik, and B. Demple, *Genome-wide transcriptional profiling of the Escherichia coli responses to superoxide stress and sodium salicylate.* J Bacteriol, 2001. **183**(13): p. 3890-902.
100. Griffith, K.L., I.M. Shah, and R.E. Wolf, Jr., *Proteolytic degradation of Escherichia coli transcription activators SoxS and MarA as the mechanism for reversing the induction of the superoxide (SoxRS) and multiple antibiotic resistance (Mar) regulons.* Mol Microbiol, 2004. **51**(6): p. 1801-16.
101. Koo, M.S., et al., *A reducing system of the superoxide sensor SoxR in Escherichia coli.* EMBO J, 2003. **22**(11): p. 2614-22.
102. Gu, M. and J.A. Imlay, *The SoxRS response of Escherichia coli is directly activated by redox-cycling drugs rather than by superoxide.* Molecular microbiology, 2011. **79**(5): p. 1136-1150.

103. Lee, J.H., et al., *SoxRS-mediated lipopolysaccharide modification enhances resistance against multiple drugs in Escherichia coli.* J Bacteriol, 2009. **191**(13): p. 4441-50.
104. Ma, D., et al., *Genes acrA and acrB encode a stress-induced efflux system of Escherichia coli.* Mol Microbiol, 1995. **16**(1): p. 45-55.
105. Rau, J. and A. Stolz, *Oxygen-insensitive nitroreductases NfsA and NfsB of Escherichia coli function under anaerobic conditions as lawsone-dependent Azo reductases.* Appl Environ Microbiol, 2003. **69**(6): p. 3448-55.
106. Pomposiello, P.J., et al., *SoxRS-regulated expression and genetic analysis of the yggX gene of Escherichia coli.* J Bacteriol, 2003. **185**(22): p. 6624-32.
107. Levin, J.D., A.W. Johnson, and B. Demple, *Homogeneous Escherichia coli endonuclease IV. Characterization of an enzyme that recognizes oxidative damage in DNA.* J Biol Chem, 1988. **263**(17): p. 8066-71.
108. Zhao, X. and K. Drlica, *Reactive oxygen species and the bacterial response to lethal stress.* Curr Opin Microbiol, 2014. **21**: p. 1-6.
109. Park, S., X. You, and J.A. Imlay, *Substantial DNA damage from submicromolar intracellular hydrogen peroxide detected in Hpx- mutants of Escherichia coli.* Proc Natl Acad Sci U S A, 2005. **102**(26): p. 9317-22.
110. Chiancone, E. and P. Ceci, *The multifaceted capacity of Dps proteins to combat bacterial stress conditions: Detoxification of iron and hydrogen peroxide and DNA binding.* Biochim Biophys Acta, 2010. **1800**(8): p. 798-805.
111. Almiron, M., et al., *A novel DNA-binding protein with regulatory and protective roles in starved Escherichia coli.* Genes Dev, 1992. **6**(12B): p. 2646-54.
112. Choi, S.H., D.J. Baumler, and C.W. Kaspar, *Contribution of dps to acid stress tolerance and oxidative stress tolerance in Escherichia coli O157:H7.* Appl Environ Microbiol, 2000. **66**(9): p. 3911-6.
113. Nair, S. and S.E. Finkel, *Dps protects cells against multiple stresses during stationary phase.* Journal of Bacteriology, 2004. **186**(13): p. 4192-4198.
114. Jeong, K.C., et al., *Acid stress damage of DNA is prevented by Dps binding in Escherichia coli O157: H7.* Bmc Microbiology, 2008. **8**.
115. Martinez, A. and R. Kolter, *Protection of DNA during oxidative stress by the nonspecific DNA-binding protein Dps.* J Bacteriol, 1997. **179**(16): p. 5188-94.
116. Meyer, A.S. and D.C. Grainger, *The Escherichia coli Nucleoid in Stationary Phase.* Adv Appl Microbiol, 2013. **83**: p. 69-86.
117. Karas, V.O., I. Westerlaken, and A.S. Meyer, *The DNA-binding protein from starved cells (Dps) utilizes dual functions to defend cells against multiple stresses.* J Bacteriol, 2015.
118. Zhao, G.H., et al., *Iron and hydrogen peroxide detoxification properties of DNA-binding protein from starved cells - A ferritin-like DNA-binding protein of Escherichia coli.* Journal of Biological Chemistry, 2002. **277**(31): p. 27689-27696.
119. Bozzi, M., et al., *A novel non-heme iron-binding ferritin related to the DNA-binding proteins of the Dps family in Listeria innocua.* J Biol Chem, 1997. **272**(6): p. 3259-65.
120. Grant, R.A., et al., *The crystal structure of Dps, a ferritin homolog that binds and protects DNA.* Nature Structural Biology, 1998. **5**(4): p. 294-303.

121. Haikarainen, T. and A.C. Papageorgiou, *Dps-like proteins: structural and functional insights into a versatile protein family.* Cell Mol Life Sci, 2010. **67**(3): p. 341-51.
122. Ceci, P., et al., *DNA condensation and self-aggregation of Escherichia coli Dps are coupled phenomena related to the properties of the N-terminus.* Nucleic Acids Research, 2004. **32**(19): p. 5935-5944.
123. Wolf, S.G., et al., *DNA protection by stress-induced biocrystallization.* Nature, 1999. **400**(6739): p. 83-5.
124. Frenkiel-Krispin, D., et al., *Nucleoid restructuring in stationary-state bacteria.* Mol Microbiol, 2004. **51**(2): p. 395-405.
125. Frenkiel-Krispin, D., et al., *Regulated phase transitions of bacterial chromatin: a non-enzymatic pathway for generic DNA protection.* EMBO J, 2001. **20**(5): p. 1184-91.
126. Ilari, A., et al., *Iron incorporation into Escherichia coli Dps gives rise to a ferritin-like microcrystalline core.* Journal of Biological Chemistry, 2002. **277**(40): p. 37619-37623.
127. Nordlund, P. and H. Eklund, *Di-iron-carboxylate proteins.* Curr Opin Struct Biol, 1995. **5**(6): p. 758-66.
128. Azam, T.A., et al., *Growth phase-dependent variation in protein composition of the Escherichia coli nucleoid.* Journal of Bacteriology, 1999. **181**(20): p. 6361-6370.
129. Altuvia, S., et al., *The dps promoter is activated by OxyR during growth and by IHF and sigma S in stationary phase.* Mol Microbiol, 1994. **13**(2): p. 265-72.
130. Grainger, D.C., et al., *Selective repression by Fis and H-NS at the Escherichia coli dps promoter.* Mol Microbiol, 2008. **68**(6): p. 1366-77.
131. Yamamoto, K., et al., *The Escherichia coli K-12 MntR miniregulon includes dps, which encodes the major stationary-phase DNA-binding protein.* J Bacteriol, 2011. **193**(6): p. 1477-80.
132. Freundlich, M., et al., *The role of integration host factor in gene expression in Escherichia coli.* Mol Microbiol, 1992. **6**(18): p. 2557-63.
133. Ali Azam, T., et al., *Growth phase-dependent variation in protein composition of the Escherichia coli nucleoid.* J Bacteriol, 1999. **181**(20): p. 6361-70.
134. Stephani, K., D. Weichart, and R. Hengge, *Dynamic control of Dps protein levels by ClpXP and ClpAP proteases in Escherichia coli.* Mol Microbiol, 2003. **49**(6): p. 1605-14.
135. Flynn, J.M., et al., *Proteomic discovery of cellular substrates of the ClpXP protease reveals five classes of ClpX-recognition signals.* Mol Cell, 2003. **11**(3): p. 671-83.
136. Studemann, A., et al., *Sequential recognition of two distinct sites in sigma(S) by the proteolytic targeting factor RssB and ClpX.* EMBO J, 2003. **22**(16): p. 4111-20.
137. Schmidt, R., et al., *ClpS is the recognition component for Escherichia coli substrates of the N-end rule degradation pathway.* Mol Microbiol, 2009. **72**(2): p. 506-17.
138. Brehm-Stecher, B.F. and E.A. Johnson, *Single-cell microbiology: tools, technologies, and applications.* Microbiol Mol Biol Rev, 2004. **68**(3): p. 538-59, table of contents.

139. Martins, B.M. and J.C. Locke, *Microbial individuality: how single-cell heterogeneity enables population level strategies.* Curr Opin Microbiol, 2015. **24**: p. 104-12.
140. Davey, H.M. and D.B. Kell, *Flow cytometry and cell sorting of heterogeneous microbial populations: the importance of single-cell analyses.* Microbiol Rev, 1996. **60**(4): p. 641-96.
141. Elowitz, M.B., et al., *Stochastic gene expression in a single cell.* Science, 2002. **297**(5584): p. 1183-6.
142. Schwabe, A. and F.J. Bruggeman, *Contributions of cell growth and biochemical reactions to nongenetic variability of cells.* Biophys J, 2014. **107**(2): p. 301-13.
143. Silander, O.K., et al., *A genome-wide analysis of promoter-mediated phenotypic noise in Escherichia coli.* PLoS Genet, 2012. **8**(1): p. e1002443.
144. Espinar, L., et al., *Circuit-level input integration in bacterial gene regulation.* Proc Natl Acad Sci U S A, 2013. **110**(17): p. 7091-6.
145. Kiviet, D.J., et al., *Stochasticity of metabolism and growth at the single-cell level.* Nature, 2014. **514**(7522): p. 376-9.
146. Locke, J.C., et al., *Stochastic pulse regulation in bacterial stress response.* Science, 2011. **334**(6054): p. 366-9.
147. Ryall, B., G. Eydallin, and T. Ferenci, *Culture history and population heterogeneity as determinants of bacterial adaptation: the adaptomics of a single environmental transition.* Microbiol Mol Biol Rev, 2012. **76**(3): p. 597-625.
148. Dubnau, D. and R. Losick, *Bistability in bacteria.* Mol Microbiol, 2006. **61**(3): p. 564-72.
149. Longo, D. and J. Hasty, *Dynamics of single-cell gene expression.* Mol Syst Biol, 2006. **2**: p. 64.
150. Moolman, M.C., et al., *Slow unloading leads to DNA-bound beta2-sliding clamp accumulation in live Escherichia coli cells.* Nat Commun, 2014. **5**: p. 5820.
151. Young, J.W., et al., *Measuring single-cell gene expression dynamics in bacteria using fluorescence time-lapse microscopy.* Nature Protocols, 2012. **7**(1): p. 80-88.
152. Fiebig, A., K. Keren, and J.A. Theriot, *Fine-scale time-lapse analysis of the biphasic, dynamic behaviour of the two Vibrio cholerae chromosomes.* Mol Microbiol, 2006. **60**(5): p. 1164-78.
153. Nghe, P., et al., *Microfabricated polyacrylamide devices for the controlled culture of growing cells and developing organisms.* PLoS One, 2013. **8**(9): p. e75537.
154. Young, J.W., et al., *Measuring single-cell gene expression dynamics in bacteria using fluorescence time-lapse microscopy.* Nat Protoc, 2012. **7**(1): p. 80-8.
155. Joyce, G., B.D. Robertson, and K.J. Williams, *A modified agar pad method for mycobacterial live-cell imaging.* BMC Res Notes, 2011. **4**: p. 73.
156. Breslauer, D.N., P.J. Lee, and L.P. Lee, *Microfluidics-based systems biology.* Mol Biosyst, 2006. **2**(2): p. 97-112.
157. Halldorsson, S., et al., *Advantages and challenges of microfluidic cell culture in polydimethylsiloxane devices.* Biosens Bioelectron, 2015. **63**: p. 218-31.
158. Walker, G.M., H.C. Zeringue, and D.J. Beebe, *Microenvironment design considerations for cellular scale studies.* Lab Chip, 2004. **4**(2): p. 91-7.

Chapter 2

Optimization of experimental conditions

The regulation of *dps* transcription is a complex mechanism that responds both to bacterial growth phase and to the surrounding environment. To accurately identify the promoter activity in response to specific stress conditions, we examined several techniques to study the effect of an individual stressor on the *dps* response. The Hi-Def Azure medium was identified as an optimal medium for cellular growth, both for the detection of *dps* expression in the presence and absence of stressor and for microscopy analysis. Cellular growth and *dps* activation were analyzed in both the *E. coli dps-mCherry* fusion and *dps::mCherry* strains. Neither of the strains were utilized for further analysis because of the aggregation of the fluorescent proteins within the *dps-mCherry* fusion cells and the increased sensitivity to external stresses of the *dps::mCherry* strain. The *dps-mCherry* strain was shown to be the most appropriate strain. Fluorescence microscopy combined with single-cell analysis was the technique selected to identify the dynamics of *dps* transcriptional regulation.

2.1 Introduction

To be able to survive and thrive in a laboratory environment, bacteria need a proper biochemical and biophysical environment. Culture media are designed to provide all the essential nutrients for bacterial proliferation. A large variety of media has been developed to fulfill the nutritional requirements of different bacterial species. A culture medium is used for the isolation of a pure bacterial culture or for the identification of a particular species according to its nutritional properties. Based on their composition, media are classified as minimal, complex or defined. A minimal medium contains the minimum possible nutrients, and it is designed for bacteria that synthesize their nutritional molecules from salts and nitrogen. A carbon source is provided and additional components, such as vitamins or amino acids, can be added. A complex medium usually contains materials of biological origin such of yeast, milk, or beef extract, in which the exact chemical composition is undetermined. These media are suitable to sustain the growth of different bacterial species. The defined media have a precisely studied chemical formulation to allow the growth of bacterial with particular nutritional needs [1] .

The composition of the medium is a key point of the experimental setup to study the bacterial metabolism or response to external stimuli. The choice is dependent not only upon the nutritional needs of the cells but also on the technique applied for the proposed investigation. In particular, to study the bacterial stress response it is important to select a growth medium that is not a primary source of nutritional or environmental stress. In fact, the optimal cell growth depends on the adequate supply of the essential nutrients that bacteria cannot synthesize themselves. The ideal medium allows for the isolation of the response of the applied stressor from the stresses derived from the external environment.

The regulation of stress response mechanisms, in response to variations in environmental conditions such as in pH, nutrients, salts, or temperature, in fact, is very complex, and the regulatory elements of each individual response often interact with each other [2]. The induction of the *Escherichia coli* general stress response sigma S (σ^S), for example, increases when the culture enters into the stationary phase with consequent nutrient deprivation, but it is also induced in adverse growth conditions, e.g. high or low temperature, variation in pH, or DNA damage [3]. The induction of the Dps (DNA-binding protein from starved cells) protein is also finely regulated during different stress conditions. Its expression is induced by OxyR when cells are exposed to H_2O_2 during exponential growth and by σ^S during stationary phase [4, 5]. This protein is in fact a key element during exposure to several stressors, such as metal exposure, temperature variations, extreme pH, oxidative stress [6]. The study of the regulation of the *dps* gene in the cell, which is the aim of this thesis, might be challenging because of its complex regulatory network. In recent years, new techniques have been developed to allow an accurate and straightforward investigation of gene expression and protein turnover.

The introduction of a gene encoding a fluorescent protein (FP) into living cells has become a well-established technique to visualize the location and dynamics of a protein [7, 8]. The FPs have been extensively studied and engineered so that a very broad range of genetic variants with emission spectral profiles covering nearly the entire visible light spectrum is now available [9]. The application of the red FPs become widely spread because of the large color separation with respect to GFP and the mCherry protein is one of the most promising. It was derived from the mRFP1 protein, which was subjected to several rounds of direct evolution. Its success derives from its monomeric form, the high photostability, the fast maturation time (15 minutes) and the low autofluorescence. The down side of the mCherry protein is the low brightness: 50% of EGFP and 27% of DsRed [10]. Recent studies have shown that autofluorescent proteins can absorb visible light and emit active electrons, producing reactive oxygen species (ROS). This reaction can lead to an increase in cell damage and photokilling processes in bacteria [11-14]. The phototoxicity is an important parameter to take into account when studying the bacterial stress response, especially for oxidative stress. The production of additional ROS in fact, might alter the cell physiology leading to an overestimation or alteration of the gene expression response. Among the red FPs, mCherry protein was seen to be the least phototoxic. The *E. coli* transformed with mCherry showed the highest survival response to illumination. After an exposure of 180 min 180 minutes, 97% of survival was observed. In contrast, after 180 minutes exposure cells transformed with KillerRed showed around 6% survival, DsRed 57% and mRFP 65% [15].

The wide adoption of FPs led to the increased use of fluorescence detection techniques. Choosing the most suitable method and the appropriate detection instrument is a key aspect for an accurate analysis of gene expression and protein detection. There are four types of instruments for fluorescence detection, each providing distinct information. Microplate readers and spectrofluorometers measure the average fluorescence of a bulk sample (cell cultures or protein solutions). They allow the analysis of the cellular growth and the fluorescence intensity of a bacterial culture [16, 17]. Fluorescence scanners are suitable to resolve the fluorescence of two-dimensional specimens, such as blots, electrophoresis gels and chromatograms. Flow cytometers detect the fluorescence in individual cells in a flowing stream, allowing the identification of subpopulations within a culture. The single cell analysis provide a snapshot of the culture, allowing the identification of the heterogeneity present in a culture, in terms of internal complexity and fluorescence signal [18]. Fluorescence microscopes resolve the fluorescence of microscopic objects as a function of spatial coordinates in two or three dimensions. The possibility to record time-lapse movies, perform lineage tracking, identify protein distribution during cell division, specify protein localization are some of the possible applications [19-21]. By combining fluorescence microscopy and microfluidic devices, the potential of single cell study expands considerably, since microfluidics allows

for continuous supply of nutrients and growth medium exchange [22]. The application of one or more specific methods depends of the desired resolution of the experimental procedure.

In this chapter, we investigated several methodologies to study the effect of an individual stressor on the *E. coli dps* promoter activity. The growth and the Dps protein expression of two genetically engineered strains were analyzed, in different growth media and in the presence of oxidative stress.

2.2 Material and methods

2.2.1 Growth curves with different media

One colony of the *E. coli* K-12 wild-type strain W3110 (CGSC# 4474) was inoculated overnight at 37°C in LB medium. The overnight culture was diluted 1:100 in one of the following media: minimal medium M9 (1x M9 salts [6 g/ L Na_2HPO_4, 3 g/ L KH_2PO_4, 0.5 g/L NaCl, 1 g/L NH_4Cl, Adjust pH 7.4], 2 mM $MgSO_4$, 0.1 mM $CaCl_2$, 0.2 %, glucose,) [23], complex medium LB (10 g/L tryptone, 5 g/L yeast extract, 10 g/L NaCl) [24] or defined Hi-Def Azure medium (3H5000, Teknova) (adapted from [25]) supplemented with 0.2% glucose. The cultures were grown at 37°C in shaking flasks, and 1 mL samples were taken at different time points to measure the growth. The optical density (O.D.) at 600 nm was measured with a cell density meter Ultrospec 10 (Amersham Bioscience).

2.2 Western blotting

An overnight culture of the *E. coli* K-12 wild-type strain W3110 (CGSC# 4474) was diluted 100 times in M9, LB or Hi-Def Azure medium supplemented with 0.2% glucose. The cultures were grown at 37°C while shaking and samples were collected at different time points to measure the *dps* expression. The cell pellet of 500 µL of cultures was combined with 2X SDS-PAGE sample buffer (5X : 10% w/v SDS, 10 mM DTT, 20% w/v glycerol, 0.2 M Tris-HCl pH 6.8, 0.05% broom phenol blue) to an $O.D._{600}$ of 10, then heated at 95°C for 10min and separated on a 15% SDS-PAGE gel. Proteins were transferred to an Immun-Blot® PVDF membrane (162-0177, Biorad) with a Novex® semi dry blotter (SD1000, Invitrogen) for 40 min at 15 volts. The PVDF membrane was blocked with 5% milk in TBS-T (10 mM Tris pH 7.5, 150 mM NaCl, 0.1% Tween-20), then incubated for 1 hour with primary antibody (rabbit anti-Dps) diluted 1:5000. It was then incubated with secondary antibody (goat anti-rabbit IgG (H+L), horseradish peroxide conjugate, 32460, Thermo Scientific) diluted 1:100,000 for 45 min. The membrane was developed using the

SuperSignal® West Pico Chemiluminescent Substrate kit (Thermo Scientific) and imaged with a Molecular Imager ChemiDoc ®XRS (Biorad). Images were analyzed with Image Lab® software (Biorad).

2.2.3 *dps::mCherry* and *dps-mCherry* fusion strain construction

The *E. coli dps::mCherry* and *dps-mCherry* fusion strains were created from the *E. coli* K-12 strain W3110 (CGSC# 4474) by replacement of the genomic *dps* gene by a counter-selectable *cat-sacB* [26] and subsequent replacement with the *mCherry* gene and the *dps-mCherry* fusion cassette respectively.

The *dps::cat-sacB* strain was created using the protocol described by [26]. The *E. coli* strain W3110 including the plasmid pKD46 [27] was grown to mid-exponential phase in LB medium added with 50 µg/mL ampicillin at 30°C while shaking at 250 rpm, followed by induction of the Lambda red proteins with the addition of L-arabinose to 0.4% final concentration. The cells were incubated for 1 hour at 37°C while shaking. They were made electrocompetent by harvesting by centrifugation and resuspending in cold sterile water to concentrate them 1000 times. The counter-selectable *cat-sacB* fragment was amplified using PCR from the plasmid pKD3V [28] using primers incorporating 50-bp homology flanks for recombination corresponding to the regions flanking the *dps* gene in the *E. coli* chromosome. The following primers were used (underlined is the homologous region): forward: 5'-TACTTAATCTCGTTAATTACTGGGACATAACATCAAGAGGATATG AAATTTGTAGGCTGGAGCTGCTTCG-3' and reverse: 5'-AGGAAGCCGCTTTTATCGGGTACTAAAGTTCTGCACCATCAGCGATGGATCATATGAATATCCTCC TTAG-3'. The PCR product was digested with the DpnI enzyme, purified, and 400 ng of were introduced into *E. coli* W3110 cells expressing the Lambda proteins with electroporation. After 3 hours of recovery in LB medium at 37°C while shaking at 250 rpm, the cells were plated on LB agar containing 25 µg/mL chloramphenicol. The *dps* mutant strain was verified with colony PCR and sequencing. To remove the pKD46 plasmid, the newly created strain was grown overnight at 37°C.

For the *dps::mCherry* strain, the *mCherry* gene was amplified from the pROD22 plasmid [29] to introduce a 50-bp upstream and downstream sequence homologous to the chromosomal region regions flanking the *dps* gene. The following primers were used (underlined is the homologous region): forward 5'-TACTTAATCTCGTTAATTACTGGGACATAACATCAAGAGGATATGAAATTATGGCTATCATTAAAG AGTT -3', reverse 5'-AGGAAGCCGCTTTTATCGGGTACTAAAGTTCTGCACCATCAGCGATGGATTTACTTGTACAGCTCG TCCA -3'.

For the creation of the *dps-mCherry* fusion strain, the *dps-mCherry* fusion cassette was created using an adapted version of the Gibson DNA assembly protocol [30].

The backbone plasmid pBAD33 [31] was amplified using PCR to create compatible ends for recombination with the *dps-mCherry* fusion cassette. The following primers were used: forward 5'-GATCCCCGGGTACCGAGCTC -3', and reverse 5'- CAAGCTTGGCTGTTTTGGCG -3'. The *mCherry* gene was amplified using PCR from the plasmid pROD22 [29] to introduce a linker sequence immediately upstream of the *mCherry* gene and 20-bp homologous region with the plasmid pBAD33 in which the assembly sequence was going to be located. The following primers were used (double underlined is the linker, underlined is the homologous region): forward 5'- CGAGTCTAACATCGAAGCTGGCTCCGCTGCTGGTTCT -3', reverse 5'- TTCTCTCATCCGCCAAAACAGCCAAGCTTGTTACTTGTACAGCTCGTCC -3'. The *dps* gene was amplified from the pET17b-dps plasmid [26] to introduce a 30-bp upstream flanking sequence homologous to the plasmid pBAD33 and an homologous region with the linker-*mCherry* gene downstream. The following primers were used (underlined is the homologous region): forward 5'-
TAGCGAATTCGAGCTCGGTACCCGGGGATCATGAGTACCGCTAAATTAGT -3', and 5'-
CCAGCAGCGGAGCCAGCTTCGATGTTAGACTCGATAA -3'. After DpnI (New England Biolabs, (NEB)) digestion at 37°C for 1 hour and purification with Wizard® SV Gel and PCR Clean-Up System (Promega), the three fragments were assembled using Gibson DNA assembly. The assembly reaction was prepared combining 15 µL of Gibson assembly master mix (320 µL of 5X ISO buffer [0.5 M Tris-HCl (Sigma) pH 7.5, 50 mM $MgCl_2$, 4 mM dNTP (Invitrogen) mix (equal concentration of the four nucleotides), 50 mM DTT (Sigma), 25% w/v PEG-8000 (Sigma), 5 mM NAD (NEB)], 0.64 µL of 10 U/µL T5 exonuclease (Epicentre), 20 µL of 2 U/µL Fusion polymerase (Finnzymes), 160 µL of 40 U/µL Taq ligase (NEB), dH_2O to 1.2 ml), 100 ng of linearized vector backbone, and 100 ng of each assembly fragment in a total volume of 20 µL. The reaction was incubated at 50°C for 60 min. Electrocompetent *E. coli* W3110 cells were transformed with 5 µL of the assembly reaction via electroporation. The positive colonies carrying the chloramphenicol resistance gene from the pBAD33 plasmid were identified, and the accuracy of the sequence was checked with sequencing analysis. The *dps-mCherry* fusion cassette was amplified from the pBAD33 plasmid to introduce a 50-bp upstream and downstream sequence homologous to the chromosomal region regions flanking the *dps* gene. The following primers were used (underlined is the homologous region): farward 5'-
TACTTAATCTCGTTAATTACTGGGACATAACATCAAGAGGATATGAAATTATGAGTACCGCTAAAT
TAG-3', and reverse 5'-
AGGAAGCCGCTTTTATCGGGTACTAAAGTTCTGCACCATCAGCGATGGATTTACTTGTACAGCTCG
TCCA-3'.

The *mCherry* and the *dps-mCherry* fusion PCR products were digested with DpnI (New England Biolabs NEB) at 37°C for 1 hour, purified with Wizard® SV Gel and PCR Clean-Up System (Promega) and introduced with electroporation into the *dps::cat-sacB* strain expressing the Lambda red proteins. The cells were grown for 3 hours in LB medium

at 37°C while shaking at 250 rpm to allow homologous recombination. The bacteria were then were plated on counterselective medium for *sacB*: NaCl-free LB 10% sucrose agar and incubated at 30°C overnight. The colonies that looked healthy were streaked on LB agar containing 25 µg/mL chloramphenicol. The screening of the colonies that did not survive on chloramphenicol was performed with colony PCR, and the replacement of the *dps* gene was confirmed by sequencing. The dps-mCherry fusion expression was confirmed with fluorescence-activated cell sorting (FACS) flow cytometry and fluorescence microscopy.

2.2.4 Fluorescence-activated cell sorting (FACS) flow cytometry

The fluorescence-activated cell sorting (FACS) flow cytometry technique was applied to detect the mCherry protein in different experimental conditions.

The presence of the fluorescent signal in the *dps-mCherry* fusion and the *dps::mCherry* strains was analyzed and compared with the *E. coli* K-12 strain W3110 (CGSC# 4474) signal. One colony of each strain was inoculated overnight into Hi-Def Azure medium supplemented with 0.2% glucose and grown overnight at 37°C. The overnight cultures were diluted 10 times in PBS (phosphate buffered saline) and analyzed using a BD FACScan® System (Becton Dickinson) equipped with DxP multi-color upgrades (Cytek). The parameters used were: forward scatter (FSC) 10X, side scatter (SSC) 413 PMT gain, and laser yellow 561/590-20 nm PMT gain 520. The data were collected using the FlowJo Collector's edition acquisition software (Cytek) and analyzed with Cyflogic software.

dps expression during bacterial culture growth was evaluated with flow cytometry to monitor mCherry production. One colony of the *dps::mCherry* strain was inoculated overnight at 37°C and then diluted 100 times Hi-Def Azure medium supplemented with 0.2% glucose to start the growth curve measurement. During the growth at 37°C in shaking flasks, 500 µL samples were collected and analyzed with FACS, using the same parameters described above. The cellular growth was evaluated by collecting 1 mL samples and measuring the $O.D._{600}$.

dps expression in the presence of 50 µM and 100 µM H_2O_2 was evaluated. One colony of the *dps-mCherry* strain (details about the strain construction are in chapter 3) was inoculated and grown overnight at 37°C. The overnight culture was diluted 100 times in Hi-Def Azure medium supplemented with 0.2% glucose and grown at 37°C with shaking. After about 2.5 hours of growth when the culture reached exponential phase ($O.D._{600}$ 0.4), it was divided into separate flasks each containing 20 mL culture, and H_2O_2 was added to a final concentration of 50 µM and 100 µM. During growth at 37°C while shaking, 500 µL samples were collected every 15 minutes for 75 minutes and analyzed with FACS, using the same parameters described above. The cellular growth was evaluated by collecting 1 mL samples every 15 min during cellular growth and measuring the $O.D._{600}$.

2.2.5 Fluorescence microscopy

The presence of the mCherry fluorescence signal in the constructed strains was confirmed with fluorescence microscopy. One colony each of the *dps::mCherry*, the *dps-mCherry* fusion and *E. coli* K-12 wild-type W3110 strains was inoculated and grown overnight at 37°C in Hi-Def Azure medium supplemented with 0.2% glucose. 5 µL were placed onto a glass slide and covered with a coverglass. The cells were visualized with an inverted microscope (Olympus IX81), equipped with an AMH-200 lamp (Andor), and a Cy3 filter cube (4040C). Images were acquired with a Luca R EMCCD camera (Andor). Andor iQ software was used to control the microscope. Brightfield images and fluorescence images were acquired.

2.2.6 Fluorimetry

Fluorimetry was applied to detect mCherry fluorescence signal both during optimal cellular growth and in the presence of H_2O_2.

For detection during cell growth, overnight cultures of the *dps::mCherry* strain and the *E. coli* K-12 wild-type W3110 strain were diluted 1:100 in Hi-Def Azure medium supplemented with 0.2% glucose and grown for about 2 hours at 37°C until early-exponential phase ($O.D._{600}$ 0.1- 0.2). 200 µL of the cultures were placed in triplicate into a 96-well plate. The cells were grown for 11 hours in a microplate reader Victor^2 1420 (Wallac) at 37°C with an orbital shaking amplitude of 5 mm. $O.D._{600}$ measurements and fluorescence emission measurements (excitation/emission filters at 550/642 nm) were performed every 7 minutes.

dps expression was evaluated in the presence of 1 mM H_2O_2. An overnight culture of the *E. coli* K-12 wild-type W3110 and *dps::mCherry* strain were diluted 1:100 in Hi-Def Azure medium supplemented with 0.2% glucose. The cultures were grown at 37°C while shaking for about 2.5 hours until early exponential phase ($O.D._{600}$ 0.3-0.4), then H_2O_2 was added to the final concentrations of 1 mM H_2O_2. 200 µL of the cultures were placed in three wells of a 96-well plate. The cells were grown for 11 hours in a microplate reader Victor^2 1420 (Wallac) at 37°C with an orbital shaking amplitude of 5 mm. The $O.D._{600}$ measurements and the fluorescence (excitation/emission filters at 550/642 nm) were performed every 7 minutes.

2.2.7 Single-cell fluorescence detection using a CellASIC microfluidics device

The fluorescence signal in single cells in the presence and in the absence of H_2O_2 was analyzed using the CellASIC® ONIX Microfluidic System (Millipore) in combination with CellASIC® ONIX B04A-02 and B04A-03 (Millipore) microfluidic bacterial plates. To control the microfluidic experiment plates, the CellASIC® ONIX FG Software (Millipore) was used. One colony of the *dps::mCherry* strain was inoculated into Hi-Def Azure medium supplemented with 0.2% glucose and grown overnight at 37°C. The preculture was diluted 1:100 and grown for around 2 hours at 37°C until early exponential phase ($O.D._{600}$ 0.2-0.3). The culture was diluted into Hi-Def Azure medium supplemented with 0.2% glucose to $O.D._{600}$= 0.001 for an optimal bacterial concentration for the single-cell detection. The media and the cells were loaded into the microfluidic plates according to the manufacturer's protocol. In the growing chamber, the bacterial cells were trapped by an elastic ceiling according to their size (0.7 µm height for *E. coli* cells). The cells were held against the bottom glass surface to maintain a single focal plane during the perfusion-based experiment. The microfluidic system allowed us to perform long-term continuous perfusion experiments and solution-exchange experiments to expose the cells to the desired growth medium and stress conditions. For 30 min the cells were fed with Hi-Def Azure medium without stress addition, then the medium was switched to supply 0.5 mM H_2O_2 in Hi-Def Azure medium supplemented with 0.2% glucose. Control experiments were performed with constant supply of medium without H_2O_2. Microcolonies were analyzed by time-lapse fluorescence microscopy using an inverted microscope (Olympus IX81) equipped with an AMH-200 lamp (Andor), and a Cy3 filter cube (4040C). Images were acquired with a Luca R EMCCD camera (Andor). Andor iQ software was used to control the microscope and to perform automatic imaging acquisition. Experiments were performed at 37°C using an incubation chamber (H201-T, Okolab) to allow precise temperature control. Brightfield images (50 ms exposure time) and fluorescence images (50 ms exposure time, 20 EM gain) were recorded every 5 min.

2.3 Results

2.3.1 Hi-Def Azure medium is the optimal medium for detection of *dps* expression

To identify the appropriate growth medium to perform stress response experiments, the growth of the *E. coli* wild-type W3110 strain was analyzed in different

growth environments. Three different media were tested: M9 minimal medium, LB complex medium and Hi-Def Azure defined medium supplemented with 0.2% glucose. An overnight culture was diluted 1:100 in the different media, and the growth was monitored over time for several hours with a spectrophotometer. In M9, the growth was very slow, and after several hours, the culture did not proceed past the mid-exponential phase (Fig. 1 A). In the LB (Fig. 2 A) and Hi-Def Azure (Fig. 3 A) media, the bacteria showed an optimal growth. There was constant cell proliferation and the cultures were able to reach late-exponential phase. The variability observed between different colonies was very low. In parallel with cell growth, the *dps* expression was detected with Western blotting. The cells in M9 medium showed a higher *dps* expression, compared to the expression in the other two media, at the start of the experiment, with a slight decrease of the protein concentration over time (Fig. 2.1 B). The Dps concentration in the cultures grown in LB and Hi-Def Azure media showed different features. The trend of the expression in LB showed an overall decrease over time, but the variability observed was very high comparing the different replicates (Fig.2.2 B). The *dps* expression in the Hi-Def Azure medium increased constantly over time and the variability observed between the cultures was low (Fig. 2.3 B). The Hi-Def Azure medium showed the best performance in term of both robust growth and *dps* expression. The low variability of growth and protein expression among the replicates and the increasing concentration of Dps over time made the Hi-Def Azure the most suitable medium for our investigations.

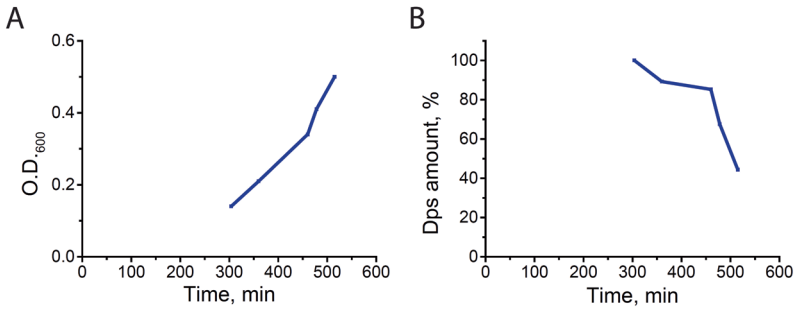

Fig. 2.1. Growth curve and Dps expression analysis of *E. coli* K-12 wild-type strain W3110 grown in M9 medium. A) Example of a growth curve. After several hours of slow growth the culture did not proceeding past the mid-exponential phase. B) Example of a Western blotting analysis of the Dps protein during growth. High Dps amount is observed at the start of the sampling with a slight decrease of the concentration over time.

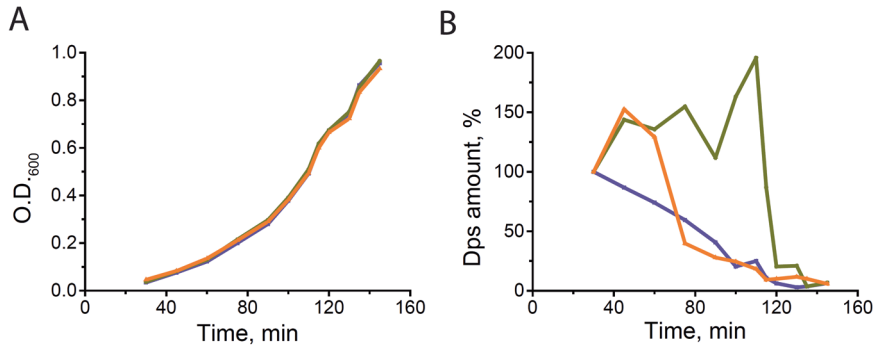

Fig. 2.2. Growth curves and Dps expression analysis of *E. coli* K-12 wild-type strain W3110 grown in LB medium. A) The three curves showed an optimal growth, with constant cell proliferation reaching the late-exponential phase. Low variability among the replicates was observed. B) The three Western blotting analysis of the Dps protein during growth showed an overall decrease over time. High variability was observed comparing the different replicates.

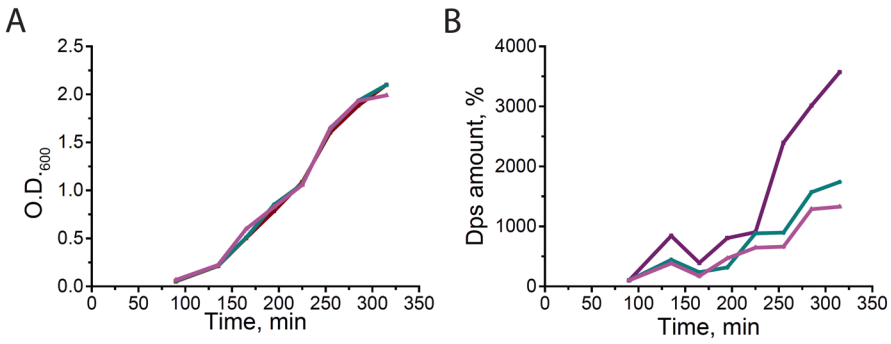

Fig. 2.3. Growth curves and Dps expression analysis of *E. coli* K-12 wild-type strain W3110 grown in Hi-Def Azure defined medium supplemented with 0.2% glucose. A) The three curves showed an optimal growth, with constant cell proliferation reaching the late-exponential phase. Low variability among the replicates was observed. B) The three Western blotting analysis of the Dps protein during growth showed an overall increase over time. Low variability was observed comparing the different replicates.

2.3.2 Construction of two reporter strains for *dps* transcription analysis

To investigate the *dps* transcriptional response, we constructed two reporter strains of *E. coli* with the *mCherry* gene as a reporter for *dps* transcription. The two strains were named "*dps::mCherry*" and "*dps-mCherry* fusion." To construct the *dps::mCherry* strain, the *dps* gene was replaced in the chromosome with the *mCherry* gene (Fig. 2.4 A). The fluorescent reporter gene was transcribed under the control of the *dps* promoter, and no copy of the *dps* gene was present in this strain. The *dps-mCherry* fusion strain carried a chimeric version of the *dps* gene, with a C-terminal fusion of the *mCherry* gene (Fig. 2.4 B). The *dps-mCherry* construct replaced the wild-type *dps* gene in the chromosome and was then under the control of the *dps* promoter. Both these constructs aimed to permit the detection of the *dps* promoter activity in single cells through the fluorescence emitted by the fluorescent reporter protein.

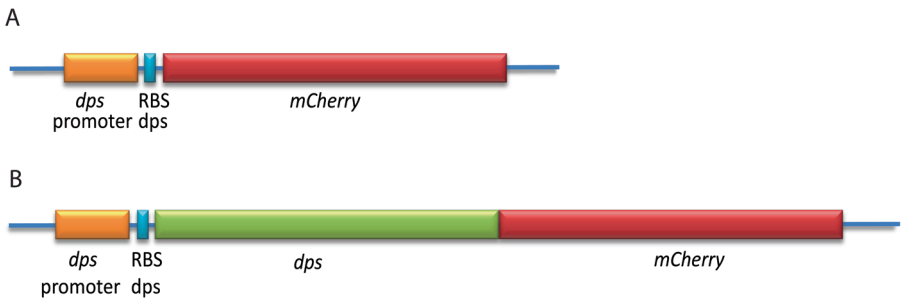

Fig. 2.4. Schematic representation of the *dps* operon present in the *dps::mCherry* (A) and *dps-mCherry* fusion (B) strains. A) In the *dps::mCherry* strain *dps* gene was replaced in the chromosome with the *mCherry* gene, under the control of the *dps* promoter. No copy of the *dps* gene was present in this strain. B) In the *dps-mCherry* fusion strain the wild-type *dps* gene in the chromosome was replaced with a chimeric version of the *dps* gene, containing a C-terminal fusion of the *mCherry* gene. The *dps-mCherry* fusion cassette was under the control of the *dps* promoter.

In order to assay the expression of the mCherry fluorescent protein, the constructed strains were analysed with flow cytometry. Overnight cultures of the *dps::mCherry* (Fig. 2.5) and the *dps-mCherry* fusion (Fig. 2.6) strains were compared with an overnight culture of the *E. coli* wild-type strain W3110 using FACS flow cytometry. Both the engineered strains showed a distinct increase in the in the emission fluorescent signal of an order of magnitude higher that the wild-type strain, indicating the expression of the mCherry protein. In addition, the presence of the mCherry signal was verified with fluorescence microscopy. Overnight cultures of the *dps::mCherry*, the *dps-mCherry* fusion and *E. coli* W3110 wild-type were analyzed using an inverted microscope equipped with a Cy3 filter cube. Both strains exhibited a distinct fluorescence signal over the background (Fig. 2.7 D, F), whereas the fluorescence signal of the W3110 wild-type strain was not detectable (Fig. 2.7 B). The *dps::mCherry* strain showed a homogeneous distribution of the fluorescence over the entire volume of the cells (Fig. 2.7 D). The *dps-mCherry* fusion strain showed a distribution of the fluorescence over the cell volume, with some puncta of more intense fluorescence clearly visible (Fig.2.7 F). The *dps-mCherry* fusion strain was considered not suitable for the *dps* expression detection because of the heterogeneous fluorescence distribution over the cell volume, maybe due to protein aggregation.

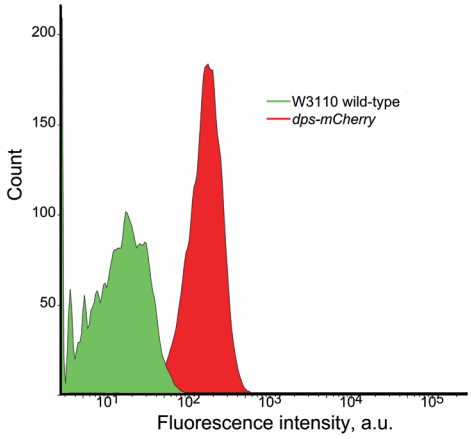

Fig. 2.5. Verification of the mCherry expression in the *dps::mCherry* strain using Fluorescence-activated cell sorting (FACS) flow cytometry. The histograms showed that the emission fluorescent signal of the engineered strain was an order of magnitude higher than the wild-type strain, confirming the expression of the mCherry.

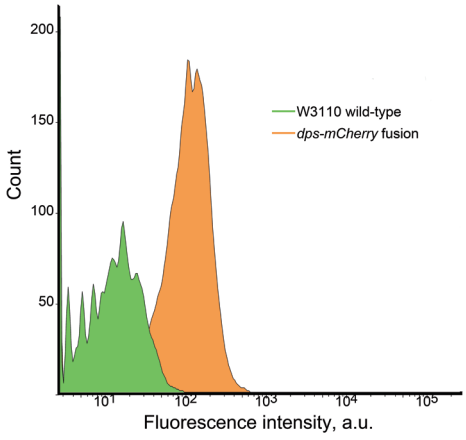

Fig. 2.6. Verification of the mCherry expression in the *dps-mCherry* fusion strain using Fluorescence-activated cell sorting (FACS) flow cytometry. The histograms showed that the emission fluorescent signal of the engineered strain was an order of magnitude higher than the wild-type strain, confirming the expression of the mCherry.

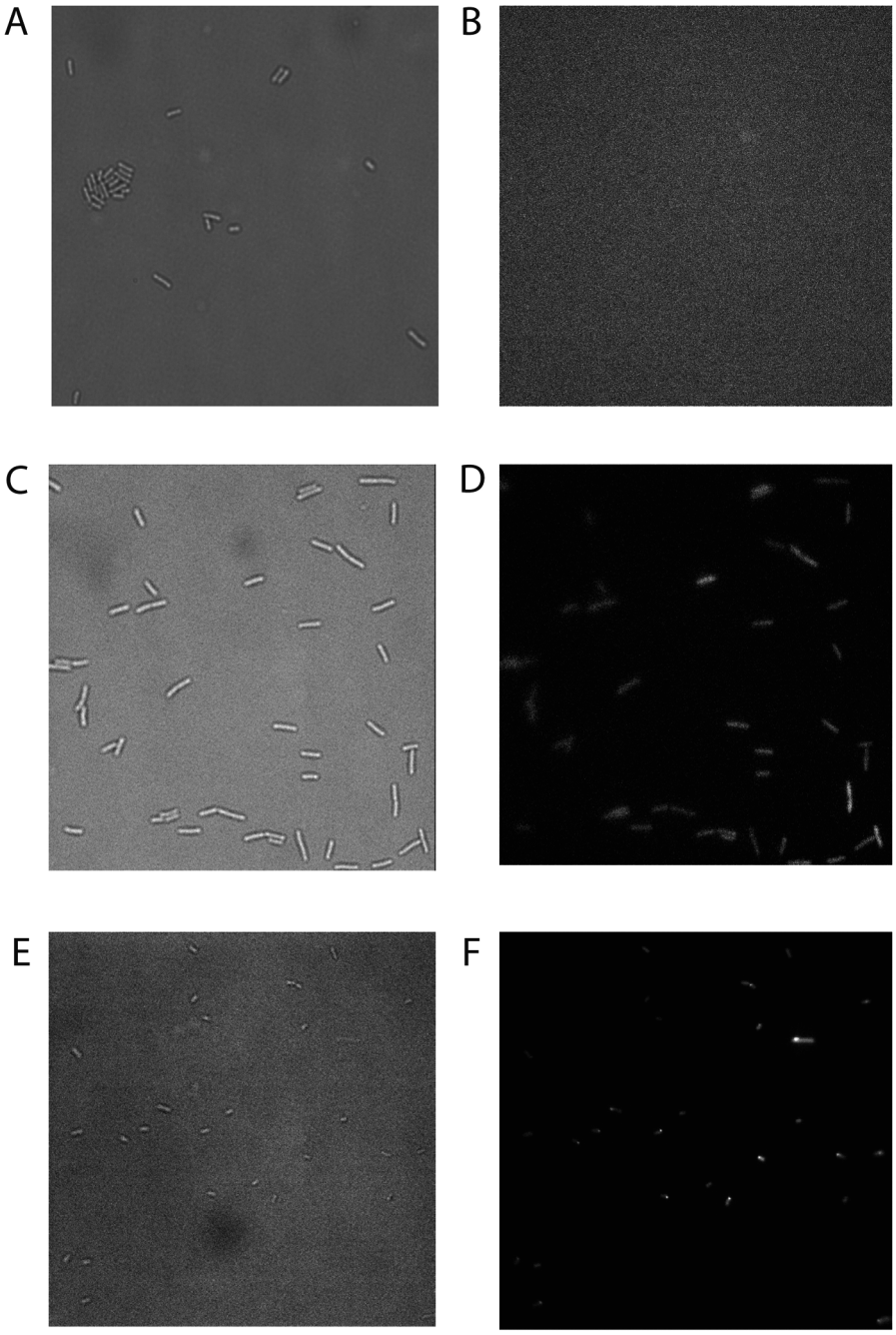

Fig. 2.7. Verification of the mCherry expression in the *E. coli* K-12 wild-type strain W3110, *dps::mCherry* and *dps-mCherry* fusion strains with fluorescence microscopy

Fig. 2.7. Verification of the mCherry expression in the *E. coli* K-12 wild-type strain W3110 (B), *dps::mCherry* (D) and *dps-mCherry* fusion (F) strains with fluorescence microscopy. A-B) The fluorescence signal of the wild-type strain is not detectable over the background (B). Brightfield image is shown in panel A. C-D) The *dps::mCherry* strain showed a homogeneous distribution of the fluorescence over the entire volume of the cells (C). Brightfield image is shown in panel D. E-F) The *dps-mCherry* fusion strain showed a non-homogeneous distribution of the fluorescence, with some puncta of more intense fluorescence (E). Brightfield image is shown in panel F.

2.3.3 *dps* expression detection

Fluorimetry and flow cytometry techniques were used to identify the optimal method of *dps* expression detection during non-stressed growth conditions. These techniques relied on the detection of the mCherry fluorescent signal. Cultures of the *E. coli* wild-type strain W3110 (Fig. 2.8 A) and the *dps::mCherry* (Fig. 2.8 C) strain were grown at 37°C while shaking in microtiter plates, and the growth and the fluorescence signal was recorded using a plate reader. Both cultures showed a healthy and constant growth reaching the stationary phase, indicating that the constructed strain was not suffering from Dps depletion or other detrimental mutations in an optimal growth environment. For both strains the fluorescence signal was not detectable over the background signal of the growth medium, and no differences in intensity were observed between the wild-type and the *dps::mCherry* strains (Fig. 2.8 B, D). The sensitivity of this method was not sufficient to detect the fluorescence signal despite the expected *dps* expression increase over time.

In order to detect the fluorescence signal from the constructed strain, flow cytometry technique was applied. An overnight culture of the *dps::mCherry* strain was diluted 100 times and the FACS profile of fluorescence was analyzed during growth at 37°C while shaking. Samples were collected at specific time points to measure the growth and the fluorescence. The culture showed an increase in mCherry fluorescent signal over time during exponential phase (Fig. 2.9 A), in parallel with constant growth (Fig 2.9 B). The strongest-intensity fluorescence signal was detected when the culture reached the stationary phase ($O.D._{600}$ 1.9). No increase in fluorescence signal was observed during the mid-exponential phase of growth, between $O.D._{600}$ 0.53 and 0.9. This detection method therefore allowed the identification of the general trend in *dps* expression during growth in our experimental conditions. However, it was not sensitive enough to detect the full dynamics of *dps* induction during the mid-exponential growth phase.

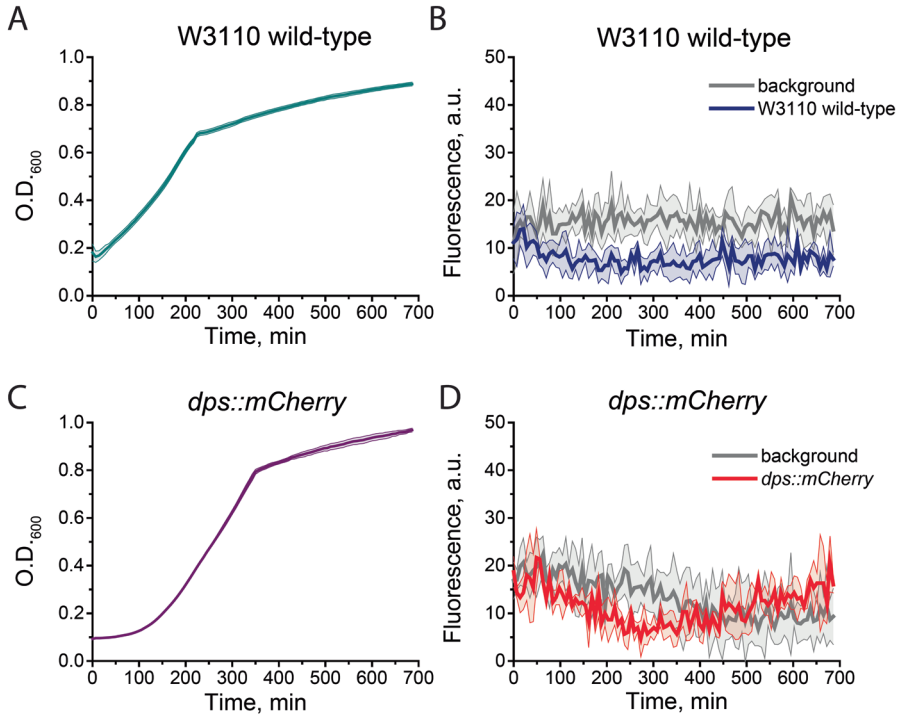

Fig. 2.8. Growth curves and Dps expression detection during non-stressed growth conditions using fluorimetry in the E. coli K-12 wild-type W3110 and dps::mCherry strains. A, C) The growth curves of the wild-type (A) and the dps::mCherry (C) strains were recorded using a plate reader. Both cultures showed a healthy and constant growth reaching the stationary phase. The shaded areas represent the standard deviation. B, D) The fluorescence signal of the wild-type (B) and the dps::mCherry (D) strains was not detectable over the background (represented by the growth medium), and no differences in intensity were observed between the two strains.

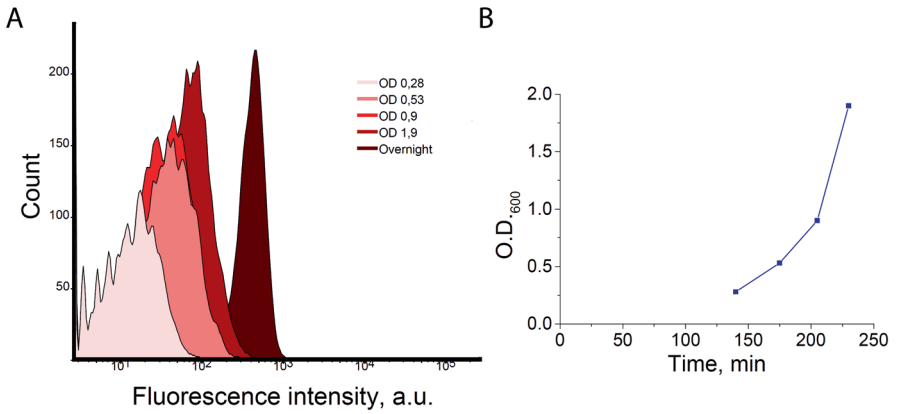

Fig. 2.9. *dps* expression in the *dps::mCherry* strain evaluated with flow cytometry to monitor the mCherry production during the bacterial culture growth. A) Histograms of the mCherry fluorescent signal. An increase in intensity signal over time is observed. No increase in fluorescence signal was observed during the mid-exponential phase of growth, between $O.D._{600}$ 0.53 and 0.9. The strongest intensity signal was detected when the culture reached the stationary phase ($O.D._{600}$ 1.9). B) The correspondent growth curve show a constant cellular growth over time.

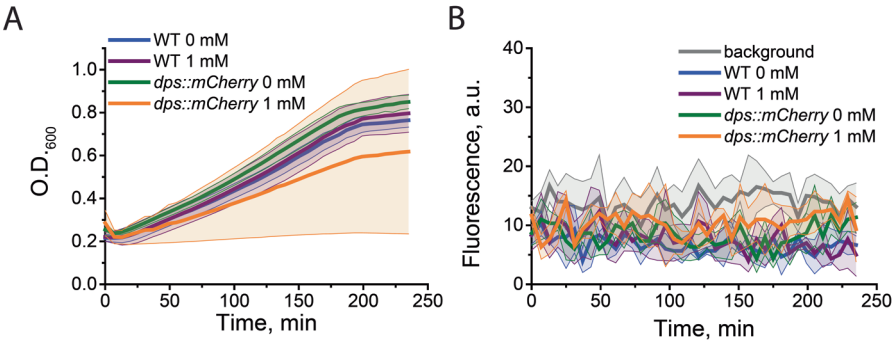

Fig. 2.10. Growth curves and *dps* expression in *E. coli* K-12 wild-type W3110 and *dps::mCherry* strains in the presence of oxidative stress investigated with fluorimetry. A) Growth curves of the two strains exposed to 0 mM and 1 mM H_2O_2. In the absence of H_2O_2, they showed robust exponential-phase growth kinetics and final optical densities. In the presence of the stressor, the engineered strain showed a stronger delay in growth and higher variability compared to the wild-type. The shaded areas represent the standard deviation. B) mCherry fluorescence signal of the two strains exposed to 0 mM and 1 mM H_2O_2. No increase in the fluorescence signal was observed for *dps::mCherry* strain when exposed to H_2O_2, compared to the background (growth medium) and the wild-type strain. The shaded areas represent the standard deviation.

2.3.4 *dps* expression during oxidative stress

The expression pattern of the *dps* gene was investigated in the presence of oxidative stress. Exponentially growing cultures of *E. coli* wild-type W3110 and *dps::mCherry* strains were exposed to 1 mM H_2O_2 and analyzed with fluorimetry (Fig. 2.10). Both the strains showed a similar growth response. In the absence of stressor, they showed similar robust exponential-phase growth kinetics and final optical densities. In the presence of H_2O_2, the *dps::mCherry* strain showed a stronger delay in growth compared to the wild-type (Fig. 2.10 A). Thus, the engineered strain exhibits higher sensitivity to oxidative stress. Moreover, a higher variability was observed in the growth of the constructed strain. No increase in the fluorescence signal was observed for *dps::mCherry* strain when exposed to H_2O_2 (Fig. 2.10 B), indicating that the sensitivity of this method was not sufficient to detect the fluorescence signal of *dps* expression in our experimental conditions.

Experiments were performed to test whether the expression of Dps protein in the presence of 50 µM and 100 µM H_2O_2 could be detected using flow cytometry (Fig. 2.11). Exponentially growing cultures of the *dps-mCherry* strain were exposed to the stressors. Samples were collected every 15 min and analysed with FACS flow cytometry. No difference in the fluorescence signal was observed comparing the bacteria not exposed to stressor and the cells in the presence of 50 µM and 100 µM H_2O_2 during the entire duration of the experiment. Increasing concentration of H_2O_2 did not lead to a distinct and detectable increase of the signal (Fig. 2.11 B-F). As well as fluorimetry, this technique showed limitations in the detection of the mCherry fluorescence signal in our experimental conditions.

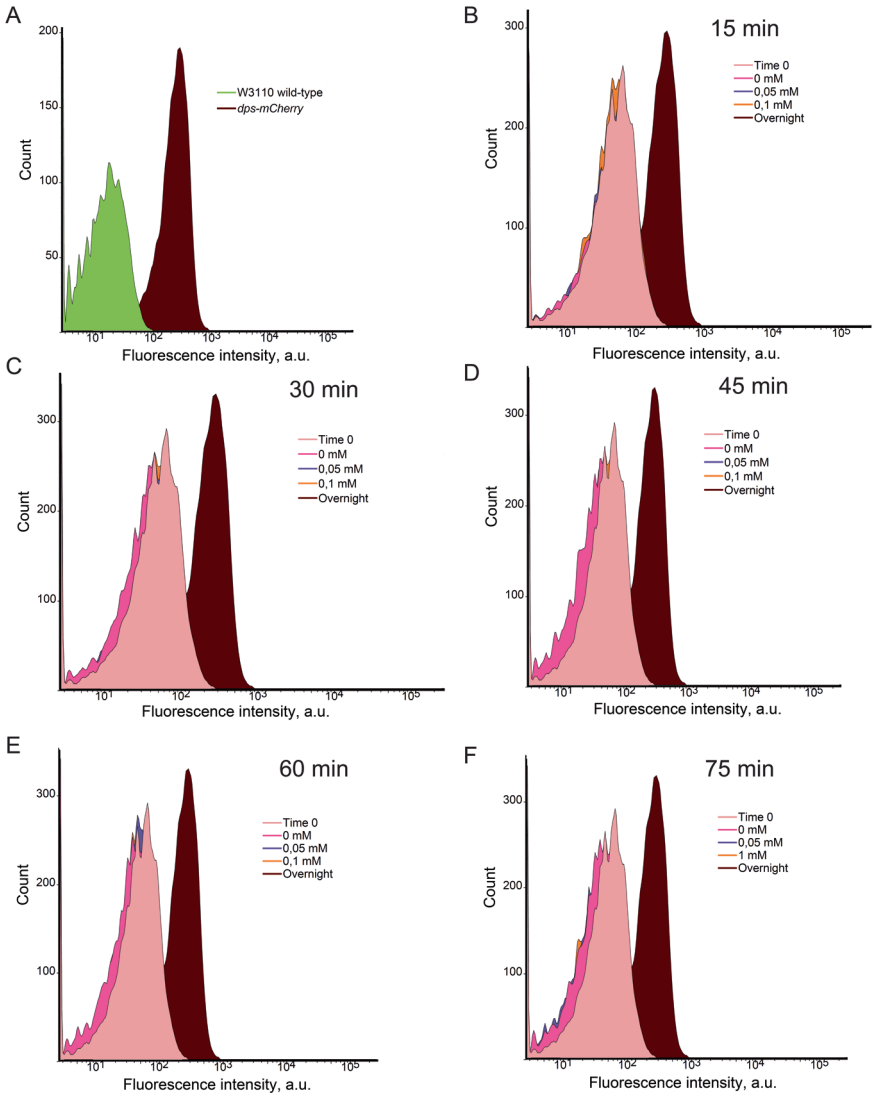

Fig. 2.11. *dps* expression in the *dps-mCherry* strain investigated in the presence of oxidative stress with Fluorescence-activated cell sorting (FACS) flow cytometry. A) The histograms showed that the emission fluorescent signal of the engineered strain *dps-mCherry* strain was an order of magnitude higher than the *E. coli* K-12 wild-type W3110 strain. B-F) The histograms showed that no difference in the emission fluorescent signal was observed comparing the cells expose 0 µM, 50 µM and 100 µM H_2O_2 during the entire duration of the experiment. Increasing concentration of H_2O_2 did not lead to and detectable increase of the signal.

2.3.5 Single-cell analysis of *dps* expression

In order to test a new detection method for the detection of *dps* promoter activity in each individual cell over time, a culture of the *dps::mCherry* strain was exposed to 0 mM or 0.5 mM H_2O_2 and analyzed using the CellASIC® ONIX microfluidic device. The bacterial cells were grown in defined medium to early exponential phase, then transferred to the microfluidic bacterial plate to apply the oxidative stressor. Cells were pressure-loaded into the plate and physically trapped by the elastic ceiling. Individual cells were selected for imaging, which would grow and divide over time to give rise to a microcolony. A difference in growth and fluorescence was observed in cells not exposed to H_2O_2 compared to those in the presence of the stressor. In the colony without applied stress, the growth was fast and vigorous, with the cells filling the growth chamber completely within 4 hours. The fluorescence of each cell remained low during the entire duration of the measurement, with a slight increase towards the end of the measurement (Fig. 2.12 A). In the presence of H_2O_2, we detected a different behavior in growth and fluorescent protein expression, compared to the no-stress condition. In the presence of both 0.5 mM (Fig. 2.12 B) and 1 mM H_2O_2 (Fig. 2.12 C), we observed a decrease in growth speed proportional to the concentration of applied stressor. The slower growth coincided with an increased mCherry expression when the cells experienced oxidative stress. Despite the big potential, the device used in these experiments showed some defective traits. The cells were not being trapped properly, and during the perfusion experiments, they were moving from their original position, not allowing an optimal cell tracking (Fig. 2.12 A-C). The defective trapping also disturbed the colony development because of the free cells carried by the medium flow. A faulty cell loading was observed as a consequence of defective structures in the microchambers. Due to these defects, the CellASIC® ONIX microfluidic device was not further utilized for the single-cell experiments.

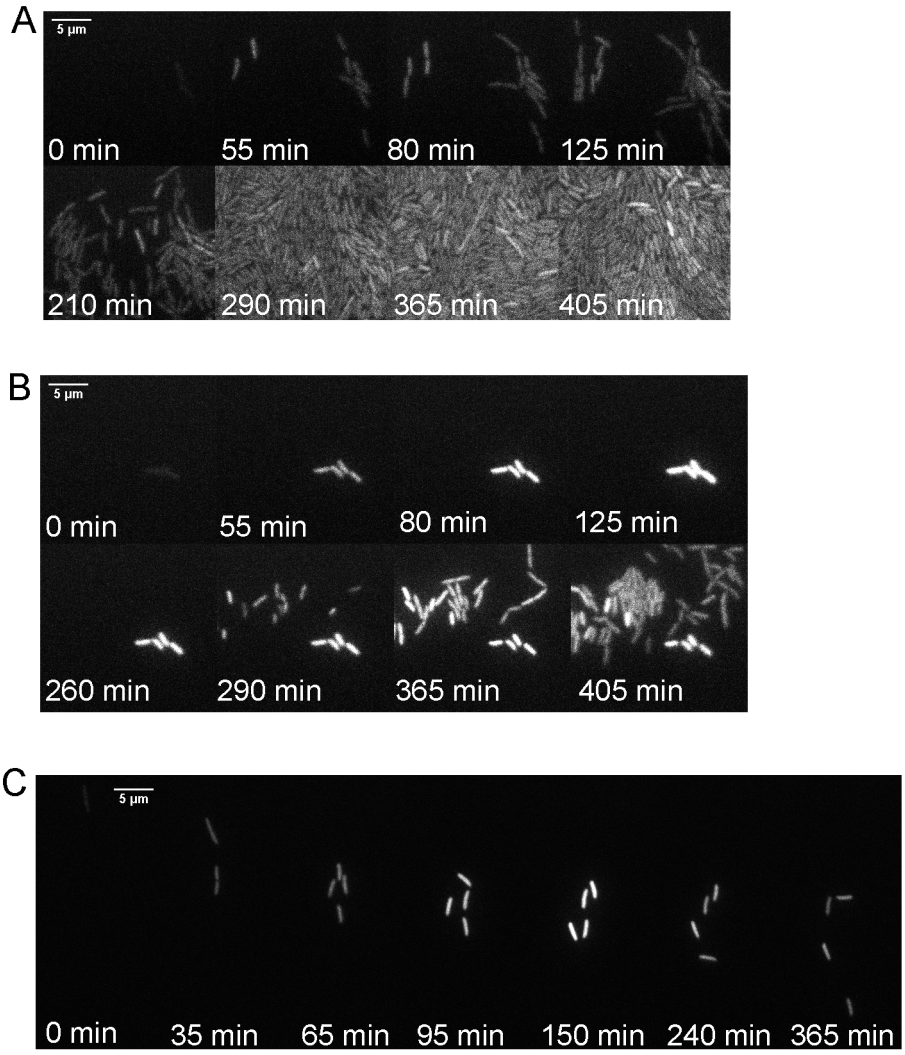

Fig. 2.12. Time-lapse fluorescence of *dps::mCherry* microcolonies exposed to 0 mM (A), 0.5 mM (B) and 1 mM (C) H_2O_2 using CellASIC® ONIX microfluidic device. A) Cells not exposed to the stressor showed a robust growth and a low fluorescence signal during the entire duration of the measurement, with a slight increase towards the end. B-C) In the presence of both concentrations of the H_2O_2 we observed a decrease in growth speed proportional to the concentration of the stressor and an increased mCherry expression. The defect in the device microfluidic structure led to a non-proper cell trapping with consequent movement of the cells during imaging (A-C).

2.4 Discussion

In this chapter, we investigated the detection of *dps* expression in different growth conditions and by applying different techniques. The cell growth in the defined Hi-Def Azure medium showed the best performance both in cell growth and in *dps* expression. The *dps::mCherry* strain proved the most suitable for the microscopy analysis because of the homogeneous distribution of the florescence over the cell surface, compared to the *dps-mCherry* fusion strain that showed more concentrated fluorescence regions in the cells. The fluorimetry and the flow cytometry detection techniques were not suitable to detect mCherry fluorescence in the presence and absence of oxidative stress. The single-cell detection of *dps* expression was possible using the microfluidic device CellASIC, but due to the fabrication defects of the bacterial plates, its use was suspended.

The minimal M9, the complex LB and the defined Hi-Def Azure media have different characteristics and effects on bacterial growth. It was necessary to identify the optimal medium that provided a stable cellular growth, a reproducible detection of Dps protein and that was suitable for fluorescent measurements. The M9 minimal medium contains the minimum nutrients possible for colony growth, salts and a carbon source. The colonies grown in this medium showed a longer lag phase, and a slower growth compared to the complex and defined media (Fig. 2.1 A, 2.2 A, 2.3 A). We excluded this medium from the experimental setup because of its unsuitability to support substantial bacterial growth, with possible consequences on the metabolism and stress reactions.

When Western blotting analysis was performed on growing cultures of the wild-type strain, a different of *dps* expression profile was observed (Fig. 2.1 B, 2.2 B, 2.3 B). In both M9 and LB media, the residual stress from the overnight culture seemed to be high. The amount of protein present at the beginning of the measurement decreased over time, showing that the recovery from the overnight stress was slower in the minimal than in the complex media. During the long-term growth, such as overnight, bacterial cultures reach the stationary phase with consequent Dps production, until it becomes the most abundant DNA-binding protein [32]. The dilution brought the culture to the beginning of the exponential phase with a subsequent reduction of nutritional stress. M9 and LB media did not allow a rapid recovery from the starvation stress of the overnight growth. In contrast, bacteria grown in the defined Hi-Def Azure medium showed a reversed pattern of *dps* expression. The amount of protein present at the beginning of growth was very low and increased steadily during the culture development. In this medium, the cells recovered faster from the overnight starvation with a faster activation of the Dps downregulatory mechanism. It is important to notice that the time scale of the growth measurements in LB and Hi-Def Azure media were different: 30 to 145 min from the inoculation for LB and 90 to 315 min from inoculation for Hi-Def Azure. The behavior of protein expression in the culture outside the measurements was not known. It might be possible that after the

initial slower stress recovery in LB, the process speeded up as the growth proceeded, reaching similar protein levels to those observed in Hi-Def Azure medium. However, the variability of the protein expression observed in LB medium was higher compared to the Hi-Def Azure medium. Thus, further experiments were performed with the defined medium for more reproducible results.

The *dps::mCherry* and the *dps-mCherry* fusion strains were investigated for their suitability as tools for Dps protein expression detection. The characteristics of the two strains were quite different. The *dps-mCherry fusion* strain was constructed to include the copy of the *dps* gene in the chromosome, whereas the *dps::mCherry* strain was a *dps* knockout strain. The chimeric protein Dps-mCherry seemed the most convenient instrument to analyze the *dps* expression because of the possibility to detect the protein turnover. However, cells expressing the protein showed a non-homogeneous distribution of the fluorescence throughout the cell volume (Fig. 2.7 F). This phenomenon indicated an aggregation of proteins, perhaps due to undesired mCherry-mCherry or Dps-mCherry interaction. Previous work has similarly shown that fusion of Dps with GFP protein led to an aggregation in the cells [33] with a result similar to the one observed in *dps-mCherry* fusion strain. This result can perhaps be explained by consideration of the dodecameric structure of Dps, with hollow cavity in the middle that provides iron storage [34]. Dps monomers have a weight of around 17 KDa [35] and mCherry of about 26 KDa [10]. A loss in activity of the Dps-mCherry chimeric protein, composed of 12 Dps monomers and 12 mCherry proteins, was possible because of the potential interference of the mCherry monomers in the DNA binding and iron storage. It was shown, in fact, that fluorescent protein tags could interfere with the regular protein activity causing clustering artifacts and resulting in an inaccurate protein localization. The cell location of ClpP and ClpX proteins tagged with several fluorescent protein, including mCherry, was not identical to the position identified with immunofluorescence [36]. The use of *dps-mCherry* fusion strain for our investigation could bring similar consequences and lead to a misleading fluorescence measurement. The aggregation of fluorescent molecules could in fact show an over- or lower-estimate of the concentration of fluorescence in the cells.

We decided to further continue our investigation with the *dps* knockout strain. The added H_2O_2 slowed the growth of this strain indicating a higher sensitivity of the strain to the oxidative stress compared to the wild-type (Fig. 2.10). The *dps::mCherry* strain did not contain the *dps* gene in the chromosome and it was previously shown that bacterial cells lacking the *dps* gene were more sensitive to external stresses, such as extreme pH, metal exposure, and temperature shift [6]. To study the impact of only one stressor on *dps* expression, we needed to limit the amount of interfering factors that could alter the Dps stress response. The effect of the application of one stressor, in fact, could be overestimated because of the increased susceptibility of the *dps* knockout strain to environmental stresses. We decided not to continue the analysis with the *dps::mCherry*

strain and instead to construct a new strain, *dps-mCherry,* described in chapter 3. This strain contained copies of both the *dps* and *mCherry* genes in the chromosome, with *mCherry* located within the *dps* operon immediately downstream of *dps,* avoiding the deleterious effect of the *dps* depletion noticed in the *dps::mCherry* strain. The *dps-mCherry* strain allowed the detection of the *dps* transcription activation through the *mCherry* fluorescence. Although this strain did not allow the identification of protein turnover because it did not contain a fusion between the Dps and mCherry protein, it was a valid strain to analyze the effect of one stressor, without the interference of other external factors.

The detection of mCherry fluorescence was the key methodology to quantify *dps* expression. To find a suitable detection method, the *dps::mCherry* and the *dps-mCherry* bacterial cultures were analyzed both in bulk and at the single-cell level. Fluorimetry allowed a bulk analysis, detecting the fluorescence increase during cellular growth caused by nutritional limitation (Fig. 2.9 A). It had previously been shown that, in normal growth conditions, the amount of Dps protein increases overtime [32]. However, we were interested to examine the *dps* expression in the presence of a stressor. The fluorimetry analysis did not allow the detection of the mCherry fluorescence increase when the culture was exposed to H_2O_2 (Fig. 2.11). Among modern fluorophores, the brightness of the mCherry protein is relatively low, 27% that of DsRed and 50% that of EGFP [10]. The sensitivity of the plate reader was not sufficient to detect any signal from the fluorescent protein, even when the colony reached the stationary phase with consequent high amount of Dps in the cells. Moreover, the results obtained from this type of analysis provided only an averaged indication of the *dps* expression among the different cells in the colony. Instead, flow cytometry analysis allowed single cell measurement with the possibility of identification of the expression in each individual bacteria. The sensitivity of the flow cytometer was higher than the sensitivity of fluorimetry. We could in fact detect the mCherry signal increase during exponential growth (Fig. 2.9). This detection was not possible with the plate reader (Fig. 2.8). However, the sensitivity was not sufficient to detect the increase of the low-brightness mCherry fluorescence signal during early and mid- exponential growth. A high signal was seen during stationary phase, where the protein reached high concentration in the cells. This technique was not sufficient to detect the difference in protein production during oxidative stress, despite the long exposure to H_2O_2.

The most suitable method for the *dps* promoter activity analysis was fluorescence microscopy. This approach was therefore chosen for the further experiments. It was possible, in fact to detect low fluorescence intensity values in cells grown in optimal conditions, as well as higher intensity values when cells were exposed to H_2O_2 (Fig. 2.12). The monolayer growth in the CellASIC® bacterial plates resulted in the most adequate technique for single-cell analysis. It was possible to follow the colony development and to

track the cell lineages, identifying the mother-to-daughter protein distribution, overcoming the averaging result of the bulk analysis. However, shortly after the introduction of the microfluidic plates, a defect in fabrication was announced by the producing company. The cell loading and trapping were not performed properly due to defects in the fabrication process. This issue was an insurmountable obstacle to use of the device. The impossibility of cell trapping did not allow regular colony growth because of the constant flow of cells in and out the colony boundaries. Single cell tracking over time was not possible, and consequently we needed to exclude this microfluidic device. Another technique was then applied to proceed with single-cell analysis of the Dps stress response. The use of agarose pads containing different concentrations of H_2O_2 is described in chapter 3.

In conclusion, we were able to identify the optimal growth conditions and technique to study *dps* promoter activity. The Hi-Def Azure medium resulted in the optimal medium for cellular growth, to study the *dps* expression detection in the presence and absence of stressor and for microscopy analysis. The *dps-mCherry* fusion strain was discovered to be unsuitable because of the aggregation of the fluorescent proteins inside the cells. The *dps::mCherry* strain was also discarded because of its sensitivity to external stresses. The *dps-mCherry* strain, described in chapter 3, resulted in the most suitable strain. Fluorescence microscopy combined with single-cell analysis was the selected technique to identify *dps* expression dynamics.

2.5 References

1. Kenneth, T. *Online textbook of bacteriology*. Available from: www.textbookofbacteriology.net.
2. Ron, E., *Bacterial Stress Response*, in *The Prokaryotes*, E. Rosenberg, et al., Editors. 2013, Springer Berlin Heidelberg. p. 589-603.
3. Battesti, A., N. Majdalani, and S. Gottesman, *The RpoS-mediated general stress response in Escherichia coli.* Annu Rev Microbiol, 2011. **65**: p. 189-213.
4. Altuvia, S., et al., *The dps promoter is activated by OxyR during growth and by IHF and sigma S in stationary phase.* Mol Microbiol, 1994. **13**(2): p. 265-72.
5. Grainger, D.C., et al., *Selective repression by Fis and H-NS at the Escherichia coli dps promoter.* Mol Microbiol, 2008. **68**(6): p. 1366-77.
6. Nair, S. and S.E. Finkel, *Dps protects cells against multiple stresses during stationary phase.* Journal of Bacteriology, 2004. **186**(13): p. 4192-4198.
7. Comeau, J.W., S. Costantino, and P.W. Wiseman, *A guide to accurate fluorescence microscopy colocalization measurements.* Biophys J, 2006. **91**(12): p. 4611-22.
8. Saffarian, S., et al., *Oligomerization of the EGF receptor investigated by live cell fluorescence intensity distribution analysis.* Biophys J, 2007. **93**(3): p. 1021-31.
9. Shaner, N.C., G.H. Patterson, and M.W. Davidson, *Advances in fluorescent protein technology.* J Cell Sci, 2007. **120**(Pt 24): p. 4247-60.
10. Shaner, N.C., et al., *Improved monomeric red, orange and yellow fluorescent proteins derived from Discosoma sp. red fluorescent protein.* Nat Biotechnol, 2004. **22**(12): p. 1567-72.
11. Carpentier, P., et al., *Structural basis for the phototoxicity of the fluorescent protein KillerRed.* FEBS Lett, 2009. **583**(17): p. 2839-42.
12. Dixit, R. and R. Cyr, *Cell damage and reactive oxygen species production induced by fluorescence microscopy: effect on mitosis and guidelines for non-invasive fluorescence microscopy.* Plant J, 2003. **36**(2): p. 280-90.
13. Jimenez-Banzo, A., et al., *Singlet oxygen photosensitization by EGFP and its chromophore HBDI.* Biophys J, 2008. **94**(1): p. 168-72.
14. Mueller, G., W. Waldeck, and K. Braun, *From green to red--To more dead? Autofluorescent proteins as photosensitizers.* J Photochem Photobiol B, 2010. **98**(1): p. 95-8.
15. Waldeck, W., et al., *ROS-mediated killing efficiency with visible light of bacteria carrying different red fluorochrome proteins.* J Photochem Photobiol B, 2012. **109**: p. 28-33.
16. Hall, B.G., et al., *Growth Rates Made Easy.* Molecular Biology and Evolution, 2014. **31**(1): p. 232-238.
17. Wong, S.S. and K. Truong, *Fluorescent protein-based methods for on-plate screening of gene insertion.* PLoS One, 2010. **5**(12): p. e14274.
18. Wojcik, M., et al., *High-Throughput Screening in Protein Engineering: Recent Advances and Future Perspectives.* Int J Mol Sci, 2015. **16**(10): p. 24918-45.
19. Kiviet, D.J., et al., *Stochasticity of metabolism and growth at the single-cell level.* Nature, 2014. **514**(7522): p. 376-9.

20. Moolman, M.C., et al., *Slow unloading leads to DNA-bound beta2-sliding clamp accumulation in live Escherichia coli cells.* Nat Commun, 2014. **5**: p. 5820.
21. Young, J.W., et al., *Measuring single-cell gene expression dynamics in bacteria using fluorescence time-lapse microscopy.* Nature Protocols, 2012. **7**(1): p. 80-88.
22. Choi, J.R., et al., *Microfluidic assay-based optical measurement techniques for cell analysis: A review of recent progress.* Biosens Bioelectron, 2015. **77**: p. 227-236.
23. Miller, J.H., *Experiments in molecular genetics.* Cold Spring Harbor Laboratory, Cold Spring Harbor, New York, 1972: p. 466.
24. Bertani, G., *Studies on lysogenesis. I. The mode of phage liberation by lysogenic Escherichia coli.* J Bacteriol, 1951. **62**(3): p. 293-300.
25. Neidhardt, F.C., P.L. Bloch, and D.F. Smith, *Culture medium for enterobacteria.* J Bacteriol, 1974. **119**(3): p. 736-47.
26. Karas, V.O., I. Westerlaken, and A.S. Meyer, *The DNA-Binding Protein from Starved Cells (Dps) Utilizes Dual Functions To Defend Cells against Multiple Stresses.* J Bacteriol, 2015. **197**(19): p. 3206-15.
27. Datsenko, K.A. and B.L. Wanner, *One-step inactivation of chromosomal genes in Escherichia coli K-12 using PCR products.* Proc Natl Acad Sci U S A, 2000. **97**(12): p. 6640-5.
28. Zhou, Q.M., et al., *A method for generating precise gene deletions and insertions in Escherichia coli.* World Journal of Microbiology & Biotechnology, 2010. **26**(7): p. 1323-1329.
29. Reyes-Lamothe, R., et al., *Independent positioning and action of Escherichia coli replisomes in live cells.* Cell, 2008. **133**(1): p. 90-102.
30. Gibson, D.G., et al., *Enzymatic assembly of DNA molecules up to several hundred kilobases.* Nature Methods, 2009. **6**(5): p. 343-U41.
31. Guzman, L.M., et al., *Tight regulation, modulation, and high-level expression by vectors containing the arabinose PBAD promoter.* J Bacteriol, 1995. **177**(14): p. 4121-30.
32. Ali Azam, T., et al., *Growth phase-dependent variation in protein composition of the Escherichia coli nucleoid.* J Bacteriol, 1999. **181**(20): p. 6361-70.
33. Otsuka, Y., et al., *GenoBase: comprehensive resource database of Escherichia coli K-12.* Nucleic Acids Res, 2015. **43**(Database issue): p. D606-17.
34. Grant, R.A., et al., *The crystal structure of Dps, a ferritin homolog that binds and protects DNA.* Nature Structural Biology, 1998. **5**(4): p. 294-303.
35. Almiron, M., et al., *A novel DNA-binding protein with regulatory and protective roles in starved Escherichia coli.* Genes Dev, 1992. **6**(12B): p. 2646-54.
36. Landgraf, D., et al., *Segregation of molecules at cell division reveals native protein localization.* Nat Methods, 2012. **9**(5): p. 480-2.

Chapter 3

Single-cell analysis of the Dps response to oxidative stress

Microorganisms have developed an elaborate spectrum of mechanisms to respond and adapt to environmental stress conditions. Among these is the expression of *dps*, coding for the DNA-binding protein from starved cells. Dps becomes the dominant nucleoid-organizing protein in stationary-phase *Escherichia coli* cells and is required for robust survival under stress conditions including carbon and nitrogen starvation, oxidative stress, metal exposure, and irradiation. To study the complex transcriptional regulation of the *dps* gene in *E. coli*, we utilized time-lapse fluorescence microscopy imaging to examine the kinetics, input-encoding, and variability of the Dps response in single cells. In the presence of an oxidative stressor, we observed a single pulse of activation of the *dps* promoter. Increased concentrations of H_2O_2 led to increased intensity and duration of the pulse. While lower concentrations of H_2O_2 robustly activated the Dps response with little effect on growth rate, higher concentrations of H_2O_2 resulted in dramatically slower and highly variable growth rates. Comparison of cells within the same concentration of H_2O_2 revealed that increased levels of *dps* expression did not confer a growth advantage, indicating that recovery from stress may rely primarily upon variation in the amount of damage caused to individual cells.

This chapter is published as: De Martino M, Ershov D, van den Berg PJ, Tans SJ, Meyer AS. 2016. Single cell analysis of the Dps response to oxidative stress. J Bacteriol 198:000 –000. doi:10.1128/JB.00239-16.
http://jb.asm.org/content/early/2016/03/22/JB.00239-16?related-urls=yes&legid=jb;JB.00239-16v1

3.1 Introduction

Bacteria encounter many stresses during their development, and they need to be able to adapt quickly to the environment to survive. Bacterial response mechanisms frequently involve specific sets of genes activated to help the cell adapt to the stress. Alternative sigma factors, of which *Escherichia coli* has seven, are a frequent regulatory mechanism [1]. While housekeeping genes expressed during exponential growth are controlled by the transcription factor σ^{70} [2, 3], alternative sigma factors act as transcription initiation factors to control the activation of specialized regulons during specific growth or stress conditions [4]. The general stress response sigma factor σ^{S} activates the transcription of more than 70 genes, conferring resistance to carbon/phosphate/nitrogen starvation, heat shock, high/low pH, UV-radiation, and oxidative stress, among others [5, 6].

Microorganisms living in an aerobic environment unavoidably encounter oxidative stress as a by-product of their aerobic metabolism [7]. The resultant formation of reactive oxygen species (ROS) can lead to the damage of cellular components including membranes, DNA, and proteins [8]. As an adaptation to this condition, bacteria produce enzymes such as superoxide dismutases and reductases to scavenge these toxic components [9]. Additionally, cells also face external sources of oxidative stress: macrophages produce superoxide and nitric oxide to kill invading bacteria [10]; following perception of pathogens, plants also induce the synthesis of organic peroxides [11]; certain communities of bacteria excrete ROS to suppress the growth of their competitors [12]; and exposure to environmental redox cycling compounds can cause damaging intracellular redox reactions [13].

In this challenging environment, bacteria have developed refined molecular mechanisms of defense. The DNA-binding protein from starved cells (Dps) plays a crucial role during stress exposure. *Escherichia coli dps* mutants experience a severe reduction in survival when exposed to any of several different stressors including oxidative stress, heat shock, metal exposure, UV and gamma irradiation, or extreme pH [14-16]. Additionally, Dps was shown to protect cells against DNA strand breakage [17]. In *E.coli*, the protective effect of Dps is attributed to its dual biochemical functions. Dps has the ability to bind DNA and form Dps-DNA crystals, which may provide mechanical shielding against damaging agents [14, 18, 19]. The ferroxidase activity of Dps may also contribute significantly to its protective abilities. Hydroxyl radicals can be formed intracellularly through chemical reaction between ferrous iron and H_2O_2, either internally generated or derived from the environment. Dps catalyzes the oxidation of ferrous iron, preferring H_2O_2 as a reactant rather than O_2, thereby preventing the formation of hydroxyl radicals [20]. Dps oligomers are composed of 12 identical monomers, each one folded into a compact four-helix bundle [21], surrounding a central cavity that can store up to 500 iron atoms

[22]. The DNA-binding and ferroxidase activities of Dps are biochemically dissociable, but they both contribute to maintain DNA integrity and cellular viability [23].

Intracellular Dps levels are controlled by a complex regulatory network. During the progression from exponential to stationary phase, the number of Dps molecules within a single *E. coli* bacterium increases from approximately 6000 to 180,000, whereby it becomes the most abundant DNA-binding protein [24]. *dps* is transcribed from a single promoter recognized by either the σ^{70} (housekeeping) or σ^{S} (stationary phase) sigma factor in response to different growth and environmental conditions [25-27]. In exponential growth, *dps* can be activated in an OxyR-dependent manner by treatment of the cells with H_2O_2, recruiting σ^{70} to initiate transcription. During stationary phase or carbon starvation, σ^{S} controls *dps* expression [25]. When bacteria are growing exponentially and not exposed to stress, the *dps* promoter is downregulated by two nucleoid-binding proteins: Fis and H-NS [24, 26].

Despite the knowledge acquired in recent years, the behavior of the Dps response is not understood at the single-cell level. Upon exposure to oxidative stress, each cell that sustains oxidative damage will require sufficient upregulation of enzymes that can counteract the damage in order to maintain its health. However, high-resolution fluctuations of the *dps* promoter activity over time and the description of the intensity and the duration of the transcription of the Dps response are still unknown at the single-cell level as well as in bulk cultures. Very little is known also about the variability of the Dps stress response in individual cells and its effect on cellular growth rate, which could play a crucial role in the ability of a bacterial population to maintain competitive advantage in adverse environmental conditions. In addition, it is unknown how the dynamics of *dps* expression are affected when the concentration of stressor is varied, a question that is central to the ability of a cell to respond appropriately to changes in its environment. Clear insights into these biological processes require recently developed single-cell technologies to overcome the limitations of bulk experiments, allowing for quantification of the cell-to-cell variability in a population as well as characterization of the dynamics of transcriptional responses [28-34].

In this work, we examined the kinetics of transcriptional activation of the *dps* promoter at the single-cell level upon exposure to oxidative stress. We observed one single pulse of *dps* activation, with an intensity and duration proportional to the concentration of H_2O_2 applied, until the highest concentration of H_2O_2 resulted in saturation of the intensity but not the duration of *dps* expression. Cell growth was not linearly correlated with the H_2O_2 concentration, such that low concentrations resulted in robust *dps* induction but only a minor decrease in initial growth rate. Higher concentrations of H_2O_2 were associated with major reductions in growth rate, accompanied by dramatically increased variation. A comparison of bacteria that were exposed to the same concentration of stressor revealed that higher levels of *dps* activation

were associated with similar or slower growth compared to cells with lower *dps* expression. This behavior was perhaps due to variation in the amount of damage experienced by individual cells that drove both reduced growth and increased *dps* transcription.

3.2 Materials and Methods

3.2.1 *dps-mCherry* strain construction

The *E. coli dps-mCherry* strain was created from the *E. coli* K-12 strain W3110 (CGSC# 4474) by replacement of the genomic *dps* gene by a counter-selectable *cat-sacB* cassette [23] and subsequent replacement with a *dps-mCherry* cassette.

The *dps-mCherry* cassette was created using an adapted version of the Gibson DNA assembly protocol [35] and introduced into the pBAD33 plasmid to create the pM1 plasmid. The backbone plasmid pBAD33 [36] was amplified using PCR to create compatible ends for recombination with the *dps-mCherry* cassette. The following primers were used: forward MDM1 5'-GATCCCCGGGTACCGAGCTC-3' and reverse MDM2 5'-CAAGCTTGGCTGTTTTGGCG-3'. The *mCherry* gene was amplified using PCR from the plasmid pROD22 [37] to introduce the *dps* ribosome binding site (RBS) sequence immediately upstream of the *mCherry* gene. The following primers were used (the sequence of the RBS is underlined): forward MDM3 5'-CATCAAGAGGATATGAAATTATGGCTATCATTAAAGAGTTC-3' and reverse MDM4 5'-TTACTTGTACAGCTCGTCCATGC-3'. This RBS-*mCherry* PCR product was further amplified to introduce an upstream flanking sequence homologous to the *dps* gene and a 30-bp downstream flanking sequence homologous to the pBAD33 plasmid. The following primers were used (the sequences of the homologous regions are underlined): forward MDM5 5'-GTTTATCGAGTCTAACATCGAATAACATCAAGAGGATATGAAATTATG-3' and reverse MDM6 5'-TTCTCTCATCCGCCAAAACAGCCAAGCTTGTTACTTGTACAGCTCGTCC-3'. The *dps* gene was amplified from the pET17b-dps plasmid [23] to introduce a 30-bp upstream flanking sequence homologous to the plasmid pBAD33 and a downstream flanking sequence homologous to the RBS-*mCherry* gene. The following primers were used (the sequences of the homologous regions are underlined): forward MDM7 5'-TAGCGAATTCGAGCTCGGTACCCGGGGATCATGAGTACCGCTAAATTAGT-3' and reverse MDM8 5'-CATAATTTCATATCCTCTTGATGTTATTCGATGTTAGACTCGATAAAC-3'.

The three fragments were DpnI (New England Biolabs (NEB))-digested at 37°C for 1 hour and purified with Wizard® SV Gel and PCR Clean-Up System (Promega), then assembled using Gibson DNA assembly [35]. The assembly reaction was prepared by

combining 15 µL of Gibson assembly master mix (320 µL of 5X ISO buffer [0.5 M Tris-HCl (Sigma) pH 7.5, 50 mM $MgCl_2$, 4 mM dNTP (Invitrogen) mix (equal concentration of the four nucleotides), 50 mM DTT (Sigma), 25% w/v PEG-8000 (Sigma), 5 mM NAD (NEB)], 0.64 µL of 10 U μL^{-1} T5 exonuclease (Epicentre), 20 µL of 2 U μL^{-1} Phusion polymerase (Finnzymes), 160 µL of 40 U μL^{-1} Taq ligase (NEB), dH_2O to 1.2 ml), 100 ng of linearized vector backbone, and 100 ng of each assembly fragment in a total volume of 20 µL. The reaction was incubated at 50°C for 60 min. Electrocompetent *E. coli* W3110 cells were transformed with 5 µL of the assembly reaction using electroporation. The positive colonies carrying the chloramphenicol resistance gene from the pBAD33 plasmid were identified, and the accuracy of the sequence was checked with sequencing analysis.

The *dps-mCherry* cassette was amplified from the pM1 plasmid using PCR to introduce 50-bp flanks homologous to the chromosomal *dps* flanks. The following primers were used (the sequences of the homologous regions are underlined): forward MDM9 5'-TACTTAATCTCGTTAATTACTGGGACATAACATCAAGAGGATATGAAATTATGAGTACCGCTAAAT TAG-3' and reverse MDM10 5'-AGGAAGCCGCTTTTATCGGGTACTAAAGTTCTGCACCATCAGCGATGGATTTACTTGTACAGCTCG TCCA-3'. The fragment was DpnI-digested and purified, then introduced with electroporation into a W3110 *dps::cat-sacB* strain [23]. The cells were grown for 3 hours in LB medium at 37°C while shaking at 250 rpm to allow homologous recombination. The bacteria were then were plated on counterselective medium for *sacB*: NaCl-free LB 10% sucrose agar and incubated at 30°C overnight. The colonies that looked healthy were streaked on LB agar containing 25 µg/mL chloramphenicol. The screening of the colonies that did not survive on chloramphenicol was performed with colony PCR, and the replacement of the *dps* gene was confirmed by sequencing. The *mCherry* expression was confirmed with fluorescence-activated cell sorting (FACS) (data not shown).

3.2.2 *dps-mCherry* growth characterization

The growth of the created *dps-mCherry* strain was compared with the wild-type W3110 strain in the presence of 0, 0.01, 0.05, 0.1, 0.5, 1, 3, 5, or 10 mM H_2O_2 . Overnight cultures of the *dps-mCherry* and W3110 strains were diluted 100 times in Hi-Def Azure medium (3H5050, Teknova) supplemented with 0.2% glucose. The cultures were grown at 37°C to early-exponential phase ($O.D._{600}$ 0.2-0.3), then H_2O_2 was added (216763, Sigma). 200 µL of each culture was placed in duplicate into a 96-well plate and covered with 50 µl of mineral oil to prevent evaporation. The cells were grown for 10 hours in a microplate reader Infinite M200 PRO (Tecan) at 37°C with an orbital shaking amplitude of 4.5 mm, and $O.D._{600}$ measurements were performed every 10 minutes.

3.2.3 Western blotting

Overnight cultures of the W3110 strain and the *dps-mCherry* strain were diluted 100 times in Hi-Def Azure medium supplemented with 0.2% glucose. The cultures were grown at 37°C until early exponential phase (O.D. $_{600}$ 0.2-0.3) before adding H_2O_2 to 0, 0.5, or 1 mM. The cultures were grown at 37°C for 45 minutes. The cell pellet of 500 µL of each culture was resuspended with 2X SDS-PAGE sample buffer (5X: 10% w/v SDS, 10 mM DTT, 20% w/v glycerol, 0.2 M Tris-HCl pH 6.8, 0.05% broom phenol blue) to a final O.D.$_{600}$ of 10, then heated at 95°C for 10min and separated on a 15% SDS-PAGE gel. Proteins were transferred to an Immun-Blot® PVDF membrane (162-0177, Biorad) with a Novex® semi dry blotter (SD1000, Invitrogen) for 40 min at 15 volts. The PVDF membrane was blocked with 5% milk in TBS-T (10 mM Tris pH 7.5, 150 mM NaCl, 0.1% Tween-20) , then incubated for 1 hour with primary antibody (rabbit anti-Dps) diluted 1:5000, followed by incubation with secondary antibody (goat anti-rabbit IgG (H+L), horseradish peroxide conjugate, 32460, Thermo Scientific) diluted 1:100,000 for 45 min. The membrane was developed using SuperSignal® West Pico Chemiluminescent Substrate kit (Thermo Scientific) and imaged with a Molecular Imager ChemiDoc ®XRS (Biorad). Images were analyzed with Image Lab® software (Biorad).

3.2.4 Growth conditions for microscopy

For the single-cell microscopy experiments, one colony of *dps-mCherry* was inoculated overnight into Hi-Def Azure medium (3H500, Teknova) supplemented with 0.2% glucose and grown overnight at 37°C. This preculture was diluted 1:100 and grown for around 2 hours at 37°C until early exponential phase (O.D.$_{600}$ 0.2-0.3). The culture was diluted to O.D.$_{600}$=0.005 for seeding onto the agarose pad.

3.2.5 Agarose pad preparation

Agarose pads were prepared with a modified version of the protocol in [38]. The pads were prepared freshly for each experiment. 2% (w/v) low-melt Agarose LE (V3125, Promega) was added to 5 mL of Hi-Def Azure medium and dissolved by microwaving. After the agarose solution had cooled, H_2O_2 was added. Agarose pads were formed immediately thereafter. Cover glass slides of 20 mm^2 (631-0122, VWR) were placed on Parafilm M® (Bemis Company, Inc.), and 900 µL of agarose were pipetted onto each. Immediately after pipetting, a second cover glass was placed on top of the agarose. The pads were allowed to solidify for 45–60 min at room temperature while covered with a lid to avoid evaporation of the edges. When the agarose was solidified, it was cut into pads of

0.5 x 0.5 cm. 2 µL of bacterial culture diluted to $O.D._{600}$ 0.005 was seeded onto individual agarose pads. The culture was allowed to evaporate and absorb into the agarose for about 10 min at room temperature. When the surface appeared to be dry, the pad was flipped with a scalpel onto a 4-well slide-base tissue culture chamber (Starstedt). The chamber was closed with a lid and sealed with Parafilm M® to avoid evaporation during the imaging. The cells were able to grow in a monolayer due to their placement between the glass bottom of the chamber and the agarose pad on top.

The variability of H_2O_2 distribution in the pads was determined using rhodamine as a fluorescent reporter. During the preparation of the agarose pads, dihydrorhodamine 123 (D1054, Sigma-Aldrich) was added to a final concentration of 20 µM after the agarose solution had cooled, and the pads were formed immediately thereafter. The pads were scanned using a Typhoon Trio (Amersham Biosciences), and the images were analyzed using ImageJ software [39]. The fluorescence intensity values of 80 different pixels in 2 different pads were averaged, and the standard deviation was calculated, showing an upper limit of variability of 12.9%. We expect a lower variability for the H_2O_2 molecule than for rhodamine, since the diffusion coefficient of H_2O_2 is 1 order of magnitude larger than that of rhodamine: $1.305\pm0.83\times10^{-5}$ cm^2s^{-1} [40] and $4x10^{-6}$ cm^2 s^{-1} respectively [41].

3.2.6 Fluorescence microscopy

Microcolonies on agarose pads were imaged by time-lapse fluorescence microscopy using an inverted microscope (Olympus IX81), an AMH-200 lamp (Andor), and a Cy3 filter cube (4040C). Images were acquired with Luca R EMCCD camera (Andor). Andor iQ software was used to control the microscope and to perform automatic imaging acquisition. Experiments were performed at 37°C using an incubation chamber (H201-T, Okolab) to allow precise temperature control. Phase contrast images (500 ms exposure time, 3 images +/- 0.2 µm from the focus) and fluorescence images (100 ms exposure time) were recorded every 5 min, for 3-4 hours.

3.2.7 Data analysis

Images were analyzed using a custom Matlab program [42] based on the Schnitzcells program [38]. Briefly, the data analysis consisted of three steps: segmentation, tracking, and extraction of cell parameters. Cell length was extracted from segment properties, and growth rate was determined from exponential fits of lengths-in-time. Individual cell fluorescence was extracted from fluorescent images using segmentation obtained from phase contrast images (more details on analysis are described in the following paragraphs). For each microcolony, the fluorescence intensity curves were fitted with the best-fitting polynomial (degree 5), and the maximum of this

function was considered to be the maximum fluorescence intensity. The duration of *dps* expression was calculated as time from the beginning of the exposure to H_2O_2. Between 11 and 19 colonies for each stress condition were analyzed for a total of 75 colonies.

3.2.7.1 Cell segmentation and tracking

Three phase-contrast images (with +/- 0,2 µm offset from the focus) were acquired at each timepoint and averaged for further analysis. The cells were isolated from the background, and groups of cells were recognized based on phase contrast maxima and concavity. Cell outlines were detected in this averaged image; the edges of the cells were identified using Laplacian of Gaussian filter. Once each frame was segmented and any errors were removed manually, lineages of cells were traced to create a genealogic tree using a tracking algorithm that looks for adjacent cells in consecutive frames.

3.2.7.2 Cell length

Cell length was extracted from the properties of its corresponding segment. The cell profile was calculated by fitting a third degree polynomial *f(x)* through all pixels of its segment:

$$f(x)=ax^3 + bx^2 + cx + d$$

where *x* is the main axis of the ellipsoid containing the segment. The length of the cell was then defined as the length of this profile between the two poles. The cell length (L) was calculated by numerical integration between pole x_0 and x_1 of each cell:

$$L = \int_{x_0}^{x_1} \sqrt{1 + [f'(x)]^2\, dx}$$

where

$$f'(x) = \frac{df(x)}{dx}$$.

3.2.7.3 Single-cell growth rate

Growth rate (μ) was determined from exponential fits of cell length over time. The cell size was proportional to cell length as no significant changes in cell width were

observed. The single-cell growth rate was calculated by fitting the cell length over time with the function:

$$L(t) = L_0 e^{\mu_e \cdot \ln(2) \cdot t} = L_0 2^{\mu_e \cdot t}$$

The elongation rate was determined for a number of consecutive time points within a cell cycle. We chose to calculate it through a window of 7 frames, to obtain an optimal balance between noise and accuracy.

3.2.7.4 Fluorescence extraction

Using a background image (I_b) and shading image (I_s), fluorescence images were corrected for camera noise and uneven illumination of the sample. The calibrated image I_c was calculated as:

$$I_c = \frac{I - I_b}{I_s - I_b}$$

where (I) is the original image. The image was further enhanced by deconvolution using the Matlab Lucy-Richardson algorithm in combination with a point-spread function for our imaging system (experimentally determined using 0.02 µm sized FluoSpheres from Invitrogen). The fluorescence intensity was determined independently of cell size to avoid artificial correlations between the two measurements. The mean fluorescence was calculated by averaging pixels within 0.2 µm of the cell axis, but more than 0.3 µm away from the cell poles, and subtracting background fluorescence (determined from pixels outside the microcolony).

3.2.8 Determination of photobleaching kinetics

The plasmid pRSETb (V351-20, Invitrogen), containing *mCherry* under a T7 promoter, was introduced into the *E. coli* wild-type strain BL21 (V351-20, Invitrogen). No inducer was applied due to leakiness of the plasmid that provided a constitutive background level of mCherry similar to that observed in our H_2O_2-treated *dps-mCherry* strain. An overnight culture of the strain was diluted 100 times in Hi-Def Azure medium supplemented with 0.2% glucose and grown at 37°C until early exponential phase ($O.D._{600}$ 0.2-0.4). The cells were imaged on agarose pads without addition of H_2O_2. Image

acquisition was performed using the same exposure time of the experiments described in the main text (100 ms) with a frequency of 30 seconds. A total of 30 frames (15 min) were recorded, to simulate the typical number of acquisitions during the oxidative stress experiments.

3.2.9 Fluorescence microscopy with reduced imaging

Time-lapse fluorescence microscopy movies were acquired of the *dps-mCherry* strain exposed to different concentrations of H_2O_2 with frames acquired every 30 minutes. A single colony was inoculated overnight into Hi-Def Azure medium supplemented with 0.2% glucose. This preculture was diluted 1:100 in Hi-Def Azure medium supplemented with 0.2% glucose and grown for around 2 hours at 37°C until early exponential phase ($O.D._{600}$ 0.2-0.3). The culture was diluted to $O.D._{600}$=0.005 and seeded onto agarose pads containing 30, 50, or 100 µM H_2O_2. The imaging frequency was set to 30 minutes instead of 5 minutes, with a total of 7 frames acquired, using the same parameters described in the main text.

3.2.10 mCherry fluorescence in the presence of H_2O_2

The *E. coli* BL21 strain containing the pRSETb::mCherry plasmid was grown overnight without inducer. This culture was diluted 100 times in Hi-Def Azure medium supplemented with 0.2% glucose and grown at 37°C until early exponential phase ($O.D._{600}$ 0.2-0.4). The cells were imaged on agarose pads containing 0 µM, 50 µM, or 100 µM of H_2O_2 for around 150 min, according to the microscope parameters described in the main text.

3.2.11 *dps* expression in the microfluidics device

One colony of the *dps-mCherry* strain was inoculated overnight into Hi-Def Azure medium supplemented with 0.2% glucose and grown overnight at 37°C. This preculture was diluted 1:100 and grown for around 2 hours at 37°C until early exponential phase ($O.D._{600}$ 0.2-0.3). The culture was diluted to $O.D._{600}$=0.04 for loading into the microfluidics device in which H_2O_2 was constantly applied to the cells over the duration of the imaging.

The microfluidics device was fabricated as in [43]. Briefly, the device consists of a multilayer structure composed of a coverglass facing the microscope objective, a polyacrylamide membrane soaked in Hi-Def Azure medium supplemented with 0.2% glucose, and a PDMS control channel for medium flow. The layers were held together by mechanical clamping. During assembly of the device, the bacterial cells were placed

between the coverglass and the polyacrylamide membrane. The PDMS flow cell allowed a continuous diffusion of the growth medium to the cells growing below the membrane.

To test the device for any possible leakage and to allow the selection of stably trapped cells, Hi-Def Azure medium supplemented with 0.2% glucose was provided to the cells through an electrical syringe pump connected to the PDMS flow cell. Then the Hi-Def Azure medium supplemented with 0.2% glucose containing 0 µM or 30 µM H_2O_2 was applied. Once the cells were stably settled in the chamber, the microcolonies were imaged by time-lapse fluorescence microscopy. The microscope parameters and the data analysis were equivalent to those described for the agarose pad experiments.

More detailed information about the microfluidic device and the experimental conditions are described in chapter 5.

3.3 Results

3.3.1 Construction of a reporter strain for *dps* transcription

To explore *dps* transcriptional dynamics, we constructed a reporter strain of *E. coli* (named "*dps-mCherry*"), with the *mCherry* gene introduced as a reporter for *dps* transcription. The two genes are both present in the *dps* promoter, with *mCherry* immediately downstream of *dps*. A ribosome binding site (RBS) sequence identical to that of the *dps* RBS was placed upstream of the *mCherry* reporter gene (Fig. 3.1). This construct allowed the detection and the quantification of *dps* promoter activity in single cells through monitoring of the collective fluorescence emitted by the fluorescent proteins. In order to characterize the health of the *dps-mCherry* strain, we compared its growth with the wild-type parental strain in the presence of H_2O_2 concentrations between 0 and 10 mM. Both the strains showed a similar growth response (Fig. 3.2). The growth kinetics were comparable at concentrations of H_2O_2 up to 1 mM, showing similar robust exponential-phase kinetics and final optical densities. At higher concentrations of H_2O_2, both strains showed growth inhibition. Thus, the engineered *dps-mCherry* strain exhibits similar growth response to H_2O_2 as the wild-type strain.

To verify *dps* expression, both strains were exposed to 0, 0.5, and 1 mM H_2O_2, and Dps protein levels were analyzed through Western blotting. An increase in Dps concentration, proportional to the stressor concentration, was detected in both strains in the presence of H_2O_2 (Fig. 3.3).

Fig. 3.1. Schematic representation of the *dps* operon present in the *dps-mCherry* strain. The *mCherry* and the *dps* genes are both present in the *dps* operon, with *mCherry* immediately downstream of *dps*. The ribosome binding site (RBS) sequence placed upstream of the *mCherry* gene is identical to that of *dps*.

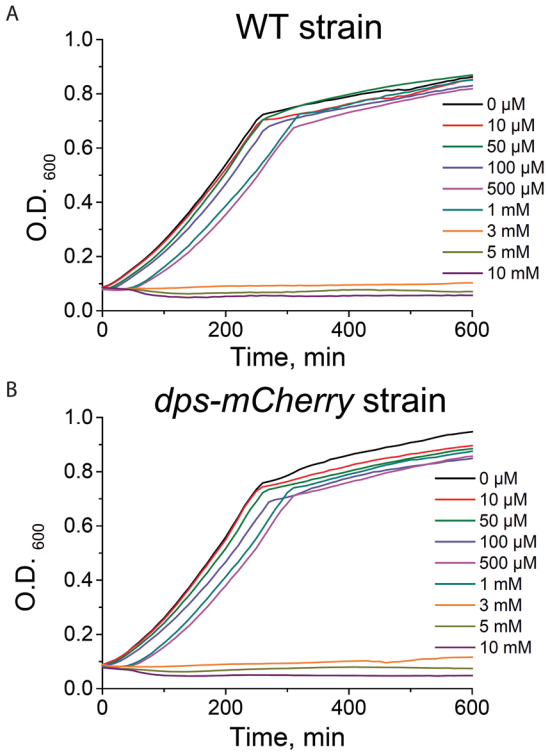

Fig. 3.2. Wild-type and *dps-mCherry* strains exhibit similar growth curves in the presence of H_2O_2. The wild-type parental (A) and *dps-mCherry* (B) strains were grown in the presence of H_2O_2 concentrations between 0 and 10 mM, and $O.D._{600}$ signal was monitored over time.

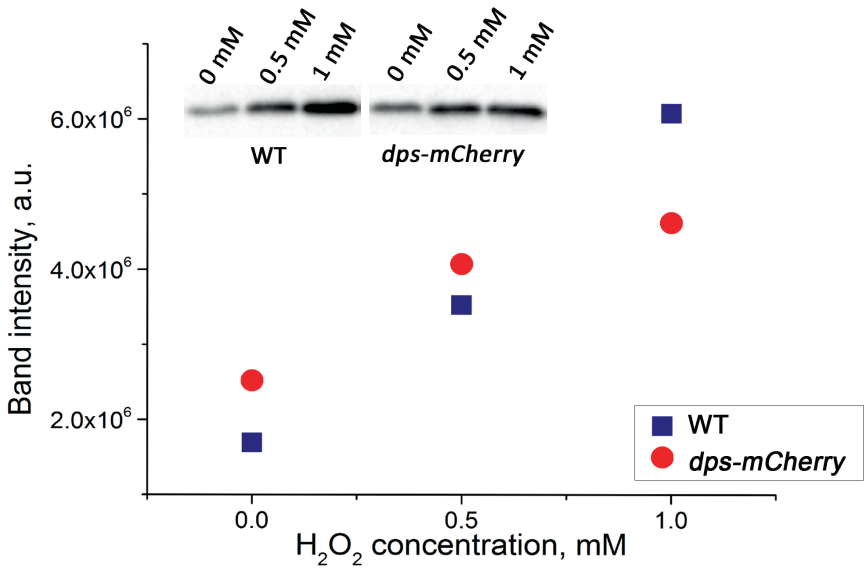

Fig. 3.3. Wild-type and *dps-mCherry* strains both exhibit increased Dps protein expression following exposure to H_2O_2. The wild-type and the *dps-mCherry* strains were exposed to 0, 0.5, or 1 mM H_2O_2 for 45 minutes, after which Dps protein levels were analyzed through Western blotting.

An engineered strain, named *dps-mCherry* fusion, carrying a chimeric version of *dps*, fused C-terminally to the *mCherry* gene as translational reporter, was also constructed. Cells expressing this protein showed a non-homogeneous distribution of fluorescence throughout the cell volume, with visible puncta of more intense fluorescence (Chapter 2). Previous work has similarly shown that fusion of Dps with the GFP protein resulted in aggregation of this fusion protein in *E. coli* cells [44]. This strain was therefore excluded from further experimentation.

3.3.2 *dps* expression dynamics during oxidative stress

Cells exposed to concentrations of H_2O_2 between 0 and 100 µM were analyzed using quantitative time-lapse fluorescence microscopy to detect *dps* promoter activity in each individual cell over time. The *E. coli* cells were grown in rich defined medium to early exponential phase, then transferred to an agarose pad in which H_2O_2 was incorporated, to begin the application of oxidative stressors. Individual cells grew and divided over time to give rise to a microcolony. A difference in growth and fluorescence could be observed in

cells not exposed to any stressor compared to those in the presence of different concentrations of H_2O_2. In the colonies without applied stress, we observed that the fluorescence of each cell is indistinguishable from background during the entire duration of the measurement (Fig. 3.4 A). In the presence of H_2O_2, we detected a fluorescent signal that was roughly proportional to the amount of applied stress (Fig. 3.4 B-E). We observed a general trend for the intensity of the fluorescence signal over time: the intensity increased during the initial period of the measurement and then decreased thereafter. Reduced growth was apparent at higher concentrations of H_2O_2, and at 100 µM H_2O_2 there was a near-complete inhibition of cell division (Fig. 3.4 D-E).

The data was analyzed using modified Schnitzcells software [38] to extract the fluorescence intensity within single cells as mean fluorescence per unit area [42]. In the absence of oxidative stress, the fluorescence intensity of each individual cell present within a microcolony over time was very low (Fig. 3.5 A). Exposure to hydrogen peroxide induced a single pulse of fluorescence that started shortly after the cell progenitor of the colony first experienced the stress (Fig. 3.5 B-E). The pulse was highly synchronized between the individual cells within each microcolony population throughout the duration of the imaging. The variability of fluorescence signal among cells within a colony at each time point was evaluated by calculation of the coefficient of variation (CV) as the ratio of the standard deviation to the mean. As the single cells divided to form a small microcolony over the course of the experiment, the CV remained low, between 0.0 and 0.25, for colonies exposed to 0, 50, or 100 µM H_2O_2. For cells exposed to 10 or 30 µM H_2O_2, the CV increased steadily over time to reach values around 0.5 (Fig. 3.5 F). This increase in CV might be due to the average higher number of cells present in the microcolonies during growth in these two stress conditions. An asymmetric dilution of oxidative components or Dps molecules during cell division could also lead to the observed increase in CV values over time.

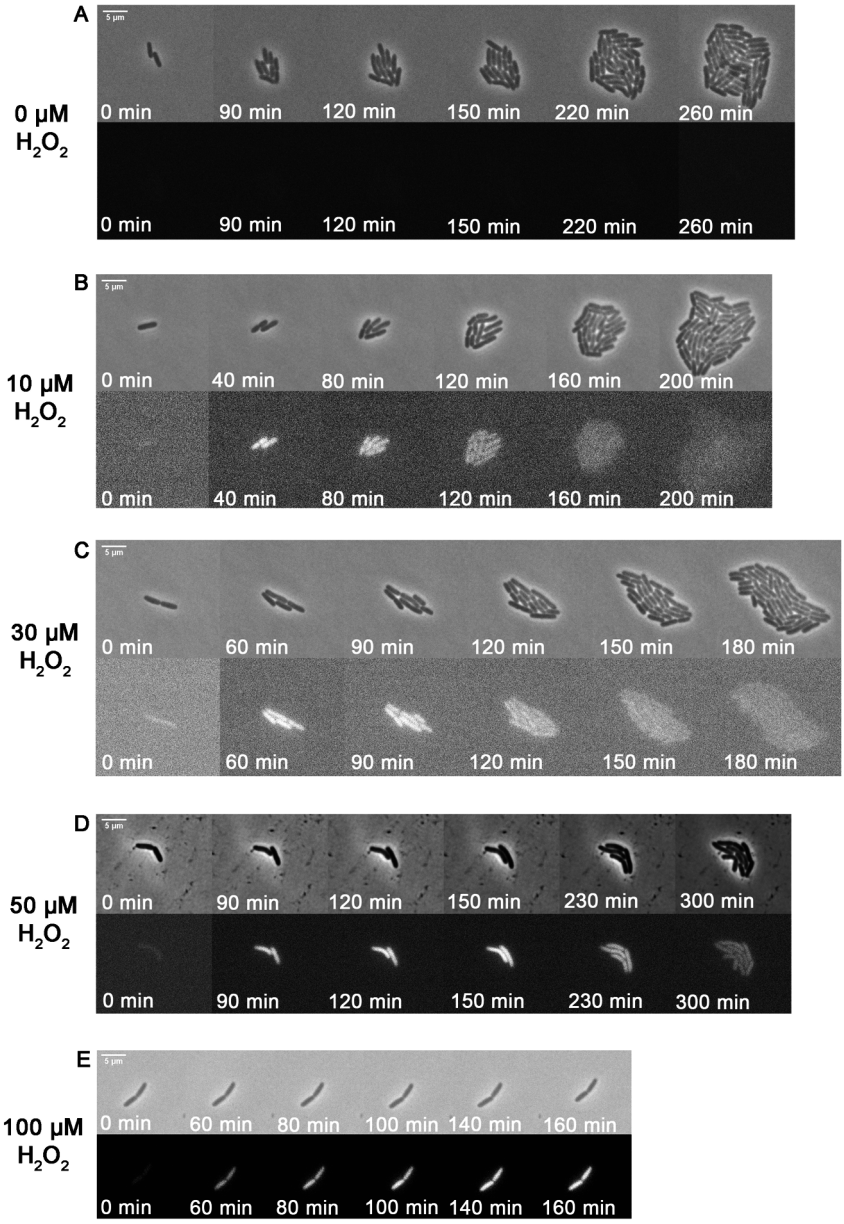

Fig. 3.4. Time-lapse fluorescence of microcolonies exposed to H_2O_2. Individual cells were exposed to concentrations of H_2O_2 between 0 µM and 100 µM (A-E) and analyzed using quantitative time-lapse fluorescence microscopy. For each panel, the upper images are phase-contrast images, and the lower images are fluorescence images from a single microcolony over time.

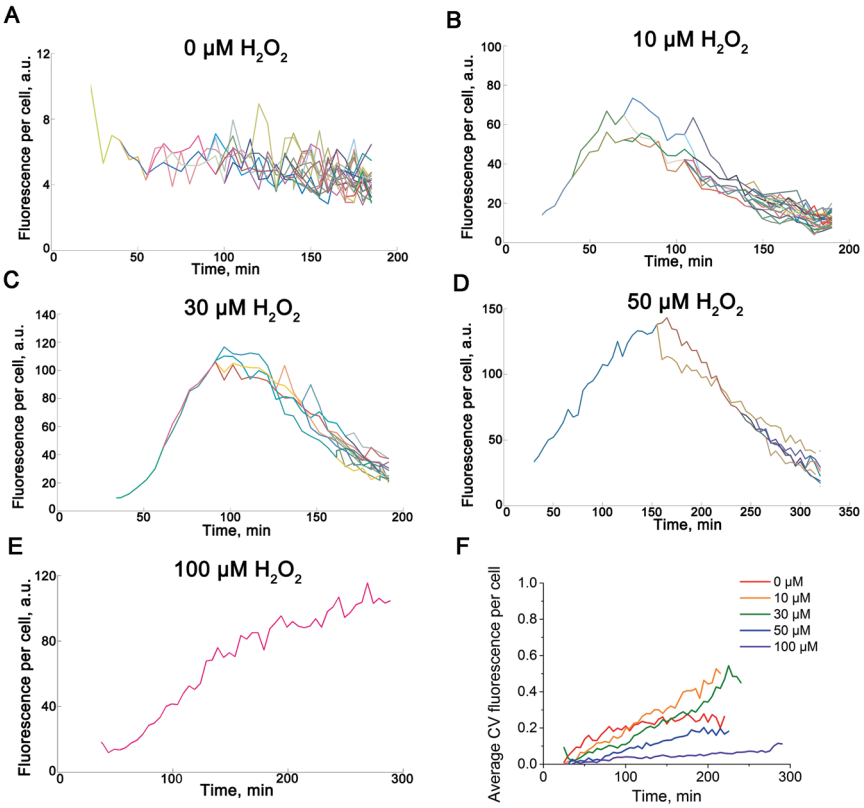

Fig. 3.5. Exposure to H_2O_2 induces a single pulse of *dps* promoter activity synchronized over the individual cells within each microcolony. A-E) Examples of fluorescence intensity over time in individual cells in a microcolony exposed to different concentrations of H_2O_2. Each line represents a single cell. F) The average coefficient of variation (CV) over time of the fluorescence intensity among all the cells exposed to the same stress condition, for varying concentrations of H_2O_2.

In order to compare fluorescent responses between microcolonies, we calculated the average of the fluorescence values of all cells within a microcolony, at each time point measured (Fig. 3.6). Every colony grown in the absence of stressor showed a low average fluorescence signal that decreased slightly over the duration of the imaging (Fig. 3.6 A). The colonies exposed to 10, 30, or 50 µM H_2O_2 showed a similar fluorescence profile: a large transient increase in fluorescence over time that took the form of one major peak. Colonies exposed to the same amount of hydrogen peroxide showed varying peak amplitudes and durations (Fig. 3.6 B-D). In contrast, at 100 µM H_2O_2 no peak of fluorescence was detected. Instead, the average fluorescence signal in each colony rose to a plateau, over a variable period of time (Fig. 3.6 E). Calculation of the average fluorescence profile over time for all colonies within each experimental condition revealed that increasing concentrations of H_2O_2 resulted in both an increase of the intensity and the duration of fluorescence signal. The standard deviations associated with certain conditions showed a large overlap, especially between 50 µM and 100 µM (Fig. 3.6 F). The variability of the average fluorescence signal among different microcolonies in the same stress condition was evaluated by calculation of the coefficient of variation at each time point. The CV values observed at 0, 30, and 100 µM H_2O_2 remained around 0.3, while at 10 and 50 µM H_2O_2 the CV values were higher, reaching a maximum value of around 0.6 at 10 µM and 0.9 at 50 µM H_2O_2 before decreasing again (Fig. 3.6 G).

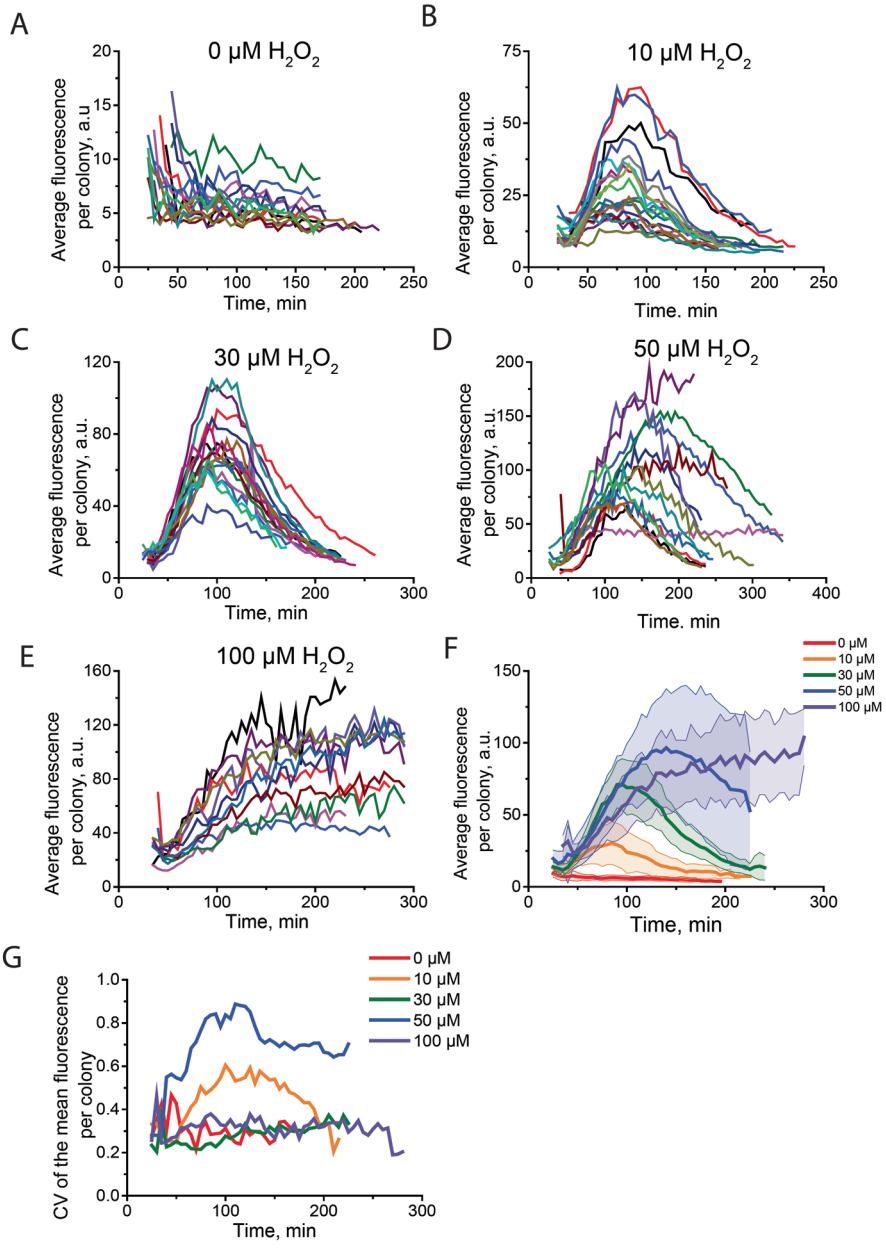

Fig. 3.6. The Dps response per microcolony exhibits variation in peak amplitude and duration.

Fig. 3.6. The Dps response per microcolony exhibits variation in peak amplitude and duration. A-E) The average fluorescence signal over time of microcolonies exposed to different concentrations of H_2O_2. Each line represents the average fluorescence intensity of all cells within one microcolony. F) The average fluorescence signal over time of all the colonies exposed to the same stress condition. The shaded area represents the standard deviation. G) The coefficient of variation (CV) over time of the average fluorescence signals of all the microcolonies exposed to the same stress condition, for varying concentrations of H_2O_2.

To assess whether the observed dynamics of Dps induction were an artifact of the experimental procedure, several control experiments were performed. To determine the consequences of the light exposure on the mCherry protein during the time-lapse fluorescence microscopy process, a photobleaching test was performed on a strain of *E. coli* with constitutive *mCherry* expression. We observed an average of about 20% decrease in the fluorescence signal due to the cumulative photobleaching effect of our image acquisition process on a single cell (Fig. 3.7). To test the effect of imaging on the cellular fluorescence, images of the *dps-mCherry* strain in the presence of 30, 50, or 100 µM H_2O_2 were acquired every 30 minutes. These fluorescence curves showed a shape similar to those obtained from image acquisition every 5 minutes (Fig. 3.8, Fig. 3.6) demonstrating that that the imaging process does not significantly affect the measured cellular behavior. Similarly shaped peaks of fluorescence were observed both in the agarose pad system and in a microfluidics device [43] in which H_2O_2 was constantly applied to the cells over the duration of the imaging (Fig. 3.9), indicating that the shape of the fluorescence curve is not due to degradation of H_2O_2 over time. The stability of mCherry signal in the presence of the oxidating effect of 50 and 100 µM H_2O_2 was also investigated, showing no statistically significant difference in mCherry degradation or loss of fluorescence intensity due to oxidation (Fig. 3.10).

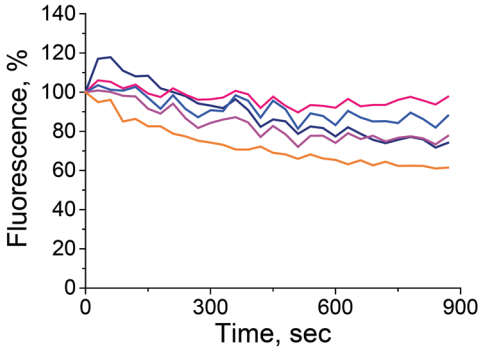

Fig. 3.7. Photobleaching of the mCherry signal. An mCherry-expressing strain was imaged on agarose pads without addition of H_2O_2, and image acquisition was performed with 100 ms exposure time and a frequency of 30 seconds, for a total of 900 seconds. An average total decrease in the fluorescence signal of individual cells of approximately 20% was recorded.

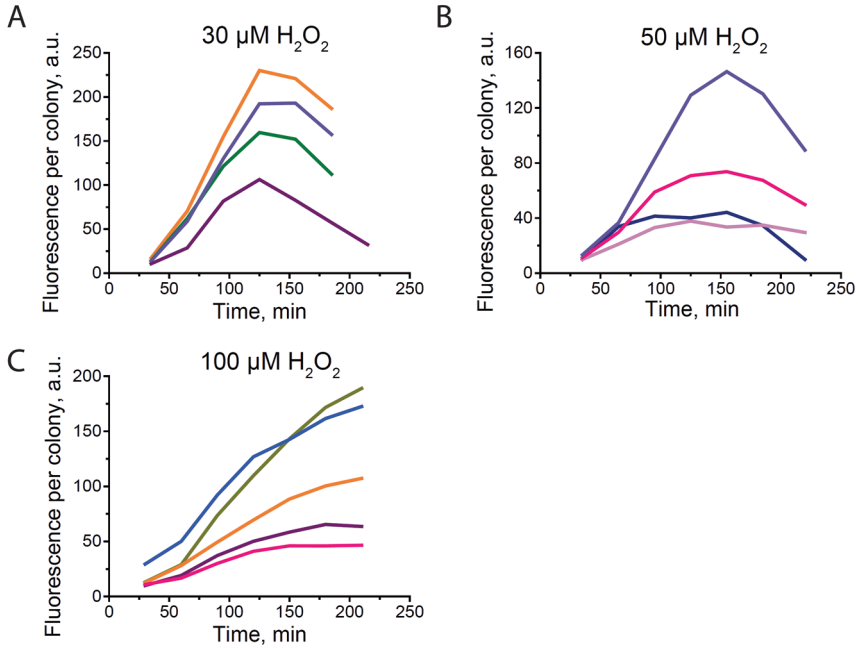

Fig. 3.8. The Dps response to H_2O_2 takes the form of a single pulse under conditions of low light exposure. The *dps-mCherry* strain in the presence of (A) 30, (B) 50, or (C) 100 μM H_2O_2 was imaged every 30 minutes with an exposure time of 100 ms for a total of 7 frames. Plots show the average fluorescence signal per microcolony over time; each line represents the average fluorescence intensity of all cells within one microcolony.

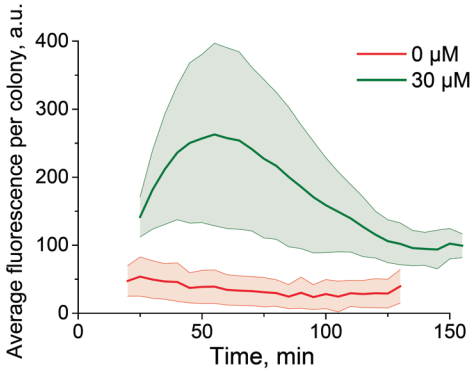

Fig. 3.9. Continuous application of H_2O_2 in a microfluidics device induces a single pulse of *dps* promoter activity. The average fluorescence signal over time of microcolonies exposed to different concentrations of H_2O_2. The cells were grown in a microfluidics device in which H_2O_2 was constantly applied to the cells over the duration of the imaging. Similarly-shaped curves of fluorescence were observed in both the microfluidics device and agarose pad experimental systems, indicating that the shape of the fluorescence curve of the cells grown onto the agarose pads is not due to degradation of H_2O_2 over time. The shaded area represents the standard deviation.

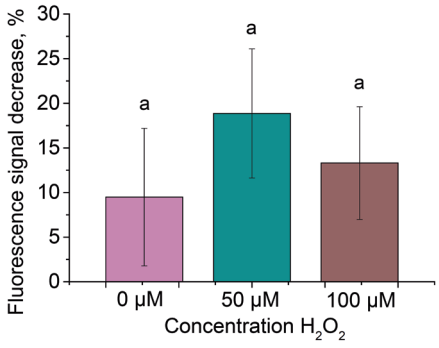

Fig. 3.10. mCherry signal is stable in the presence of high H_2O_2 concentrations. An mCherry-expressing strain was imaged on agarose pads containing 0 μM, 50 μM, or 100 μM of H_2O_2 for approximately 150 min. Imaging was performed every 5 min with 100 ms exposure time. The chart shows the average difference in the average fluorescence signal per microcolony between the first and the final image of the experiment, for each concentration of H_2O_2. The error bars represent the standard deviation. The letters represent the statistical significance: samples labeled with the same letters are not statistically different (ANOVA test, $p < 0.05$).

3.3.3 Correlations between oxidative stressor concentration and the intensity and duration of *dps* induction

For a quantitative analysis of Dps induction in the presence of oxidative stress, we analyzed the intensity and the length of the fluorescence peak. For each microcolony, the curve representing the average fluorescence intensity among its constituent cells was fitted with a polynomial function in order to extract both the maximum value of the fluorescence and the time point at which it was reached. Calculation of the average maximum fluorescence values of colonies exposed to the same amount of H_2O_2 revealed that higher concentrations of stressor were correlated with higher peak amplitude for H_2O_2 concentrations between 0 µM and 50 µM (Fig. 3.11 A). No increase in average maximum fluorescence value was observed when the H_2O_2 concentration was increased from 50 µM to 100 µM (Fig. 3.11 A). The variability in the maximum fluorescence intensity among different colonies in the presence of the same concentration of stressor was evaluated by calculation of the coefficient of variation. These values ranged between 0.23 and 0.47, with the maximum variability observed at 10 µM H_2O_2 (Fig. 3.11 B). No overall trend was seen between the coefficient of variation and the maximum fluorescence values over the various concentrations of H_2O_2 (Fig. 3.11 C). No significant differences were observed in the distribution of maximum fluorescence values when microcolonies were grown on the same agarose pad versus different agarose pads.

The average time at which the maximum fluorescence signal was observed for microcolonies in each experimental condition increased steadily with the amount of H_2O_2 applied to the culture (Fig. 3.12 A). The coefficient of variation for the time of maximum fluorescence intensity was calculated between different microcolonies in the same stress condition and ranged between 0.10 and 0.29, lower than the variability observed for the strength of the induction (Fig. 3.12 B). No relationship was observed between the coefficient of variation values and the time to the maximum fluorescence, over the concentrations of H_2O_2 (Fig. 3.12 C). Taken together, our data indicate that an increase in hydrogen peroxide concentration led to an increase of *dps* promoter activity. In addition, the duration of the protein synthesis also increased with the concentration of the stressor.

Correlation analyses were performed on the extracted values for the maximum fluorescence intensity and the duration of the increase in fluorescence for individual microcolonies. When comparing all the stress conditions simultaneously, the Pearson correlation coefficient (R) between the time to reach the fluorescence peak and its intensity was 0.80 with a p value < 0.0001 (Fig. 3.13 A). Fluorescence peaks that were higher in amplitude were therefore strongly correlated with a longer period of *dps* expression. While this strongly positive correlation was observed through analyzing the pooled data, the data for each individual H_2O_2 concentration considered separately

showed a weaker positive correlation, ranging from 0.23 to 0.82 with an average of 0.49 (Fig. 3.13 A).

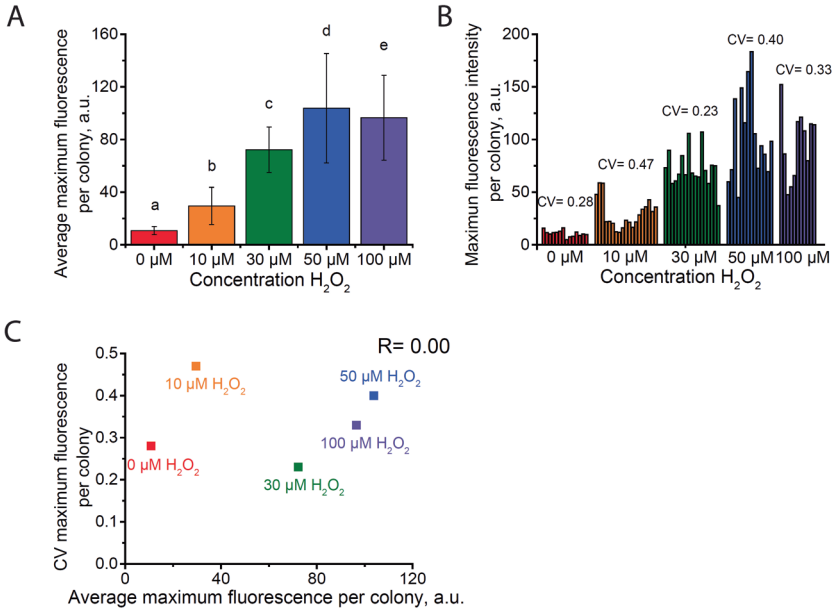

Fig. 3.11. Dps induction intensity increases with exposure to higher concentrations of H_2O_2. A) The average maximum values of the fluorescence signal for each microcolony, for each concentration of H_2O_2. The error bars represent the standard deviation. The letters represent the statistical significance: samples labeled with different letters are statistically different (ANOVA test, $p < 0.05$). B) The maximum values of the fluorescence signal for each microcolony, and the coefficient of variation (CV) of the maximum fluorescence intensity among microcolonies, for each H_2O_2 concentration. C) Scatter plot of the coefficient of variation vs. the average maximum fluorescence value for each concentration of H_2O_2. R represents the Pearson correlation coefficient.

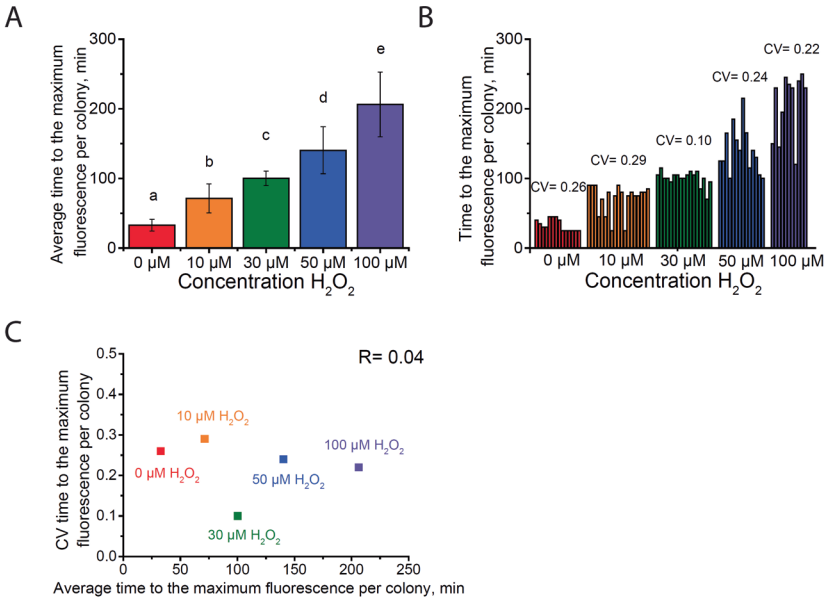

Fig. 3.12. The duration of Dps induction increases with exposure to higher concentrations of H_2O_2. A) The average time at which the maximum value of the fluorescence signal was observed for each microcolony, for each concentration of H_2O_2. The error bars represent the standard deviation. The letters represent the statistical significance: samples labeled with different letters are statistically different (ANOVA test, $p < 0.05$). B) The time to the maximum value of the fluorescence signal for each microcolony, and the coefficient of variation (CV) of the time to the maximum fluorescence intensity among microcolonies, for each H_2O_2 concentration. C) Scatter plot of the coefficient of variation vs. the time to the average maximum fluorescence value for each concentration of H_2O_2. R represents the Pearson correlation coefficient.

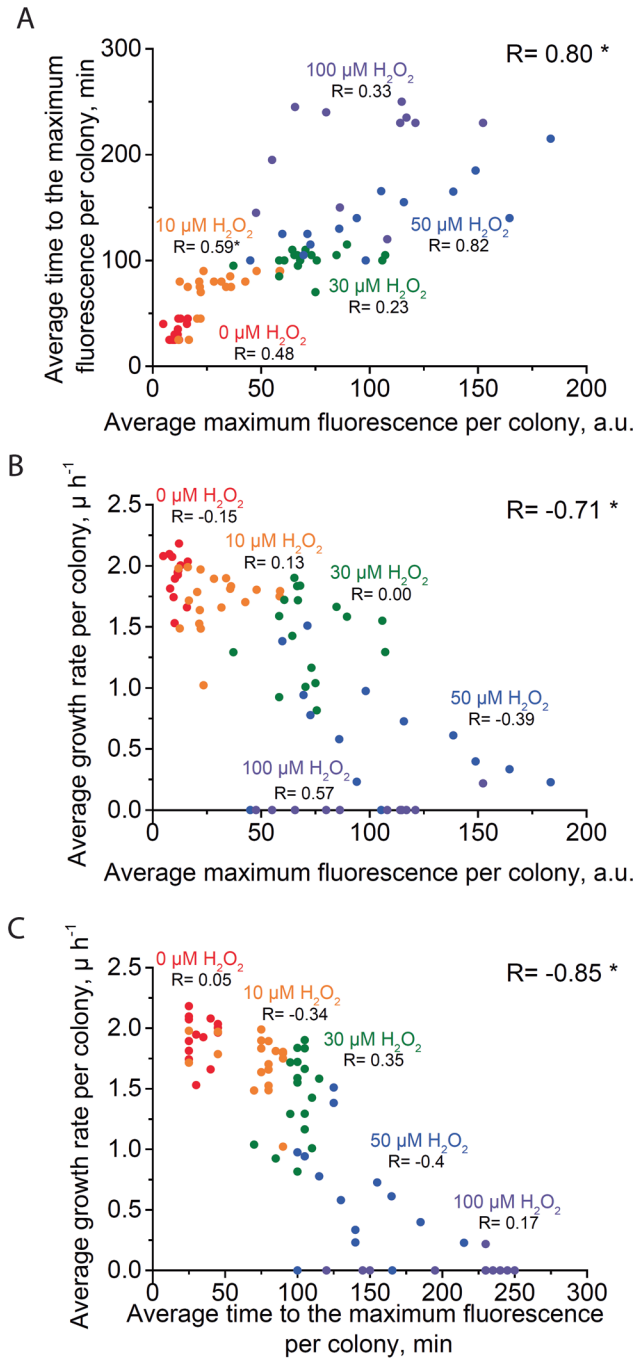

Fig. 3.13. Correlations between growth rate, intensity, and duration of Dps induction.

Fig. 3.13. Correlations between growth rate, intensity, and duration of Dps induction. A) Scatter plot of the average maximum fluorescence intensity vs. the average time to the maximum fluorescence for individual microcolonies. B) Scatter plot of the average growth rate per colony vs. the average maximum fluorescence intensity for individual microcolonies. C) Scatter plot of the average growth rate per colony vs. the average time to the maximum fluorescence intensity for individual microcolonies. Each dot represents a single microcolony. Microcolonies exposed to the same H_2O_2 concentration are represented in the same color. The R value in the top right corner of each graph represents the **Pearson** correlation coefficient over all the data. The R below the label for each concentration of H_2O_2 represents the R value calculated over all microcolonies in each stress condition. * = $p<0.05$.

3.3.4 Effects of oxidative stress on cellular growth

Cellular length and growth rate can be - indicators of cellular fitness. The parameter of cell length was calculated as the length of the axis between the two poles of a cell [42]. We compared the average length of all cells within each microcolony over time for all the microcolonies analyzed (Fig. 3.14). If 0 µM or 10 µM H_2O_2 was applied we observed the trend that the cell length slightly decreased over time, declining from an average of 5.5 µm down to 3.5 µm (Fig. 3.15, Fig. 3.14 A- B). Application of higher H_2O_2 concentrations of 30 µM or 50 µM resulted in little increase in the average cell length, but a higher proportion of elongated cells, reaching a length of up to 12.5 µm (Fig. 3.15, Fig. 3.14 C- D). The highest concentration of H_2O_2 applied, 100 µM, caused a complete halt of cell growth and division; each cell remained at the same length throughout the course of the experiment. (Fig. 3.15, Fig. 3.14 E). The standard deviation for average cell length per microcolony overlapped greatly between conditions, such that the amount of stressor applied is a poor predictor of cell length (Fig. 3.15). We observed that the variability of cell length increased over time for colonies exposed to 0-50 µM H_2O_2, rising from near-zero at the start of imaging to 0.6, but remained close to zero for 100 µM H_2O_2 (Fig 3.14 F).

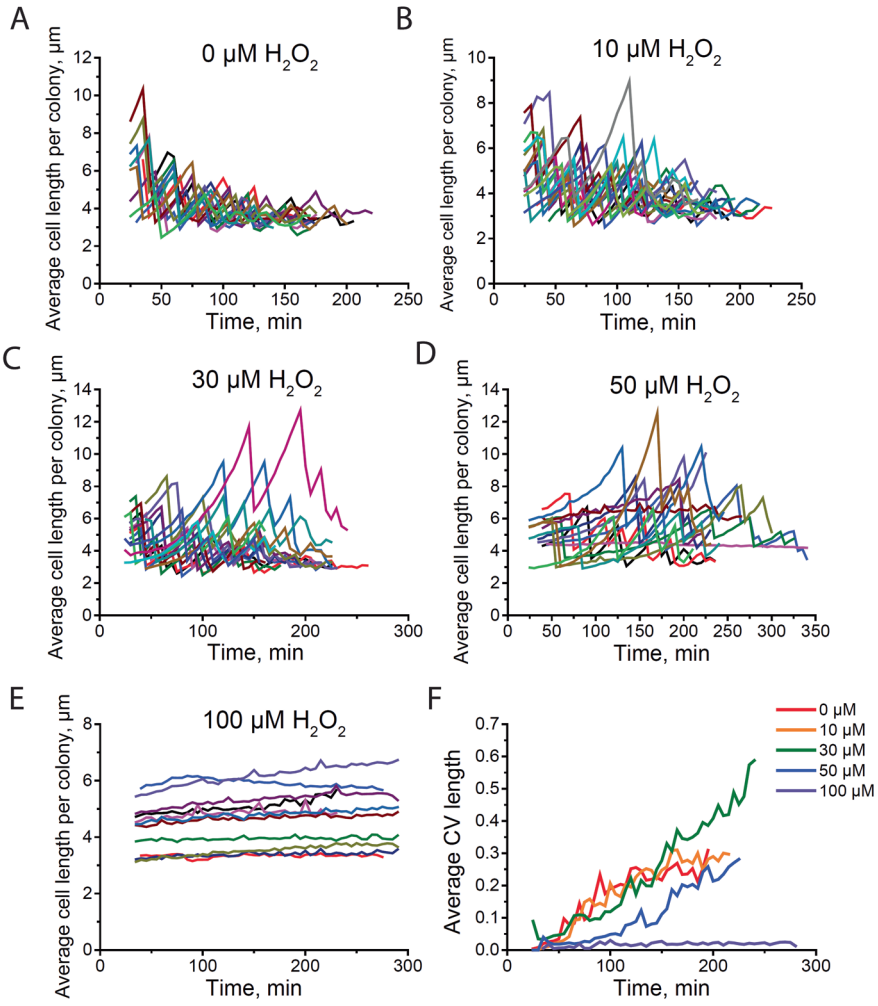

Fig. 3.14. Average cellular length over time. A-E) The average cellular length over time of microcolonies exposed to different concentrations of H_2O_2. Each line represents the average cellular length of all cells within one microcolony. F) The average coefficient of variation (CV) over time of the cell length of all the microcolonies exposed to the same stress condition, for varying concentrations of H_2O_2.

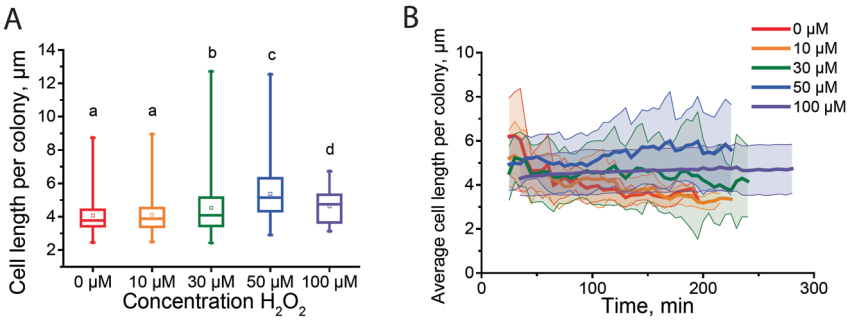

Fig. 3.15. Effects of oxidative stress on cellular length. A) Distribution of the length of all cells in a microcolony, averaged over all timepoints within each experiment, for different concentrations of H_2O_2. The top and bottom of the vertical bars represent the maximum and the minimum length values, respectively; the top and bottom of the rectangular box represent the 75th and the 25th percentile; the horizontal line within the box is the median; and the square in the box is the mean value. The letters represent the statistical significance: samples with different letters are statistically different (ANOVA test, $p < 0.05$). B) The average length of all cells within the microcolonies over time, for varying concentrations of H_2O_2. The shaded areas represent the standard deviation.

The measurement of growth rate over time also allowed us to evaluate cellular fitness over time upon exposure to oxidative stress. The instantaneous growth rate, µ, was calculated by fitting the cell length over time to an exponential function [42]. Cell width was not seen to vary significantly during the experiments. We calculated the average instantaneous growth rate of all the cells within a microcolony at each point in time (Fig. 3.16). The cells exposed to either 0 µM or 10 µM hydrogen peroxide showed a similar, slightly increasing growth rate over time, ranging between 1.1 and 1.8 $\mu\ h^{-1}$ (Fig. 3.16 A-B). Each further increase of the stressor concentration led to a reduction of cell growth. We observed that at 30 µM H_2O_2 the colonies grew only moderately during the initial part of the experiment, with an average starting growth rate of approximately 0.6 $\mu\ h^{-1}$, but showed a complete recovery of growth over several hours (Fig. 3.16 C). At 50 µM concentration of hydrogen peroxide, the growth was severely affected. Initial growth rates of 0.2- 0.3 $\mu\ h^{-1}$ increased slowly over time but only partially recovered over the course of imaging (Fig. 3.16 D). When the hydrogen peroxide was increased to 100 µM, cellular growth was completely stalled during the entire duration of the imaging (Fig. 3.16 E). Overall, increasing concentrations of H_2O_2 resulted in a greater initial decrease in cell growth and increasingly impaired recovery of cell growth over time (Fig. 3.16 F).

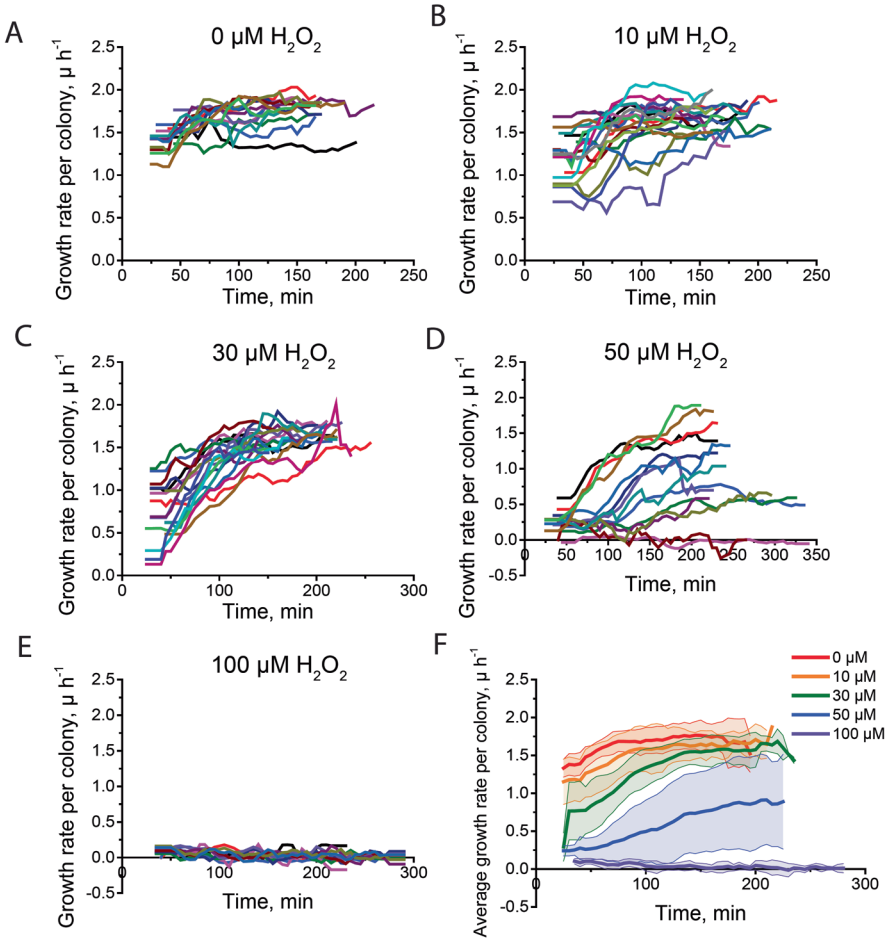

Fig. 3.16. Oxidative stress suppresses initial rates of cellular growth. A-E) The average instantaneous growth rate of all the cells within a colony over time, for different concentrations of H_2O_2. Each line represents the average growth rate of all cells within one microcolony. F) The average growth rate over time of all the colonies in the presence of the same concentration of H_2O_2. The shaded areas represent the standard deviation.

Analysis of the average growth rate per microcolony over the duration of the experiment revealed that concentrations of H_2O_2 up to 30 µM had moderate effects on the average growth rate, producing a decrease from 1.9 µ h^{-1} at 0 µM to 1.4 µ h^{-1} at 30 µM. Strong reduction of growth was observed at exposure to 50 µM H_2O_2 with an average of 0.6 µ h^{-1}, and at 100 µM cell growth was negligible, with an average growth rate of 0.01 µ h^{-1} (Fig. 3.17 A). The coefficients of variation for the average growth rates were low for the 0-30 µM H_2O_2 conditions, ranging from 0.09-0.24, while the variation for 50 µM H_2O_2 was extremely high at 0.75 (Fig. 3.17 B). For 100 µM H_2O_2 the coefficient of variation could not be accurately calculated because the mean value of the growth rate was close to zero for most microcolonies. Higher H_2O_2 concentrations were correlated with higher coefficient of variation values (Fig. 3.17 C). Thus, an increase in H_2O_2 concentration was strongly correlated with both a decrease in growth rate and an increase in growth rate variability, primarily for the higher concentrations of stressor.

To analyze the relationship between Dps induction parameters and cellular growth, we determined Pearson correlation coefficients between the average growth rate within microcolonies and the intensity and the duration of induction peaks. Between the average growth rate and amplitude of Dps induction for all stress conditions compared simultaneously, we observed a strong negative correlation (R= -0.71) with a p value < 0.0001 (Fig. 3.13 B). Interestingly, the correlation coefficients calculated within each stress condition were dramatically weaker, with an average of 0.03, and not significantly correlated. Similarly, the correlation coefficient comparing the growth rate and the time to reach the maximum fluorescence was strongly negative when calculated over all conditions (R= -0.85) with a p value < 0.0001, but much weaker within each individual condition (average R= -0.18) (Fig. 3.13 C). Lower average growth rate was therefore seen to be strongly associated with both higher *dps* expression and a longer induction time over a range of H_2O_2 concentrations.

We further analyzed the relationship between the mean fluorescence signal per colony and the mean growth rate per colony over time, identifying three response categories. The first category consisted of colonies that showed a small-amplitude decrease over time of the fluorescence signal with a constant high growth rate. All the colonies grown without H_2O_2 and 37% of the colonies grown in 10 µM H_2O_2 showed this response (Fig. 3.18 A, D). In the second category, the colonies exhibited a steady increase of growth rate over time, starting around 0.5 µ h^{-1} and reaching values around 1.8-2 µ h^{-1}. The fluorescence signal initially increased, reached its peak value, and then decreased again. 63% of colonies exposed to 10 µM H_2O_2, 100% of the colonies at 30 µM H_2O_2, and 79% of the colonies at 50 µM H_2O_2 showed this behavior (Fig. 3.18 B, D). The third category contained colonies in which the fluorescence signal increased robustly over time while the growth rate remained constantly low. This category captured 21% of the colonies exposed to 50 µM H_2O_2 and 100% of the colonies at 100 µM H_2O_2 (Fig. 3.18 C, D).

The presence of these three distinct patterns may suggest a threshold model of *dps* promoter activation, perhaps due to still-uncharacterized internal regulatory processes.

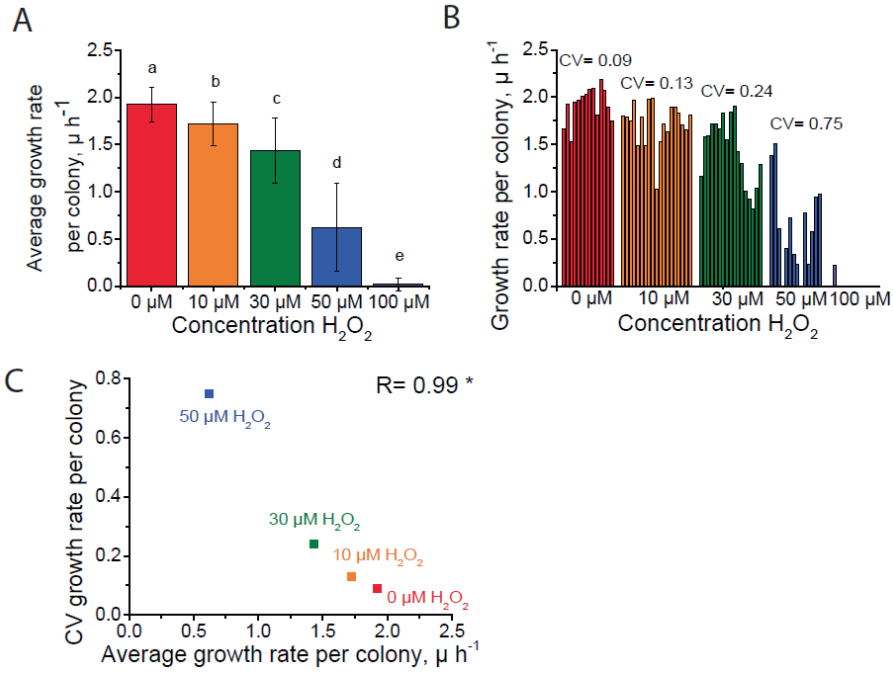

Fig. 3.17. Variation in microcolony growth rate increases at lower growth rates. A) The average growth rate per microcolony, averaged over all cells over all timepoints for each microcolony, for each concentration of H_2O_2. The error bars represent the standard deviation. The letters represent the statistical significance: samples labeled with different letters are statistically different (ANOVA test, $p < 0.05$). B) The average growth rate for each microcolony, and the coefficient of variation (CV) of growth rate among microcolonies, for each H_2O_2 concentration. Two of the microcolonies exposed to 50 μM H_2O_2 and ten of the microcolonies exposed to 100 μM H_2O_2 are not visible in the plot because their average growth rate is 0. C) Scatter plot of the coefficient of variation vs. the average growth rate for each concentration of H_2O_2. R represents the correlation coefficient. *= $p < 0.05$.

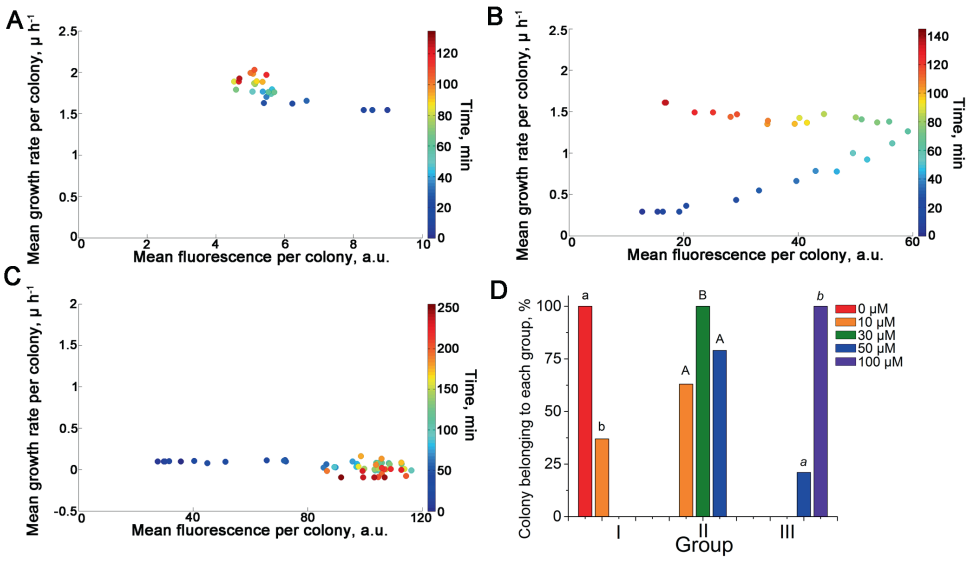

Fig. 3.18. Microcolonies exhibited three categories of Dps response. A-C) Scatter plots of the mean fluorescence signal and the mean growth rate per microcolony, over time, for example microcolonies in each category. Each dot represents the average fluorescence and the average growth rate of a single microcolony at a specific timepoint, colored to indicate the timepoint. A) Category I: a constant high growth rate associated with a slightly decreasing, low fluorescence signal . B) Category II: a steady increase in growth rate over time associated with a pulse of fluorescence signal. C) Category III: a robust increase in fluorescence signal over time associated with a constant low growth rate. D) The percentage of microcolonies in each response category, for each concentration of H_2O_2.

3.4 Discussion

In this study we have investigated for the first time the Dps stress response at the single-cell level. When exposed to H_2O_2, *E. coli* cells exhibit a single pulse of activation of the *dps* promoter. Higher concentrations of H_2O_2 induce an increase in both the intensity and duration of the activation pulse. The correlation between cellular growth and stressor intensity is quite non-linear. Low H_2O_2 concentrations initiate a robust Dps response but have little effect on cellular growth, while higher concentrations of H_2O_2 slow down the growth rate dramatically and cause high variability. Cells exposed to the same H_2O_2 concentration do not receive a growth advantage in case of higher Dps induction. The

recovery from stress may thus rely more upon the degree of damage generated in individual cells than to the strong induction of specific stress response proteins.

3.4.1 Stressor intensity predicts pulse amplitude and duration but not growth rate variability

The single pulse of induction of the *dps* promoter likely arises from more general features of the oxidative stress-induced response in *E. coli*. In the presence of H_2O_2, *dps* activation is regulated by the OxyR protein [25], a key regulator of the adaptive response to oxidative stress [45, 46]. During exponential growth, H_2O_2 converts OxyR protein to an oxidized active form that recruits σ^{70}-RNA polymerase to initiate *dps* transcription [25]. In *E. coli* cells treated with 200 µM H_2O_2, OxyR was fully converted to its oxidized form within 30 seconds of exposure to the stressor. Thereafter, OxyR reverted back to its reduced form with a half-life of ~ 5 minutes, and no oxidized OxyR was detected after 10 minutes [47]. This transient activation response provides a potential window for *dps* transcription lasting only on the order of minutes. Specific analysis of *dps* transcription kinetics in cells exposed to 10 µM H_2O_2 revealed *dps* induction to be active for a limited period of time as well. Maximum levels of *dps* transcript were detected at 1 minute after exposure, followed by a steady decrease until returning to background levels by 20 minutes post exposure [48]. Following the decrease of OxyR activity, transcriptional repression of *dps* occurs via the formation of an unproductive complex between the nucleoid-associated protein Fis and σ^{70} on the *dps* promoter [26], that may provide stringent downregulation of *dps* transcription at the end of its pulse of activation. The observed pulse in the produced protein related to the transcriptional pulse. When the burst of dps expression ends, the dilution occurred due to substantial colony growth and a small contribution of photobleaching may be responsible for the decrease in the fluorescence signal observed.

We observe a correlation between the amount of stress applied to the cells and the peak intensity of the Dps response, which saturates at the highest concentrations of stressor (Fig. 3.11). A correlation between the magnitude of the stress and the duration of the Dps response is also indicated by our observations (Fig. 3.12), so that stronger stresses are associated with both longer and stronger *dps* expression. The speed of the initial increase of gene expression was seen to be similar under all conditions, such that stronger Dps responses are achieved by modulation of the duration of expression. However, not all bacterial stress response genes show a similar pattern of expression. In *Bacillus subtilis*, the addition of increasing concentrations of stressors results in transcription of the general stress response factor σ^B with either an increase in peak amplitude but no alteration in the duration of the response [34] or an increase in the frequency of pulses of induction, accompanied by only weak changes in pulse amplitude and duration [32]. In

contrast, the highly modulated duration of the Dps response under varying intensities of oxidative stress may be a strategy to allow for an extended period of repair under conditions of more extensive damage.

Over a range of H_2O_2 concentrations, lower average growth rate is strongly correlated with both stronger *dps* expression and a longer induction time (Fig. 3.13). Interestingly, cells exposed to the same concentration of H_2O_2 do not receive a growth advantage from increased levels of *dps* expression but instead exhibit similar or slower growth, even in the 50 μM H_2O_2 condition where *dps* expression levels varied by up to 4-fold. This observation indicates that the kinetics of recovery from stress are not dictated by the magnitude of induction of specific stress response enzymes. Rather, we propose that individual cells may vary significantly in their amount of oxidative damage, such that cells sustaining more damage both have slower growth and induce a larger stress response. The development of real-time *in vivo* markers of oxidative damage will be quite interesting for study of the relationship between damage and stress response induction.

Analysis of the stress conditions separately reveals that a low dose of H_2O_2 does not result in a major reduction in cell growth rate, although the *dps* gene is already transcribed (Fig. 3.15, 3.16). When the H_2O_2 concentration reaches a critical level, the bacteria exhibit extremely high variability in growth rate. This variability does not correlate with either the intensity or the variability of *dps* expression (Fig. 3.11, 3.17). Noise in metabolic gene expression has been shown to affect the growth stability of a cell under conditions of active metabolism [31]. While metabolic reactions are crucial to synthesize enzymes and molecules necessary for cell development, stress response processes are responsible for maintaining the stability of cellular equilibrium under disruptive conditions. The observed variation in cell growth during exposure to high levels of oxidative stress might be linked to increased stochastic noise of one or more essential metabolic pathways under these conditions.

3.4.2 Cell-to-cell variability in *dps* expression is greater between microcolonies

The Dps response to oxidative stress shows some features of excitable dynamics, a class of transient cellular differentiation in which cells probabilistically enter into an ON state and return to the initial OFF state after a certain stereotypical period of time [49]. Within the resolution of our experiments, we detect a single burst of transcription that rapidly activates a temporary stress-response state (Fig. 3.5, 3.6). Unlike a true excitable noise-triggered system, the return to an OFF state is not stereotypical in the case of *dps* transcription. Instead, the return to the initial state occurs after a variable period of time that partially depends on growth kinetics. Additionally, we do not observe probabilistic

entry into the ON state. Instead, every cell that was exposed to hydrogen peroxide was seen to initiate *dps* transcription, and the kinetics and amplitude of the stress response were synchronized over each microcolony throughout the duration of imaging.

Cells lacking the *dps* gene are more sensitive to oxidative stress, showing dramatically reduced viability and elevated DNA damage [16, 18, 23]. Because the Dps protein is a key protector in stress survival, especially during the initial stage of the exposure, the non-probabilistic initiation of *dps* transcription allows all affected cells to respond to the oxidative damage. The similar kinetics of the *dps* response among individual cells within microcolonies is likely a consequence of the majority of the active *dps* transcription taking place in the single-cell stage, before the founding cell has undergone cell division. Once an oxidatively damaged cell resumes growth, the profile of the response is primarily reflective of dilution only, which seems to exhibit low variation (Fig. 3.5).

The profile of the *dps* response showed greater variability between different microcolonies exposed to the same amount of stress than among different cells within microcolonies (Fig. 3.5, 3.6). While some of this variability may originate from non-homogeneous distribution of hydrogen peroxide in the environment, a relatively moderate amount of site-to-site variability was observed on the agarose pads. Most of the variability observed in the *dps* responses is likely due to differences between the progenitor cells of each individual colony. Non-genetic cell-to-cell heterogeneity within a clonal population is common to many biological processes [33] and can arise from a broad range of phenomena including noise in gene expression or intracellular protein concentration, stochastic biochemical interactions, or non-synchronicity in cell cycle stage [29, 50-52]. A genome-wide survey of phenotypic noise over approximately 75% of *E. coli* promoters found that stress-response genes such as *dps* exhibit particularly variable expression during non-stressful growth [52]. On top of this baseline variability, we find that the variability in *dps* promoter activity can increase more than three-fold between non-stress and high-stress conditions (Fig. 3.6). Whether this dramatic increase in variability under stress or upregulation is a common feature of all bacterial genes or is limited to certain functional classes will require further investigation.

3.5 Tables

Table 1

List of the strains, plasmids and oligonucleotides.

Strain	**Genotype**	**Source**
dps-mCherry	*E. coli* K-12 strain W3110, *dps::dps-mCherry*	This work
Plasmids	**Genotype**	**Source**
pM1	pBAD33 containing the *dps-mCherry* cassette	This work
pROD22	pUC18 containing the *mCherry* gene	[37]
pET17b-dps	pET17b containing the *dps* gene	[23]

Table 2

List of the primers

Primers	**Sequence (5'-3')**
MDM1	GATCCCCGGGTACCGAGCTC
MDM2	CAAGCTTGGCTGTTTTGGCG
MDM3	CATCAAGAGGATATGAAATTATGGCTATCATTAAAGAGTTC
MDM4	TTACTTGTACAGCTCGTCCATGC
MDM5	GTTTATCGAGTCTAACATCGAATAACATCAAGAGGATATGAAATTATG
MDM6	TTCTCTCATCCGCCAAAACAGCCAAGCTTGTTACTTGTACAGCTCGTCC
MDM7	TAGCGAATTCGAGCTCGGTACCCGGGGATCATGAGTACCGCTAAATTAGT
MDM8	CATAATTTCATATCCTCTTGATGTTATTCGATGTTAGACTCGATAAAC
MDM9	TACTTAATCTCGTTAATTACTGGGACATAACATCAAGAGGATATGAAATTA TGAGTACCGCTAAATTAG
MDM10	AGGAAGCCGCTTTTATCGGGTACTAAAGTTCTGCACCATCAGCGATGGATT TACTTGTACAGCTCGTCCA

3.6 References

1. Ron, E., *Bacterial Stress Response*, in *The Prokaryotes*, E. Rosenberg, et al., Editors. 2013, Springer Berlin Heidelberg. p. 589-603.
2. Gross, C.A., et al., *The functional and regulatory roles of sigma factors in transcription.* Cold Spring Harb Symp Quant Biol, 1998. **63**: p. 141-55.
3. Paget, M.S. and J.D. Helmann, *The sigma70 family of sigma factors.* Genome Biol, 2003. **4**(1): p. 203.
4. Gruber, T.M. and C.A. Gross, *Multiple sigma subunits and the partitioning of bacterial transcription space.* Annu Rev Microbiol, 2003. **57**: p. 441-66.
5. Hengge-Aronis, R., *Signal transduction and regulatory mechanisms involved in control of the sigma(S) (RpoS) subunit of RNA polymerase.* Microbiol Mol Biol Rev, 2002. **66**(3): p. 373-95.
6. Battesti, A., N. Majdalani, and S. Gottesman, *The RpoS-mediated general stress response in Escherichia coli.* Annu Rev Microbiol, 2011. **65**: p. 189-213.
7. Korshunov, S. and J.A. Imlay, *Two sources of endogenous hydrogen peroxide in Escherichia coli.* Mol Microbiol, 2010. **75**(6): p. 1389-401.
8. Imlay, J.A., *The molecular mechanisms and physiological consequences of oxidative stress: lessons from a model bacterium.* Nat Rev Microbiol, 2013. **11**(7): p. 443-54.
9. Imlay, J.A., *Cellular defenses against superoxide and hydrogen peroxide.* Annu Rev Biochem, 2008. **77**: p. 755-76.
10. Robinson, J.M., *Phagocytic leukocytes and reactive oxygen species.* Histochem Cell Biol, 2009. **131**(4): p. 465-9.
11. Lamb, C. and R.A. Dixon, *The Oxidative Burst in Plant Disease Resistance.* Annu Rev Plant Physiol Plant Mol Biol, 1997. **48**: p. 251-275.
12. He, X., et al., *Oral-derived bacterial flora defends its domain by recognizing and killing intruders--a molecular analysis using Escherichia coli as a model intestinal bacterium.* Microb Ecol, 2010. **60**(3): p. 655-64.
13. Cohen, G.M. and M. d'Arcy Doherty, *Free radical mediated cell toxicity by redox cycling chemicals.* Br J Cancer Suppl, 1987. **8**: p. 46-52.
14. Almiron, M., et al., *A novel DNA-binding protein with regulatory and protective roles in starved Escherichia coli.* Genes Dev, 1992. **6**(12B): p. 2646-54.
15. Choi, S.H., D.J. Baumler, and C.W. Kaspar, *Contribution of dps to acid stress tolerance and oxidative stress tolerance in Escherichia coli O157:H7.* Appl Environ Microbiol, 2000. **66**(9): p. 3911-6.
16. Nair, S. and S.E. Finkel, *Dps protects cells against multiple stresses during stationary phase.* Journal of Bacteriology, 2004. **186**(13): p. 4192-4198.
17. Jeong, K.C., et al., *Acid stress damage of DNA is prevented by Dps binding in Escherichia coli O157: H7.* Bmc Microbiology, 2008. **8**.
18. Martinez, A. and R. Kolter, *Protection of DNA during oxidative stress by the nonspecific DNA-binding protein Dps.* J Bacteriol, 1997. **179**(16): p. 5188-94.
19. Meyer, A.S. and D.C. Grainger, *The Escherichia coli Nucleoid in Stationary Phase.* Adv Appl Microbiol, 2013. **83**: p. 69-86.

20. Zhao, G.H., et al., *Iron and hydrogen peroxide detoxification properties of DNA-binding protein from starved cells - A ferritin-like DNA-binding protein of Escherichia coli.* Journal of Biological Chemistry, 2002. **277**(31): p. 27689-27696.
21. Grant, R.A., et al., *The crystal structure of Dps, a ferritin homolog that binds and protects DNA.* Nature Structural Biology, 1998. **5**(4): p. 294-303.
22. Bozzi, M., et al., *A novel non-heme iron-binding ferritin related to the DNA-binding proteins of the Dps family in Listeria innocua.* J Biol Chem, 1997. **272**(6): p. 3259-65.
23. Karas, V.O., I. Westerlaken, and A.S. Meyer, *The DNA-Binding Protein from Starved Cells (Dps) Utilizes Dual Functions To Defend Cells against Multiple Stresses.* J Bacteriol, 2015. **197**(19): p. 3206-15.
24. Ali Azam, T., et al., *Growth phase-dependent variation in protein composition of the Escherichia coli nucleoid.* J Bacteriol, 1999. **181**(20): p. 6361-70.
25. Altuvia, S., et al., *The dps promoter is activated by OxyR during growth and by IHF and sigma S in stationary phase.* Mol Microbiol, 1994. **13**(2): p. 265-72.
26. Grainger, D.C., et al., *Selective repression by Fis and H-NS at the Escherichia coli dps promoter.* Mol Microbiol, 2008. **68**(6): p. 1366-77.
27. Yamamoto, K., et al., *The Escherichia coli K-12 MntR miniregulon includes dps, which encodes the major stationary-phase DNA-binding protein.* J Bacteriol, 2011. **193**(6): p. 1477-80.
28. Brehm-Stecher, B.F. and E.A. Johnson, *Single-cell microbiology: tools, technologies, and applications.* Microbiol Mol Biol Rev, 2004. **68**(3): p. 538-59, table of contents.
29. Elowitz, M.B., et al., *Stochastic gene expression in a single cell.* Science, 2002. **297**(5584): p. 1183-6.
30. Junker, J.P. and A. van Oudenaarden, *Every cell is special: genome-wide studies add a new dimension to single-cell biology.* Cell, 2014. **157**(1): p. 8-11.
31. Kiviet, D.J., et al., *Stochasticity of metabolism and growth at the single-cell level.* Nature, 2014. **514**(7522): p. 376-9.
32. Locke, J.C., et al., *Stochastic pulse regulation in bacterial stress response.* Science, 2011. **334**(6054): p. 366-9.
33. Martins, B.M. and J.C. Locke, *Microbial individuality: how single-cell heterogeneity enables population level strategies.* Curr Opin Microbiol, 2015. **24**: p. 104-12.
34. Young, J.W., J.C. Locke, and M.B. Elowitz, *Rate of environmental change determines stress response specificity.* Proc Natl Acad Sci U S A, 2013. **110**(10): p. 4140-5.
35. Gibson, D.G., et al., *Enzymatic assembly of DNA molecules up to several hundred kilobases.* Nature Methods, 2009. **6**(5): p. 343-U41.
36. Guzman, L.M., et al., *Tight regulation, modulation, and high-level expression by vectors containing the arabinose PBAD promoter.* J Bacteriol, 1995. **177**(14): p. 4121-30.
37. Reyes-Lamothe, R., et al., *Independent positioning and action of Escherichia coli replisomes in live cells.* Cell, 2008. **133**(1): p. 90-102.

38. Young, J.W., et al., *Measuring single-cell gene expression dynamics in bacteria using fluorescence time-lapse microscopy.* Nat Protoc, 2012. **7**(1): p. 80-8.
39. Schneider, C.A., W.S. Rasband, and K.W. Eliceiri, *NIH Image to ImageJ: 25 years of image analysis.* Nat Methods, 2012. **9**(7): p. 671-5.
40. Csoka, B. and G. Nagy, *Determination of diffusion coefficient in gel and in aqueous solutions using scanning electrochemical microscopy.* Journal of Biochemical and Biophysical Methods, 2004. **61**(1-2): p. 57-67.
41. Gendron, P.O., F. Avaltroni, and K.J. Wilkinson, *Diffusion Coefficients of Several Rhodamine Derivatives as Determined by Pulsed Field Gradient-Nuclear Magnetic Resonance and Fluorescence Correlation Spectroscopy.* Journal of Fluorescence, 2008. **18**(6): p. 1093-1101.
42. Boulineau, S., et al., *Single-cell dynamics reveals sustained growth during diauxic shifts.* PLoS One, 2013. **8**(4): p. e61686.
43. Nghe, P., et al., *Microfabricated polyacrylamide devices for the controlled culture of growing cells and developing organisms.* PLoS One, 2013. **8**(9): p. e75537.
44. Otsuka, Y., et al., *GenoBase: comprehensive resource database of Escherichia coli K-12.* Nucleic Acids Res, 2015. **43**(Database issue): p. D606-17.
45. Christman, M.F., G. Storz, and B.N. Ames, *OxyR, a positive regulator of hydrogen peroxide-inducible genes in Escherichia coli and Salmonella typhimurium, is homologous to a family of bacterial regulatory proteins.* Proc Natl Acad Sci U S A, 1989. **86**(10): p. 3484-8.
46. Tao, K., et al., *Purification and characterization of the Escherichia coli OxyR protein, the positive regulator for a hydrogen peroxide-inducible regulon.* J Biochem, 1991. **109**(2): p. 262-6.
47. Aslund, F., et al., *Regulation of the OxyR transcription factor by hydrogen peroxide and the cellular thiol-disulfide status.* Proc Natl Acad Sci U S A, 1999. **96**(11): p. 6161-5.
48. Michan, C., et al., *In vivo transcription of the Escherichia coli oxyR regulon as a function of growth phase and in response to oxidative stress.* J Bacteriol, 1999. **181**(9): p. 2759-64.
49. Eldar, A. and M.B. Elowitz, *Functional roles for noise in genetic circuits.* Nature, 2010. **467**(7312): p. 167-73.
50. Davey, H.M. and D.B. Kell, *Flow cytometry and cell sorting of heterogeneous microbial populations: the importance of single-cell analyses.* Microbiol Rev, 1996. **60**(4): p. 641-96.
51. Schwabe, A. and F.J. Bruggeman, *Contributions of cell growth and biochemical reactions to nongenetic variability of cells.* Biophys J, 2014. **107**(2): p. 301-13.
52. Silander, O.K., et al., *A genome-wide analysis of promoter-mediated phenotypic noise in Escherichia coli.* PLoS Genet, 2012. **8**(1): p. e1002443.

Chapter 4

Single-cell analysis of the Dps response to alkaline pH stress

During their development, bacteria encounter adverse growth conditions. Exposure to alkaline environment is one the challenges that microorganisms face. The Dps response mechanism, crucial to cell survival, is triggered by several factors including the basic pH environment. In this chapter, we investigated at the single-cell level the transcriptional dynamics of *dps* promoter activity during exposure to pH 7, 8, 9 and 10 utilizing time-lapse fluorescence microscopy imaging. One single pulse of *dps* activation was detected, with an amplitude and a duration proportional to the pH increase. Cellular growth was not related to the intensity of the stressor. pH values up to 9 did not lead to a growth decrease. Correlation analysis showed that increased levels of *dps* expression did not confer a growth advantage among cells exposed to the same stress condition. Higher levels of *dps* transcription were associated with similar or slower growth compared to cells with lower *dps* expression. These results strengthen the thesis that it is the amount of damage experienced by each cell more than the expression of a stress protein that determines the recovery from stress.

4.1 Introduction

The ability of bacterial cells to grow and survive under alkaline environmental conditions is crucial for their survival. Many natural bacterial environments have an alkaline pH. In the human body, enteric bacteria need to possess alkali resistance in order to survive in the pancreatic duct where the pH is ≥ 10 [1]. The gut of many insects has also been measured to have high pH [2, 3]. The marine environment has an alkaline pH of around 8.3 [4].

Bacteria need to preserve their cytosolic pH to be compatible with the structure and the functionality of the proteins responsible for their metabolism and development. The pH of cytosol is actively controlled and stabilized at around 7.4 to 7.8 [5, 6]. The main strategy applied by bacteria to maintain this homeostatic condition is the use of proteins that catalyze the active transport of protons (H^+) across their membranes. These transporters generate the proton motive force (PMF), an electrochemical gradient of H^+ across the cell membrane, composed of a transmembrane pH gradient and a transmembrane electrical potential [7]. Primary proton pumps (i.e. respiratory or proton-pumping ATPase complexes) or secondary active transporters (i.e. ATPases that uptake external protons in exchange for cations, such as K^+ and Na^+) are the key factors responsible for PMF generation [8].

During growth at pH 7, neutralophilic bacteria such as *E. coli* show a small pH gradient, with internal pH higher than the external environment and a considerable transmembrane electrical potential, with negatively charged internal contents compared with the external surrounding [7, 9]. When exposed to alkaline environments, bacteria need to actively transport H^+ ions into the cytosol by using cation/proton antiporters. This mechanism leads to the generation of an inverted pH gradient (acidic inside) that produces a lightly alkaline cytoplasmic pH [6]. In this type of environment, *E. coli* cells increase the expression of the non-proton-pumping cytochrome *bd* and decrease the expression of the proton-pumping respiratory chain complexes. The increased expression of the F_1F_O-ATP synthase further contributes to the retention of H^+ in the cell [6, 10, 11]. The role of the cation/proton antiporters is crucial during high pH exposure to maintain an adequate transmembrane electrical potential [12]. They catalyze the intake of protons in exchange for Na^+ or K^+ with an unequal ratio between the intake and the extrusion of ions [13]. In *E. coli* this major role is played by the Na^+/H^+ antiporter NhaA during alkaline pH homeostasis [14].

In this challenging environment, the Dps protein plays an important role. Its protective function during exposure to several types of stress, including oxidative stress, metal exposure, heat shock, UV and gamma irradiation, is well-established [15, 16]. In *E.coli*, the survival of *dps* mutants exposed to both extreme acidity (pH 5) and alkaline condition (pH 12) drops drastically compared to wild-type cells [16]. The *dps* gene was

shown to be more highly expressed than at pH 7 during both acid (pH 5) and alkaline (pH 8.7) pH exposure [10]. The protective effect of Dps is attributed to its dual biochemical functions: the ability to binds to DNA and the ferroxidase activity [17]. A complex regulatory network controls intracellular levels of Dps. In different growth and environmental conditions, the *dps* promoter is recognized by the σ^{70} (housekeeping) or σ^{S} (stationary phase) sigma factor [18-20]. Despite the knowledge acquired about the regulation of the Dps protein during several stress exposure, very little is known of the molecular mechanism of the *dps* regulation in alkaline pH conditions. Moreover, the Dps response is not yet understood at the single-cell level.

In this work, we investigated the transcriptional activation kinetics of the *dps* promoter at the single-cell level during exposure to alkaline pH stress. We detected one single pulse of *dps* activation, with an intensity and duration proportional to the pH increase. Cellular growth was not correlated with the stress exposure. Increased pH values did not lead to a decrease in growth when the pH was lower than 9. pH 10 resulted in robust *dps* induction and a decrease of the growth rate. Correlation analysis of cells exposed to the same stressor revealed that increased levels of *dps* expression did not confer a growth advantage. Higher levels of *dps* activation were associated with similar or slower growth compared to cells with lower *dps* expression. As also demonstrated during oxidative stress exposure in chapter 3, this behavior indicated that perhaps the extent of damage perceived by each cell led to both reduced cell growth and increased *dps* promoter activation.

4.2 Material and methods

4.2.1 Growth conditions for microscopy

The bacterial strain *dps-mCherry* used in this work was created from the *E. coli* K-12 strain W3110 (CGSC# 4474) by replacement of the genomic *dps* gene with a *dps-mCherry* cassette as described in chapter 3 (3.2.1).

To perform the single-cell experiments, a colony of the strain was inoculated into Hi-Def Azure medium (3H500, Teknova) supplemented with 0.2% glucose. After an overnight growth at 37°C, the preculture was diluted 1:100 and grown for around 2 hours at 37°C until early exponential phase ($O.D._{600}$ 0.2-0.3). The culture was diluted into Hi-Def Azure medium supplemented with 0.2% glucose to $O.D._{600}$=0.005 for seeding onto the agarose pad.

4.2.2 Agarose pad preparation

Agarose pads were prepared with a modified version of the protocol described in chapter 3 (3.2.3). To expose the cells to different pH values, the pads were assembled with Hi-Def Azure medium supplemented with 0.2% glucose at pH 7, 8, 9 and 10, pH-adjusted through the addition of 1 M NaOH. The media were filter sterilized and stored at 4°C.

The agarose pads were freshly prepared for each experiment. 2% (w/v) low-melt Agarose LE (V3125, Promega) was added to 5 mL of Hi-Def Azure medium at different pH and dissolved by microwaving. Agarose pads were formed immediately thereafter, and the bacterial culture was seeded onto individual agarose pads. The pad was inverted onto a 4-well slide-base tissue culture chamber (Starstedt), and the chamber was sealed. The monolayer growth of the cells was detected through a fluorescence microscope.

4.2.3 Fluorescence microscopy and data analysis

As described in chapter 3 (3.2.4), individual microcolonies were imaged by time-lapse fluorescence microscopy using an inverted microscope (Olympus IX81), equipped with an AMH-200 lamp (Andor) and a Cy3 filter cube (4040C). Images were acquired with a Luca R EMCCD camera (Andor). Experiments were performed at 37°C using an incubation chamber (H201-T, Okolab). Phase contrast images (500 ms exposure time, 3 images +/- 0.2 µm from the focus) and fluorescence images (100 ms exposure time) were recorded every 5 min.

Images were analyzed using a custom Matlab program [21] based on the Schnitzcells program [22], as described in chapter 3 (3.2.5). Briefly, the data analysis consisted of three steps: segmentation, tracking, and extraction of cell parameters (fluorescence, length, growth rate). Each phase contrast image (average of three) was segmented, and the cell tracking was performed. Lastly, the desired parameter of each cell were extracted. For every microcolony, the fluorescence intensity curves were fitted with the best-fitting polynomial (degree 5), and the maximum of this function was considered to be the maximum fluorescence intensity. The duration of *dps* expression was calculated as time from the beginning of the exposure to pH stress. The cell length was calculated as the length of the axis between the two poles of a cell, and instantaneous growth rate was extracted by fitting the cell length over time to an exponential function.

4.3 Results

4.3.1 *dps* expression dynamics during alkaline pH exposure

To investigate the transcriptional dynamics of the *dps* gene in individual *E. coli* cells exposed to a growth medium with alkaline pH, we utilized the *dps-mCherry* reporter strain. This strain was previously described in the prior chapter as a reporter to study the *dps* transcriptional response to oxidative stress. The *mCherry* and the *dps* genes were both present in the *dps* operon, with *mCherry* immediately downstream of *dps* and under the transcriptional control of the *dps* promoter. mCherry operated as reporter for *dps* transcription, allowing the detection of *dps* promoter activity in single cells through the detection of its fluorescence.

The bacterial cells were grown to early exponential phase in growth medium with a neutral pH 7, then transferred to agarose pads prepared with alkaline pH media, between pH 7 and 10. Bacterial microcolonies were then analyzed using quantitative time-lapse fluorescence microscopy to determine the *dps* promoter activity in each cell over time.

Analysis of the fluorescence images showed a different fluorescence signal in cells exposed to a neutral pH 7 compared to those in the presence of a basic pH. The colonies grown on pH 7 exhibited a fluorescence indistinguishable from background during the entire duration of the measurement (Fig. 4.1 A). At pH 9, we detected a distinct fluorescent signal (Fig. 4.1 B).

The microscopy data was analyzed using modified Schnitzcells software [22] to extract the cell parameters. The fluorescence intensity values were calculated within each cell as average fluorescence per unit area [21]. At pH 7 and 8, the fluorescence intensity of each individual bacteria within a microcolony over time was very low (Fig. 4.2 A-B). Exposure to higher pH led to an increase in the fluorescence signal. The cells exposed to pH 9 showed an increase in fluorescence signal, with a smaller amplitude of the pulse (Fig. 4.2 C). pH 10 induced a single pulse of fluorescence, highly synchronized between the cells constituting each microcolony throughout the duration of the imaging (Fig. 4.2 D).

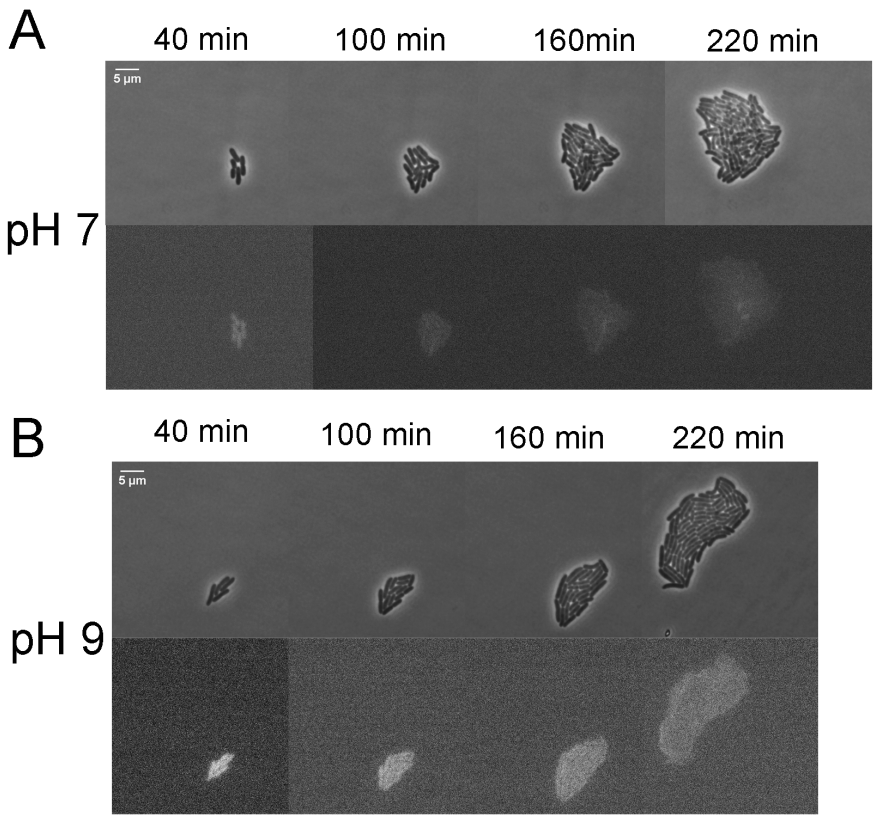

Fig. 4.1 Time-lapse fluorescence of microcolonies exposed to pH 7 (A) and 9 (B). For each panel, the upper images are phase-contrast images, and the lower images are fluorescence images from a single microcolony over time.

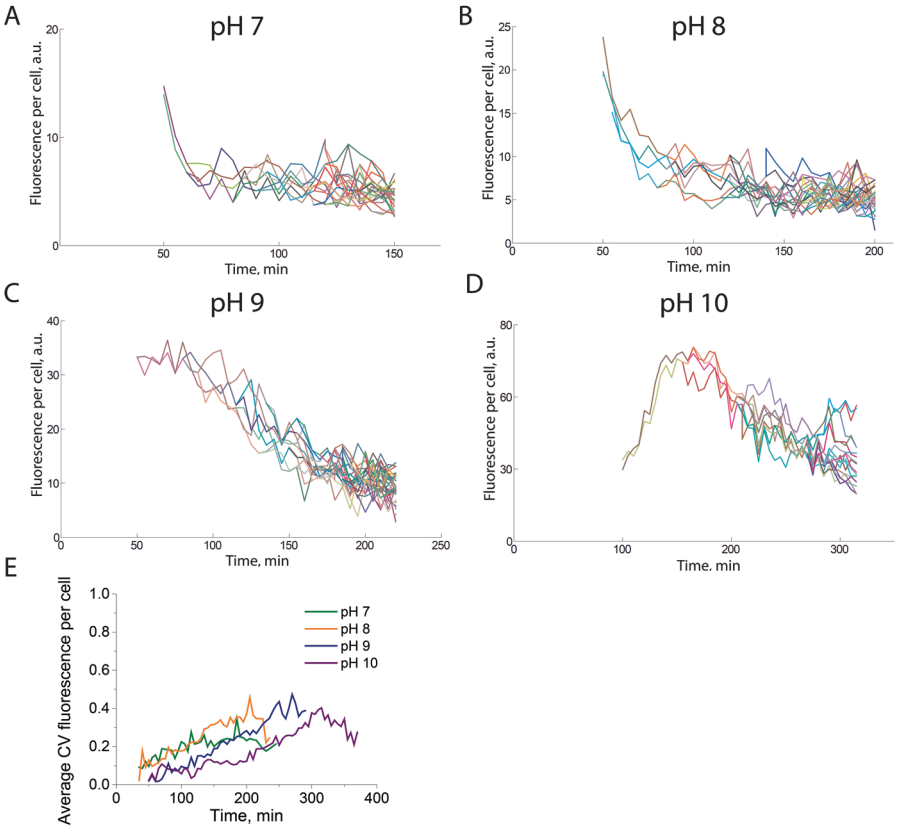

Fig. 4.2 Exposure to alkaline pH induces a single pulse of *dps* promoter activity synchronized over the individual cells within each microcolony. A-D) Examples of fluorescence intensity over time in individual cells in a microcolony exposed to pH between 7 and 10. Each line represents a single cell. F) The average coefficient of variation (CV) over time of the fluorescence intensity ithin a microcolony

The comparison of fluorescent responses between microcolonies was performed by determining the average fluorescence values of all the cells within a microcolony, at each time point (Fig. 4.3). Comparison of the average fluorescence signal per microcolony over time for all colonies within each condition revealed that all the colonies exposed to pH 7 and 8 showed a low average fluorescence signal that decreased slightly over the duration of the imaging (Fig. 4.3 A-B). When exposed to pH 9, the cells showed an average increase in the fluorescence signal over time. Two distinct subgroups could be observed: colonies that showed an increase in fluorescence over time that took the form of one major peak and colonies that displayed a monotonic decrease of the fluorescence signal (Fig. 4.3 C). The fluorescence signal of the colonies at pH 10 typically appeared as a single peak over time (Fig. 4.3 D). Colonies exposed to the same condition showed varying peak amplitudes and durations (Fig. 4.3 C-D).

At pH 7 and 8 the average fluorescence profile over time for all colonies within each stress condition showed a large overlap in the standard deviations, whereas the increase in the signal for the cells exposed to pH 9 and 10 is associated with the amount of the applied stress (Fig. 4.3 E). The curve of the pH 9 fluorescence values showed a pulse of expression with a very small amplitude, with a maximum fluorescence around 25 a.u. The average fluorescence curve of the colonies exposed to pH 10 displayed a major peak 2-fold higher than the pulse observed at pH 9 (Fig. 4.3 E). Overall, increasing pH values resulted in an increase of the duration and the intensity of fluorescence signal.

To evaluate the variability of the average fluorescence signal among different microcolonies in the same stress condition, the coefficient of variation at each time point was calculated. The average CV values among microcolonies within each condition was calculated over time, and these CV values observed at pH 7 and 8 remained between 0.2 and 0.3. At pH 9 and 10 the CV values were higher, reaching a maximum value of around 0.4 at pH 9 and 0.5 at pH 10 before decreasing again (Fig. 4.3 F).

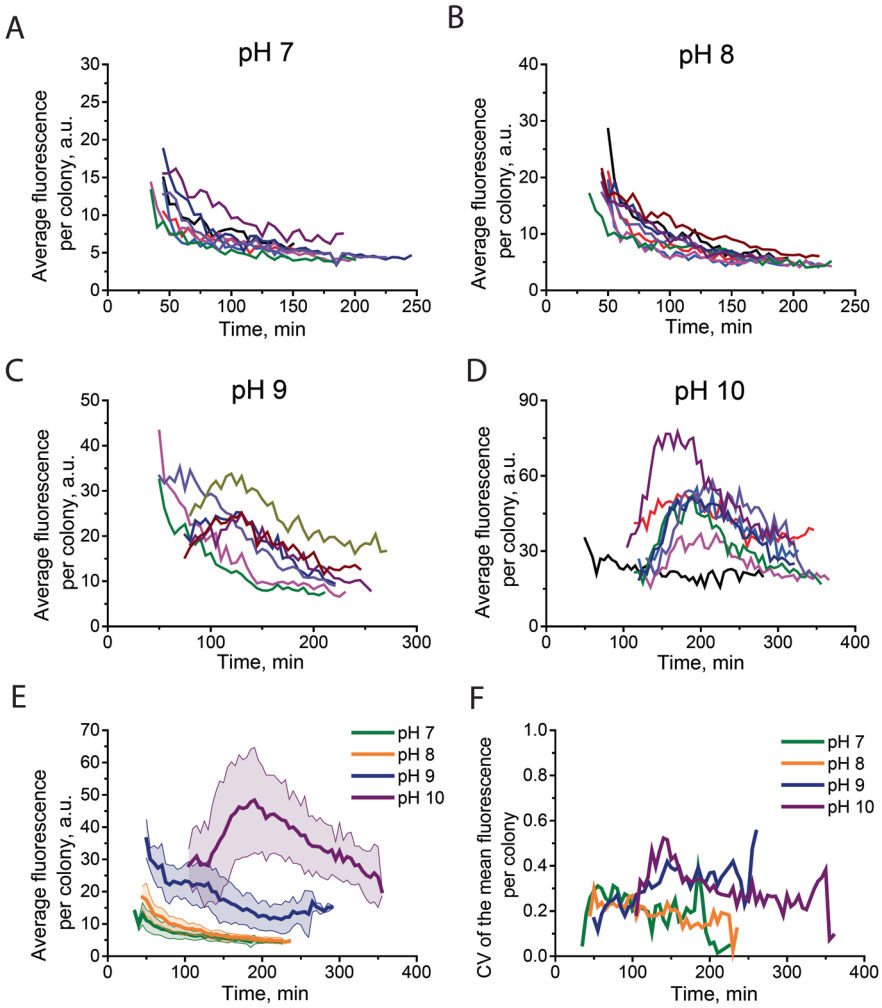

Fig. 4.3 *dps* response per microcolony. Increase in pH leads to a single pulse of *dps* transcription activation. A-D) The average fluorescence signal over time of microcolonies exposed to different pH. Each line represents the average fluorescence intensity of all cells within one microcolony. E) The average fluorescence signal over time of all the colonies exposed to the same stress condition. The shaded area represents the standard deviation. F) The coefficient of variation (CV) over time of the average fluorescence signals of all the microcolonies exposed to the same stress condition.

4.3.2 Correlations between alkaline pH exposure and the dynamics of *dps* induction

Analysis of the intensity and duration of the peak of fluorescence signal was performed for each individual colony by fitting the curve by describing the average fluorescence intensity with a polynomial function to extract the maximum value of the fluorescence and the time point at which it was reached. We calculated the average maximum fluorescence values of colonies exposed to the same pH value. Higher pH values correlated with higher peak amplitude for all the conditions analyzed (Fig. 4.4 A). The variability in the maximum fluorescence intensity among different colonies growing in the same pH was evaluated by calculation of the coefficient of variation. These values ranged between 0.12 and 0.33, with the maximum variability observed at pH 10 (Fig. 4.4 B). A positive correlation was observed between the coefficient of variation and the maximum fluorescence values over the different pH values. Increasing pH values corresponded to an increase of maximum fluorescence and coefficient of variation (Fig. 4.4 C).

The average time at which the maximum fluorescence signal was determined for colonies in the same experimental condition. No statistical differences in the average time of maximum fluorescence were observed for microcolonies exposed to pH 7 and pH 8. The time to the peak was significantly higher for pH 9 and 10, with an increase proportional to the increase in the pH (Fig. 4.5 A). The coefficient of variation for the time at which microcolonies reached the maximum fluorescence intensity was calculated between colonies in the same stress condition. The values ranged between 0.11 and 0.45 (Fig. 4.5 B). No statistically significant trend was observed between the coefficient of variation values and the time to the maximum fluorescence, over the several stresses (Fig. 4.5 C). An overall analysis of our data revealed that an increase of pH value in the growth media drove an increase of *dps* promoter activity, in both intensity and duration.

In order to test for correlations between the strength and the duration of the *dps* stress induction, the correlation coefficient value was calculated of the average values for individual microcolonies of the maximum fluorescence intensity versus the duration of the increase in fluorescence were compared. When all the stress conditions were examined simultaneously, the Pearson correlation coefficient (R) was 0.78 (p value < 0.00001.) (Fig. 4.6 A). Thus, a longer period of *dps* gene expression were correlated with fluorescence peaks of higher amplitude. Contrarily, the data for each individual pH value of the growth media considered separately showed a weaker, non-significant correlation, ranging from 0.32 to 0.73 (Fig. 4.6 A).

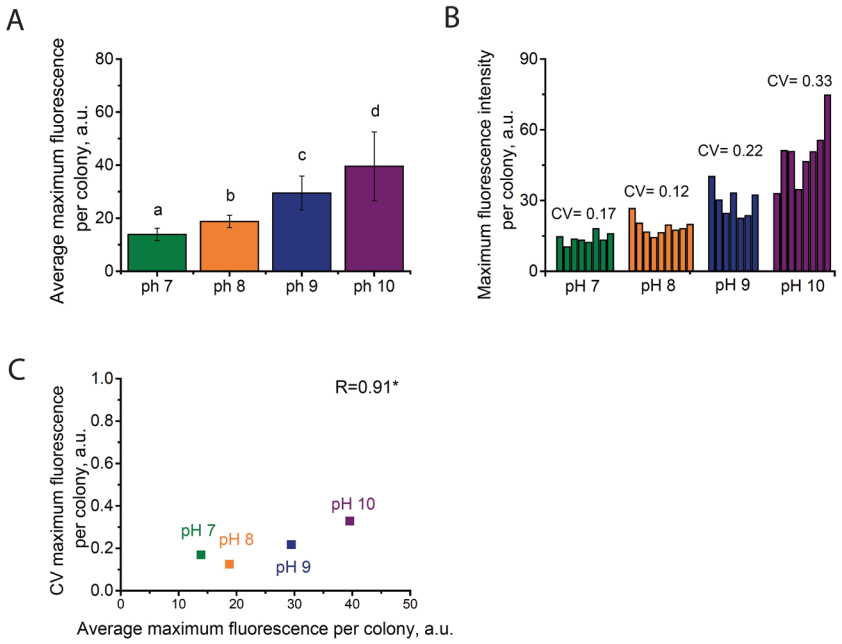

Fig. 4.4 The intensity of the *dps* induction increases with more alkaline pH. A) The average maximum values of the fluorescence signal for each microcolony, for each pH value. The error bars represent the standard deviation. The letters represent the statistical significance: samples labeled with different letters are statistically different (ANOVA test, $p < 0.05$). B) The maximum values of the fluorescence signal for each microcolony, and the coefficient of variation (CV) of the maximum fluorescence intensity among microcolonies, for each for each pH value. C) Scatter plot of the coefficient of variation vs. the average maximum fluorescence value for each concentration of H_2O_2. R represents the Pearson correlation coefficient. * = $p<0.05$

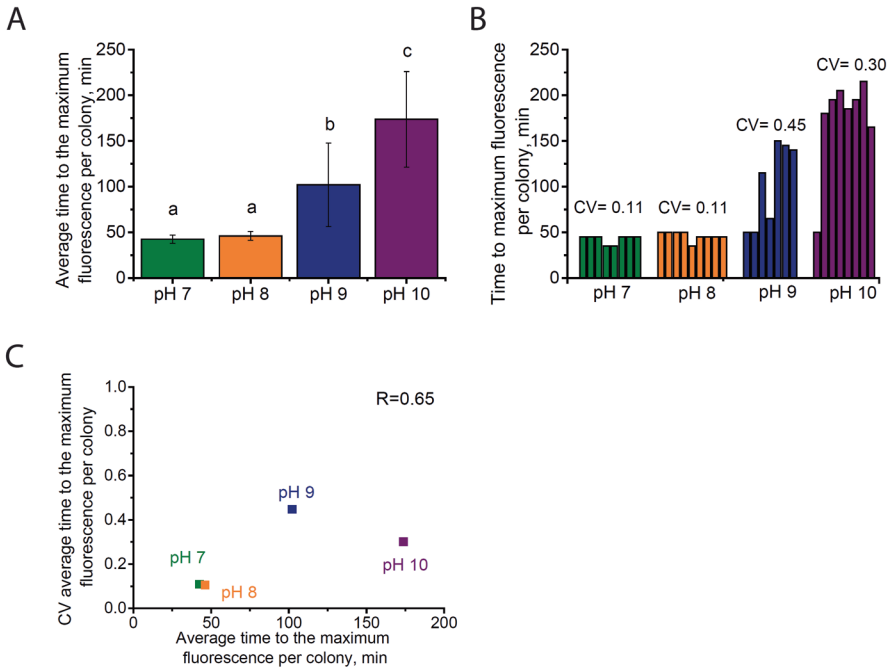

4

Fig. 4.5 The duration of *dps* induction increases with exposure to more alkaline pH. A) The average time at which the maximum value of the fluorescence signal was observed for each microcolony, for each pH analyzed. The error bars represent the standard deviation. The letters represent the statistical significance: samples labeled with different letters are statistically different (ANOVA test, $p < 0.05$). B) The time to the maximum value of the fluorescence signal for each microcolony, and the coefficient of variation (CV) of the time to the maximum fluorescence intensity among microcolonies, for each pH analyzed. C) Scatter plot of the coefficient of variation vs. the time to the average maximum fluorescence value for each pH condition. R represents the Pearson correlation coefficient.

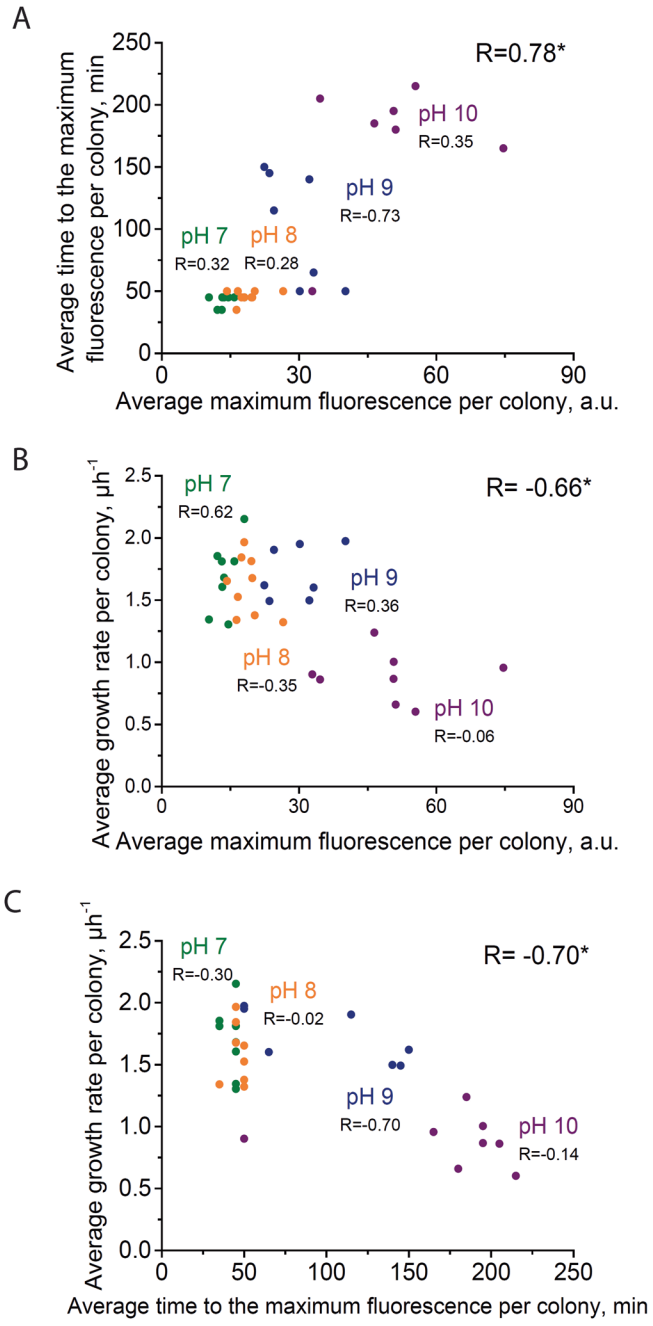

Fig. 4.6 Correlations coefficients between growth rate, intensity, and duration of Dps induction.

Fig. 4.6 Correlations coefficients between growth rate, intensity, and duration of Dps induction. A) Scatter plot of the average maximum fluorescence intensity vs. the average time to the maximum fluorescence for individual microcolonies. B) Scatter plot of the average growth rate per colony vs. the average maximum fluorescence intensity for individual microcolonies. C) Scatter plot of the average growth rate per colony vs. the average time to the maximum fluorescence intensity for individual microcolonies. Each dot represents a single microcolony. Microcolonies exposed to the same pH are represented in the same color. The R value in the top right corner of each graph represents the **Pearson** correlation coefficient over all the data. The R below the label for each concentration of H_2O_2 represents the R value calculated over all microcolonies in each stress condition. * = $p<0.05$.

4.3.3 Effect of alkaline pH stress on the cellular growth

In order to assess the effect of alkaline pH exposure on bacterial health, the cell length and growth rate were evaluated. The cellular length was calculated as the length of the axis between the two extremities of a cell [21]. The comparison of the average length of all cells within a colony over time for all the colonies analyzed showed a trend for the cells exposed to pH 7, 8 and 9: the cell length slightly decreased over time, from an average of around 4-5 µm down to around 3 µm (Fig. 4.7 A, B, C, E). Exposure to pH 10 led to a higher proportion of elongated cells, reaching a length of up to 11 µm (Fig. 4.7 D, E). The standard deviation for average cell length per microcolony overlapped greatly between exposure to pH 7, 8 and 9, with a clear distinction of the values for pH 10. This indicates that the cell length may be an indicator of the amount of pH stress applied, at high pH values (Fig. 4.7 E, F).

The second parameter to evaluate cellular health over time upon exposure to basic pH stress was the measurement of growth rate over time. The instantaneous growth rate, µ, was calculated by fitting the cell length over time with an exponential function [21]. The average instantaneous growth rate of all the cells within a microcolony at each point in time was calculated (Fig. 4.8). The cells exposed to pH 7 and pH 8 showed a similar and constant growth rate over time, ranging between 1.4 and 2 $\mu\ h^{-1}$ (Fig. 4.8 A, B). An increase of the stressor intensity resulted in a reduction of cell growth rate. We observed that at pH 9 the growth rate ranged between 0.7 and 1.8 $\mu\ h^{-1}$, maintaining for most microcolonies a steady trend during the time of the measurement (Fig. 4.8 C). pH values of 10 severely affected the growth. The cell proliferation was nearly constant over time, ranging between 0.6 and 0.8 $\mu\ h^{-1}$ during the entire duration of the measurements (Fig. 4.8 D). The analysis of the average growth rate values of all the colonies exposed to the same stress condition showed an overlap of the standard deviations between the vales at pH 7, 8 and 9, with higher standard deviation observed for pH 9. The pH 10 condition led to a strong growth decrease. (Fig. 4.8 E).

The analysis of the average growth rate per microcolony showed that pH values between 7 and 9 did not affect the average cell growth, which was around 1.6 μ h^{-1} for each of these pH conditions. A significant reduction of growth was observed when the cells were exposed to pH 10 with an average of 0.9 μ h^{-1} (Fig. 4.9 A). For all the stress conditions analyzed, the coefficients of variation for the average growth rates were low, ranging from 0.12 and 0.16 (Fig. 4.9 B). Higher average growth rate was not associated with lower average CV (R not statistically significant) (Fig. 4.9 C), although the coefficient of variation values were low.

In order to calculate correlation coefficients a correlation between *dps* promoter activity and cellular growth, we compared the average growth rate within microcolonies and the intensity and the duration of the fluorescence peaks. A negative correlation (R= -0.66, p value= 3.8E-05) was identified between the average growth rate and maximum fluorescence intensity of *dps* induction for all stress conditions compared simultaneously (Fig. 4.6 B). Interestingly, the correlation coefficients calculated within each stress condition were weaker, with an average of 0.07, and not significantly correlated. Similarly, the comparison of the average growth rate and the average time to reach the maximum fluorescence showed a strongly negative correlation when calculated over all conditions (R= -0.70, p value < 0.0001), but much weaker within each condition (average R= -0.15, p > 0.05) (Fig. 4.6 C). Our observations indicated that lower average growth rates were strongly associated with both stronger *dps* gene expression and a longer induction time over all the stresses investigated.

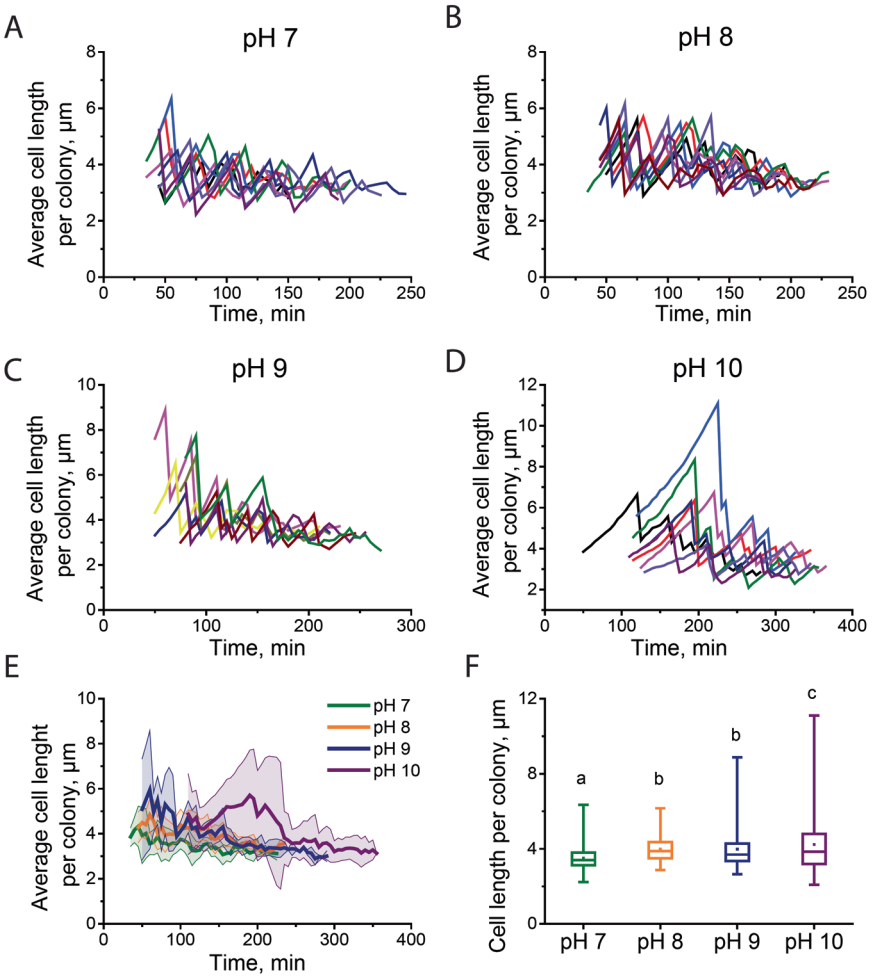

Fig. 4.7 Effect of alkaline pH exposure on cellular length. A-D) The average cellular length over time of microcolonies exposed to different alkaline pH. Each line represents the average cellular length of all cells within one microcolony. E) The average length of all cells within the microcolonies over time, for each pH analyzed. The shaded areas represent the standard deviation. F) Distribution of the length of all cells in a microcolony, averaged over all timepoints within each experiment, for different alkaline pH. The top and bottom of the vertical bars represent the maximum and the minimum length values, respectively; the top and bottom of the rectangular box represent the 75th and the 25th percentile; the horizontal line within the box is the median; and the square in the box is the mean value. The letters represent the statistical significance: samples with different letters are statistically different (ANOVA test, $p < 0.05$).

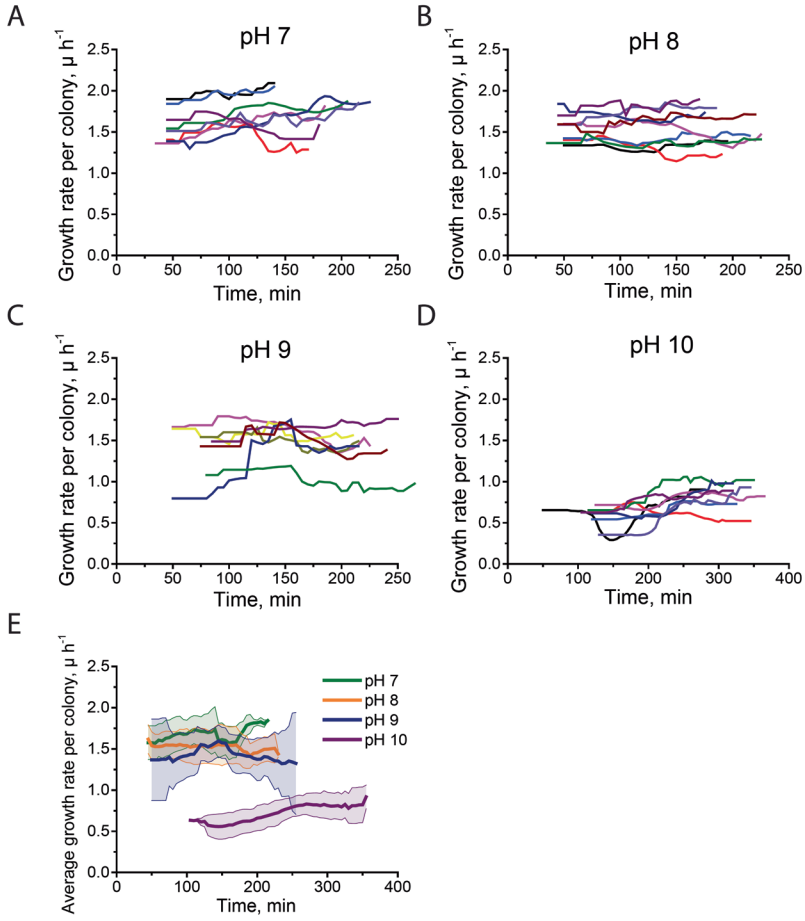

Fig. 4.8 Colonies exposed to the same alkaline pH showed a constant growth over time. A-D) The average instantaneous growth rate of all the cells within a microcolony over time, for different pH. Each line represents the average growth rate of all cells within one microcolony. E) The average growth rate over time of all the microcolonies in the presence of the same alkaline pH. The shaded areas represent the standard deviation.

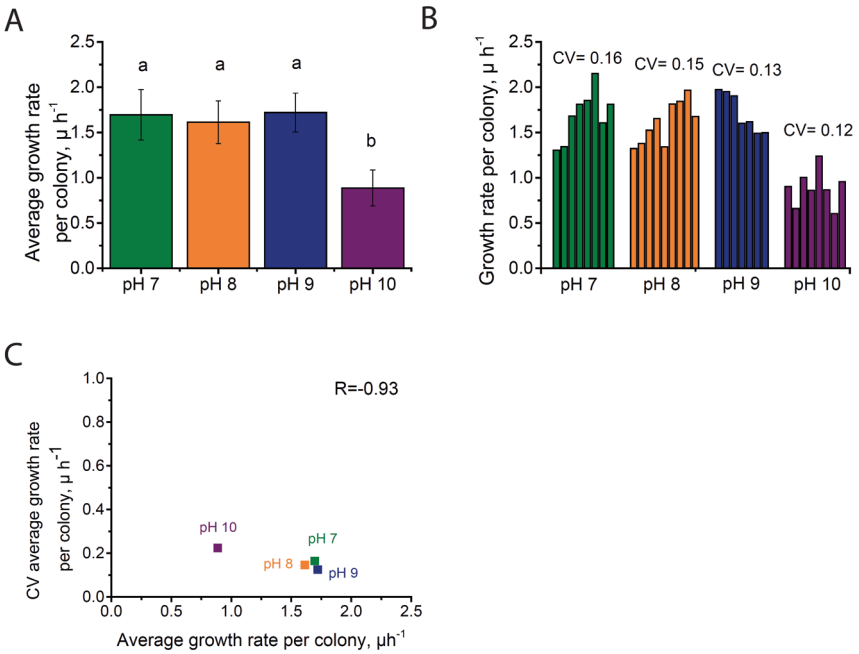

Fig. 4.9 Higher alkaline pH strongly affects the average colony growth. A) The average growth rate per microcolony, averaged over all cells over all timepoints for each microcolony, for each pH value. The error bars represent the standard deviation. The letters represent the statistical significance: samples labeled with different letters are statistically different (ANOVA test, $p < 0.05$). B) The average growth rate for each microcolony, and the coefficient of variation (CV) of growth rate among microcolonies, for each pH value. C) Scatter plot of the coefficient of variation vs. the average growth rate for each concentration of H_2O_2. R represents the correlation coefficient.

4.4 Discussion

In this work, we have investigated for the first time the Dps stress response upon exposure to alkaline pH at the single-cell level. Similar features can be observed when comparing this response to the oxidative stress response described in chapter 3. As in the response to H_2O_2, *E. coli* cells exposed to alkaline media display a single pulse of *dps* promoter activation. The increase in the intensity and the duration of the induction pulse are associated with an increase of the pH in the growth media. Contrarily, the correlation

between growth rate and stress intensity is not so evident as for oxidative stress. Cells with stronger and longer *dps* induction do not show an improvement in growth, as also observed during hydrogen peroxide exposure. Our findings suggest that the severity of the damages in each individual cell may be more responsible for the stress recovery than the strong induction of a specific stress response protein such as Dps.

A single pulse of induction of the *dps* promoter appeared upon exposing bacterial cells to pH 9. An increase in both the intensity and duration of this pulse occurred at pH 10. We previously described in chapter 3 the hypothesis that the transcriptional response of *dps* during exposure to H_2O_2 is related to the lifetime of the oxidized form of OxyR [18, 19]. A similar mechanism might occur during alkaline pH conditions, although a mechanistic similarities between oxidative stress and alkaline exposure have not yet been observed. The molecular mechanism and the regulatory enzymes that control the transcriptional regulation of *dps* upon exposure to alkaline stress are still an open question. During alkaline stress, *E.coli* cells showed high membrane permeability and a reduced membrane potential, associated with reduced cell viability. Increase in the production of reactive oxygen species (ROS) was observed only at pH 12 [23]. The *dps* gene has been shown to be expressed during both acid (pH 5) and alkaline (pH 8.7) pH exposure [10]. *E. coli* cells lacking the *dps* gene are more sensitive to extreme pH [16]. It was also shown that σ^S is required in *E. coli* and *S. typhimurium* for survival during severe alkaline pH 9.8 and to induce stationary-phase acid resistance [24]. During stationary phase or starvation, it was shown in fact that σ^S controls the expression of the *dps* gene (Altuvia et al., 1994, Freundlich et al., 1992). We hypothesize that *dps* is σ^S-regulated during exposure to alkaline media. The demonstration of this hypothesis will require a wider experimental investigation.

During exposure to alkaline pH, cells activate several response mechanisms. Microarray analysis has demonstrated that *E. coli* represses flagellar genes and genes involved in chemotaxis that dissipate the PMF. It represses also the proton pump cytochrome o and the NADH dehydrogenases I and II. *E. coli* induces instead the proteins that reduce the proton export, including the ATP synthase F_1F_0 and the cytochrome d [10]. *E. coli* also activates the SOS response [25], heat shock response [26] and CpxP envelope stress response [27]. The activation of these mechanisms may contribute to the observed Dps response.

We see a correlation between the amount of applied stress and both the intensity (Fig. 4.4) and the duration (Fig. 4.5) of the *dps* response. Thus, exposure to more alkaline pH is associated with both longer and stronger *dps* expression. The analysis of the average fluorescence of colonies exposed to the same condition over time (Fig. 4.3) showed that pH 7 and 8 do not lead to an induction of the *dps* transcription. pH 9 seems to be the point at which some bacterial cells need protection from the stressful condition. The intensity profile observed at pH 10 suggests that a higher amount of the protein

appears relevant for the survival. Exposure of *E. coli* to H_2O_2 also showed a correlation between the amount of stress and the intensity and duration of the Dps response (Chapter 3). The *dps* response curve plateaued at the highest concentrations of H_2O_2 stressor, 100 µM, due to a halt in the cell division. When the pulse of the expression ended, the dilution of the fluorescent protein seen at lower concentrations of H_2O_2 did not occur because the colonies did not expand. The stressful environment analyzed with alkaline stress, led to a reduced cell growth without the complete halt that was seen for oxidative stress. More extensive experiments are required to further characterize the response and identify the upper limit of pH that causes the saturation of the response.

Slower bacterial average growth rate is correlated with both stronger *dps* expression and a longer time of induction during exposure to alkaline stress (Fig. 4.6). The analysis of separate colonies exposed to the same stress condition showed that prolonged and stronger *dps* expression do not provide a growth advantage. This observation reflects a similar behavior observed during oxidative stress. Both considerations strengthen the hypothesis that the kinetics of recovery from stress do not rely on the induction of specific stress response proteins, but on the degree of damage caused by the exposure to hostile environmental condition in each individual cell. We suggest that cells that experience more damage have both slower growth and a larger induction of the Dps protein.

Analysis of cell growth in the separate stress conditions reveals that low alkaline pH values do not induce the reduction in cell growth rate that is instead observed at high alkalinity (Fig. 4.8, 4.9). At pH 8, *dps* transcription is not detectable, and the bacterial growth rate is comparable to that at pH 7, indicating that these environments do not represent a stressful condition that results in Dps expression. When the pH reaches 9, the *dps* response is induced with no alteration in the growth (Fig 4.2, 4.9). When pH is increased to 10, the cell growth is severely slowed but not completely halted (Fig. 4.8, 4.9). Increasing still farther the alkalinity of the growth medium may lead to a critical condition where the damages do not allow bacterial proliferation, as was observed during exposure to 100 µM H_2O_2 (Chapter 3).

The Dps response to oxidative stress exhibits excitable dynamics. The stress exposure induce in the bacteria a probabilistic ON state, and they subsequently return to the initial OFF state after a certain period of time (Chapter 3) [28]. Although a deeper analysis of the alkaline response is necessary, and a broader range of pH needs to be tested, an identical behavior was observed during exposure to alkaline pH. A single burst of transcription occurred in each cells, with no probabilistic event observed. The kinetics and amplitude of the response were synchronized over each colony through the entire duration of imaging. The induction of Dps protein occurred in all the cells in alkaline pH, with very low variability of response observed among cells in each individual colony (Fig 4.2). The transcription takes place in a limited time window at the initial stage of colony

development. Once the initial cells overcome the damages induced by the alkaline medium, the dilution factor appears to take the leading role in the response pattern.

Contrary to what we observed during exposure to H_2O_2 (Chapter 3), a low variability of response between microcolonies is observed during exposure to all the alkaline conditions tested. We hypothesize that the differences in *dps* transcription initiation in the case of H_2O_2 originate from differences in the level of stress experienced by the progenitor cells of the progenitor cells of the microcolony. Within cells in a clonal population, the heterogeneity or noise in the response is an important source of non-genetic variability [29]. The high homogeneity of *dps* activation during exposure to alkaline media both within and among microcolonies indicates a reduced relevance of the noise in this regulatory pathway. Moreover, this observation strengthens the hypothesis of a separate regulatory pathway that regulates the alkaline response, distinct from the control occurring during oxidative stress. Further investigations are required to confirm this hypothesis.

The results supported the hypothesis that the healing from the stress is interconnected with the amount of damage experienced by each cell. These observations suggested that, during alkaline pH exposure, the *dps* gene is subjected to a transcriptional regulation similar to the one observed during H_2O_2 stress. Further investigation will help to unravel the common regulatory members involved in both the responses.

4.5 References

1. Evans, D.F., et al., *Measurement of gastrointestinal pH profiles in normal ambulant human subjects.* Gut, 1988. **29**(8): p. 1035-41.
2. Brune, A. and M. Kühl, *pH profiles of the extremely alkaline hindguts of soil-feeding termites (Isoptera: Termitidae) determined with microelectrodes.* Journal of Insect Physiology, 1996. **42**(11–12): p. 1121-1127.
3. Lemke, T., et al., *Physicochemical conditions and microbial activities in the highly alkaline gut of the humus-feeding larva of Pachnoda ephippiata (Coleoptera: Scarabaeidae).* Appl Environ Microbiol, 2003. **69**(11): p. 6650-8.
4. Harvey, H.W., *The Chemistry and Fertility of Sea Waters, H. W. Harvey, Sc.D., F.R.S. Cambridge: Cambridge University Press, 1955.* Journal of the Marine Biological Association of the United Kingdom, 1956. **35**(01): p. 289-289.
5. Padan, E., D. Zilberstein, and H. Rottenberg, *The proton electrochemical gradient in Escherichia coli cells.* Eur J Biochem, 1976. **63**(2): p. 533-41.
6. Slonczewski, J.L., et al., *Cytoplasmic pH measurement and homeostasis in bacteria and archaea.* Adv Microb Physiol, 2009. **55**: p. 1-79, 317.
7. Kashket, E.R., *The proton motive force in bacteria: a critical assessment of methods.* Annu Rev Microbiol, 1985. **39**: p. 219-42.
8. Krulwich, T.A., G. Sachs, and E. Padan, *Molecular aspects of bacterial pH sensing and homeostasis.* Nat Rev Microbiol, 2011. **9**(5): p. 330-43.
9. Rottenberg, H., *The measurement of membrane potential and deltapH in cells, organelles, and vesicles.* Methods Enzymol, 1979. **55**: p. 547-69.
10. Maurer, L.M., et al., *pH regulates genes for flagellar motility, catabolism, and oxidative stress in Escherichia coli K-12.* J Bacteriol, 2005. **187**(1): p. 304-19.
11. Stancik, L.M., et al., *pH-dependent expression of periplasmic proteins and amino acid catabolism in Escherichia coli.* J Bacteriol, 2002. **184**(15): p. 4246-58.
12. Padan, E., et al., *Na(+)/H(+) antiporters.* Biochim Biophys Acta, 2001. **1505**(1): p. 144-57.
13. Macnab, R.M. and A.M. Castle, *A variable stoichiometry model for pH homeostasis in bacteria.* Biophys J, 1987. **52**(4): p. 637-47.
14. Padan, E., et al., *Alkaline pH homeostasis in bacteria: new insights.* Biochim Biophys Acta, 2005. **1717**(2): p. 67-88.
15. Almiron, M., et al., *A novel DNA-binding protein with regulatory and protective roles in starved Escherichia coli.* Genes Dev, 1992. **6**(12B): p. 2646-54.
16. Nair, S. and S.E. Finkel, *Dps protects cells against multiple stresses during stationary phase.* Journal of Bacteriology, 2004. **186**(13): p. 4192-4198.
17. Karas, V.O., I. Westerlaken, and A.S. Meyer, *The DNA-Binding Protein from Starved Cells (Dps) Utilizes Dual Functions To Defend Cells against Multiple Stresses.* J Bacteriol, 2015. **197**(19): p. 3206-15.
18. Altuvia, S., et al., *The dps promoter is activated by OxyR during growth and by IHF and sigma S in stationary phase.* Mol Microbiol, 1994. **13**(2): p. 265-72.
19. Grainger, D.C., et al., *Selective repression by Fis and H-NS at the Escherichia coli dps promoter.* Mol Microbiol, 2008. **68**(6): p. 1366-77.

20. Yamamoto, K., et al., *The Escherichia coli K-12 MntR miniregulon includes dps, which encodes the major stationary-phase DNA-binding protein.* J Bacteriol, 2011. **193**(6): p. 1477-80.
21. Boulineau, S., et al., *Single-cell dynamics reveals sustained growth during diauxic shifts.* PLoS One, 2013. **8**(4): p. e61686.
22. Young, J.W., et al., *Measuring single-cell gene expression dynamics in bacteria using fluorescence time-lapse microscopy.* Nat Protoc, 2012. **7**(1): p. 80-8.
23. Baatout, S., et al., *Physiological changes induced in bacteria following pH stress as a model for space research.* Acta Astronautica, 2007. **60**(4–7): p. 451-459.
24. Small, P., et al., *Acid and base resistance in Escherichia coli and Shigella flexneri: role of rpoS and growth pH.* J Bacteriol, 1994. **176**(6): p. 1729-37.
25. Schuldiner, S., et al., *Induction of SOS functions by alkaline intracellular pH in Escherichia coli.* J Bacteriol, 1986. **168**(2): p. 936-9.
26. Taglicht, D., et al., *An alkaline shift induces the heat shock response in Escherichia coli.* J Bacteriol, 1987. **169**(2): p. 885-7.
27. DiGiuseppe, P.A. and T.J. Silhavy, *Signal detection and target gene induction by the CpxRA two-component system.* J Bacteriol, 2003. **185**(8): p. 2432-40.
28. Eldar, A. and M.B. Elowitz, *Functional roles for noise in genetic circuits.* Nature, 2010. **467**(7312): p. 167-73.
29. Martins, B.M. and J.C. Locke, *Microbial individuality: how single-cell heterogeneity enables population level strategies.* Curr Opin Microbiol, 2015. **24**: p. 104-12.

Chapter 5

A microfluidics approach to study the Dps response to oxidative stress

Microfluidics is a powerful tool for the deeper investigation of many aspects of cell biology. The precise control of the growth environment, the automation of the data acquisition, and the small volume of fluids required are some of the advantages of this technique that has promoted its increasing utilization in several research fields. In this chapter, we applied a PDMS-based device in combination with a polyacrylamide hydrogel to study *dps* promoter activity in response to oxidative stress in single cells. A PDMS flow cell connected to an electric pump provided continuous medium perfusion within a growth chamber. The bacteria grew in a monolayer and were separated from the flow chamber by a polyacrylamide membrane. When the *E. coli* cells were exposed to H_2O_2 concentrations between 0 and 500 μM, a single pulse of *dps* activation was detected. The intensity of the *dps* induction was correlated to the amount of the applied stress, but no correlation was identified between the duration of the induction and the stress concentration. H_2O_2 amounts up to 30 μM did not alter the growth rate despite initiating *dps* transcription. Comparison of cells in the same stress condition showed that cells with more intense *dps* induction did not receive a growth advantage. The overall analysis of these results confirmed the observation of *dps* promoter activity dynamics from cells grown on agarose pads. It also reinforce the thesis that the stress recovery may rely more on the extent of damage in each individual cell than to the strong induction of specific stress proteins.

5.1 Introduction

Microfluidics is defined as "The science and technology of systems that process or manipulate small (10^{-9} to 10^{-18} liters) amounts of fluids, using channels with dimensions of tens to hundreds of micrometres" [1]. In recent years, the technological progress of research tools has led to the increasing use of microfluidic devices for deeper study of many aspects of cell biology [2], tissue culture [3], and microbiology [4]. One of the main advantages of the application of this technique include the possibility to precisely control the environment of the cell culture. This feature allows a continuous and regulated perfusion of nutrients to closely mimic the cellular microenvironment, an efficient exposure to chemical agents, and the creation of chemical gradients. The possibility of automation increases drastically the amount of parallel data acquisition with high temporal and spatial resolution. Another important advantage of microfluidic devices is the use of miniaturized components. Using smaller volume of fluids reduces the consumption of reagents, reducing the costs and the waste production [5-7].

In this chapter, we describe the application of a PDMS (polydimethylsiloxane)-based device in combination with a polyacrylamide hydrogel [8] to study the Dps response to oxidative stress. PDMS-based devices are a powerful platform for biology studies because of certain chemical characteristics of the polymer: biocompatibility [9, 10], transparency and low autofluorescence [11].These features support the creation of very narrow channels (few nanometers) that allow flow perfusion and prevent the escape of cells [12, 13]. PDMS is also permeable to gas but not to aqueous solutions, a feature that allows gas exchange for cell cultures and an accurate compartmentalization of separate chambers [14, 15].

Polyacrylamide hydrogels also present many advantages for the development of microfluidics devices. They are commonly used in the laboratory for DNA and protein studies, with low costs and simple handling protocols. Polyacrylamide is biocompatible [16, 17] and mechanically stronger than agarose gel, making it more suitable for microfabricated devices [8]. This gel is permeable to aqueous solutions and allows the diffusion of fluids. Moreover, this synthetic polymer cannot be metabolized by bacteria, ensuring precise control of the growth environment [8].

The device utilized in this work combines the advantages of both materials. The PDMS flow cell ensures a continuous perfusion of growth medium, through the connection to an electrical pump. The bacteria are separated from the flow chamber by polyacrylamide, in such a way that growth medium diffuses, but cells are not able to pass through it. The choice of studying the *dps* response with this device relies on the precise control of stressor delivery. The possibilities to regulate the timing of the stress exposure, to supply continuous fresh H_2O_2 solution to the cells and the homogeneous circulation of the stress solution in the growth chamber are the primary contributing factors for its

utilization. Contrarily, the cells grown on the agarose pads were exposed to the oxidative stress as soon as they were transferred on the pad, with no possibility of stress removal. Moreover, the H_2O_2 was added during the preparation of the pad with no possibility to control a potential degradation and with a modest variability of distribution observed.

The application of such microfluidics systems allowed the single-cell analysis of the Dps response during application of H_2O_2. One single pulse of promoter activity was identified during the exposure to concentrations of stressor between 0 and 500 µM, as was also shown during the utilization of agarose pads (Chapter 3). The intensity of the *dps* induction was correlated to the amount of the applied stress, but no correlation was identified between the duration of the induction and the stress concentration. Concentrations of H_2O_2 up to 30 µM initiated the *dps* transcription but did not affect cellular growth. The comparison of bacteria exposed to the same condition showed that cells with more intense *dps* induction did not receive a growth advantage. A similar behavior was observed also in microcolonies grown on agarose pads, supporting the thesis that this response was perhaps due to variation in the amount of damage experienced by individual cells.

5.2 Material and methods

5.2.1 Strain and growth conditions for microscopy

In this work, we used the *dps-mCherry* strain created from *E. coli* K-12 strain W3110 (CGSC# 4474) by replacement of the genomic *dps* gene with a *dps-mCherry* cassette as described in chapter 3 (3.2.1). One colony was inoculated overnight at 37°C into Hi-Def Azure medium (3H500, Teknova) supplemented with 0.2% glucose. The preculture was diluted 1:100 and grown at 37°C for around 2 hours until it reached early exponential phase ($O.D._{600}$ 0.2-0.3). The culture was diluted to $O.D._{600}$= 0.02 into Hi-Def Azure medium supplemented with 0.2% glucose and subsequently introduced into the microfluidic device.

5.2.2 Microfluidic device

5.2.2.1 Fabrication

The microfluidics device was manufactured as described in [8]. The fabrication of the device components was performed by D. Ershov (S. Tans research group, AMOLF,

Amsterdam). Briefly, the flow cell consisted of a PDMS control channel, a thin polyacrylamide gel, and a coverglass facing the microscope objective. Metal clamps held the layers together. Bacterial cells were placed between the coverglass and the polyacrylamide membrane. When connected to an electric syringe pump using tubing, the PDMS flow cell allowed a continuous and strictly regulated diffusion of the growth medium to the cells growing below the membrane (Fig. 5.1 A).

In more detail, the PDMS (Dow Corning) flow cell was shaped on a silicon wafer with SU-8 photoresist. The flow channel had a height of 113 µm, a width of 5 mm and a total length of 30 mm. The channel contains pillars to provide a uniform pressure on the polyacrylamide membrane surface. A 10% polyacrylamide gel was poured in a mold composed of a silanized glass slide and a silanized coverslip glass side held together by 3 layers of double- sided tape to allow a thickness of the gel of around 70 µm. Once solidified, the gel was stored in deionized water. At least two hours before conducting experiments, the gel was soaked in Hi-Def Azure medium supplemented with 0.2% glucose to allow the diffusion of nutrients to the bacteria. A glass cover slip 24x60x1.5 mm in size was placed as a bottom layer facing the membrane. The layers were held together by mechanical clamping (Fig. 5.1 A-B-C). The metal holders were custom-made. They consisted of two metal plates, held together by 4 screws. Each plate had a total dimension of 7.6x3.6x0.2 cm. In both plates, a square-shaped hole of 2x2 cm and centered in the middle of the plates was present to allow light to pass through during imaging. The top plate presented two identical rectangular openings on either side of the square to allow the positioning of the tubing for the input and output of fluids. When the device was constructed, the two layers fit on top of each other so that bolts were used to fix the plates.

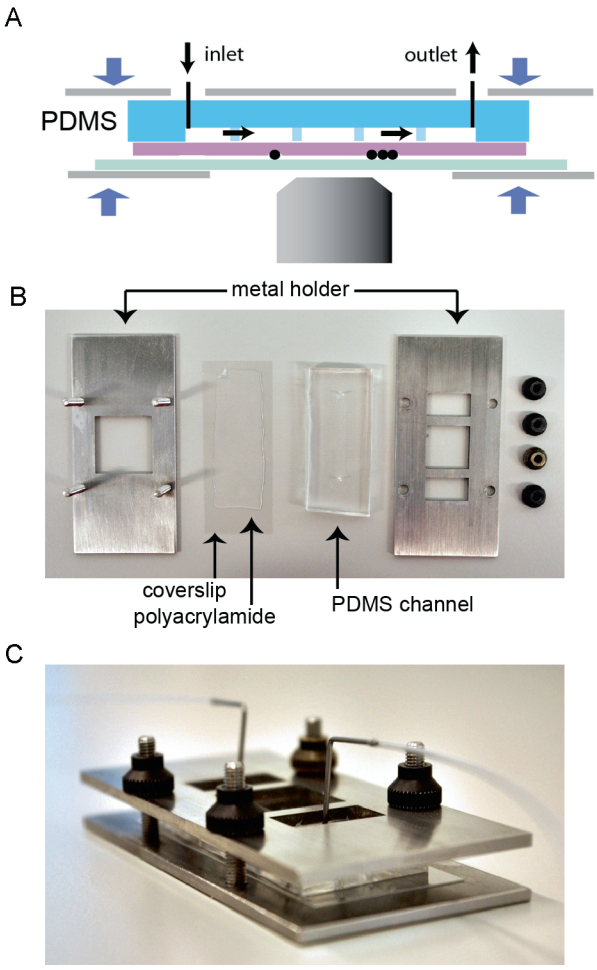

Fig. 5.1 Microfluidic device PDMS-based used to study the *dps* activation under oxidative stress (images adapted from [8]). A) Schematic representation. A multilayer structure composed of a coverglass facing the microscope objective (green), a polyacrylamide membrane (violet) and a PDMS control channel for a continuous diffusion of the growth medium to the cells (blue). The cells were placed between the coverglass and the polyacrylamide layer (black circles). B-C) Photographs of the separate parts (B) and the assembled device (C).

5.2.3.1 Assembly of the device

10 µL of cells were pipetted onto the coverglass before the assembly of the device. The cells were carefully covered by an acrylamide gel of 24x60 mm in size,

previously soaked in the growth medium, and any air bubble formation was avoided. The PDMS flow cell was deposited on top of the gel, with the fluid channel facing towards the gel. Lastly, the top plate was placed on top of the PDMS, and the entire device was fixed by screwing nuts onto the bolts. The plates were fixed to allow a proper flow of the growth medium through the flow cell, without any leakage. The preferred tightness was found by trial-and-error. Two bend connectors were inserted into the prefabricated holes in the PDMS channel and were connected to two silicon tubes, representing the entry and exit flows.

The flow chamber was filled using a syringe with Hi-Def Azure medium supplemented with 0.2% of glucose, and the device was checked for any possible leakage. The syringe was placed in an electric pump (NE-1200, New Era Pump Systems, Inc.), and the flow was set to 20 µL/min for approximately 20 to 30 minutes before the selection of stably trapped bacteria.

The device was placed in the fluorescence microscope to start the application of the oxidative stress. The inlet tube was connected to a syringe containing the Hi-Def Azure medium supplemented with 0.2% glucose and 0 µM, 10 µM, 30 µM or 500 µM H_2O_2. Once the cells were stably settled in the chamber, the microcolonies were imaged by time-lapse fluorescence microscopy.

5.2.3 Time lapse fluorescence microscopy and data analysis

As described in chapter 3 (3.2.4), the individual microcolonies were imaged by time-lapse fluorescence microscopy using an inverted microscope (Olympus IX81), equipped with an AMH-200 lamp (Andor), and a Cy3 filter cube (4040C). Images were acquired with Luca R EMCCD camera (Andor). Experiments were performed at 37°C using an incubation chamber (H201-T, Okolab). Phase contrast images (500 ms exposure time, 3 images +/- 0.2 µm from the focus) and fluorescence images (100 ms exposure time) were recorded every 5 min.

Images were analyzed using a custom Matlab program [18] based on the Schnitzcells program [19], as described in chapter 3 (3.2.5). Briefly, the data analysis was performed in three steps, consisting of segmentation, tracking, and extraction of cell parameters (fluorescence, length, growth rate). The average of three phase contrast images was segmented, and cell tracking was performed to follow the colony development. Then, for every microcolony the fluorescence intensity curves were fitted with the best-fitting polynomial (degree 5). The maximum of this function was considered to be the maximum fluorescence intensity, and the time at which the maximum was reached is calculated. The duration of *dps* expression was calculated as time from the

beginning of the exposure to pH stress. The individual cell length and growth rate were also extracted from the data.

5.3 Results

In this work, we have studied the *dps* response to oxidative stress at the single-cell level using a PDMS-based microfluidic device. *E. coli dps-mCherry* cells were exposed to concentrations of H_2O_2 between 0 µM and 500 µM and analyzed with time lapse fluorescence microscopy. The strain was grown until early exponential phase in a flask containing a rich medium and then transferred onto the coverglass of the device. The device was assembled and, after testing for leakage, transferred into the microscope chamber to start the application of stress. Microscopy analysis showed a monolayer growth in the device, allowing for identification of the fluorescence within each cell of the microcolony (Fig. 5.2). A difference was observed between cells exposed to the stressor and cells grown in the absence of H_2O_2. Cells that were not exposed to the stressor showed strong growth associated with a very weak fluorescence signal (Fig 5.2 A). Cells in the presence of oxidative stress showed a strong fluorescence signal that increased at the beginning of the data acquisition before declining (Fig. 5.2 B-C). The intensity of the fluorescent signal appeared proportional to the amount of the stress. The highest concentrations of H_2O_2 were also associated with complete halt of the growth (Fig. 5.2 D).

5.3.1 Dynamics of the *dps* expression

The images acquired were analyzed with modified Schnitzcells software [19] to extract the fluorescence intensity within single cells as mean fluorescence per unit area [18]. In the absence of stressor, the fluorescence signal displayed a decreasing trend over time (Fig 5.3 A). During exposure to 10 and 30 µM H_2O_2, a single pulse of fluorescence signal was measured, with a nearly synchronized response in all the cells of the colony (Fig. 5.3 B-C). Cells exposed to 500 µM H_2O_2 did not exhibit a fluorescence pulse but showed a constant strong signal over time (Fig 5.3 D). The variability of fluorescence signal among cells within a colony at each time point was evaluated by calculation of the coefficient of variation (CV) as the ratio of the standard deviation to the mean (Fig. 5.3 E). For the colonies exposed to 0, 10, or 30 µM H_2O_2 the CV values increased over time, starting from a minimum of around 0.1 and reaching a maximum of around 0.5. Possible explanations for the increasing of the variability are the average increasing number of cells in the colony or the unequal distribution of the fluorescent proteins in the daughter cells during cell division. The colonies exposed to the maximum concentration of stressor showed constant low CV values of around 0 because only one cell was present.

We calculated the average fluorescence values of all the cells within a microcolony at each time point to compare the response of different colonies exposed to the same stressor amount (Fig. 5.4). All the microcolonies grown in the absence of stress showed an average decrease in fluorescence signal over time, with a distinct fluorescence signal observed for some of the colonies (Fig. 5.4 A). The colonies exposed to 10 and 30 µM H_2O_2 showed an initial increase in the fluorescence signal before a subsequent decrease, having the shape of a peak. Colonies exposed to 10 µM displayed a fluorescence decrease followed by peak with a small amplitude (Fig. 5.4 B). Exposure to 30 µM H_2O_2 resulted in a distinct peak formation with a big amplitude (Fig. 5.4 C). Colonies exposed to the same amount of hydrogen peroxide showed varying peak amplitudes and durations (Fig. 5.4 B-C). During the exposure to 500 µM H_2O_2 we did not detect a fluorescence peak. The average fluorescence signal in each colony was fairly constant over time (Fig. 5.4 D). The average fluorescence analysis over time for all colonies within each experimental condition showed that increasing concentration of H_2O_2 resulted in an increase in intensity of the fluorescence signal (Fig. 5.4 E). The variability of the average fluorescence signal among different microcolonies in the same stress condition was evaluated by calculation of the coefficient of variation at each time point (Fig. 5.4 F). The CV values for the colonies not exposed to stress slightly increased over time, reaching a maximum of around 0.9. For the colonies exposed to 10 µM H_2O_2 the CV showed a slight decrease and a subsequent increase to reach the initial values around 0.3, while at 30 µM the CV curve showed a peak with a maximum around 0.5. The CV value observed for 500 µM decreased over time from around 0.5 to around 0.1.

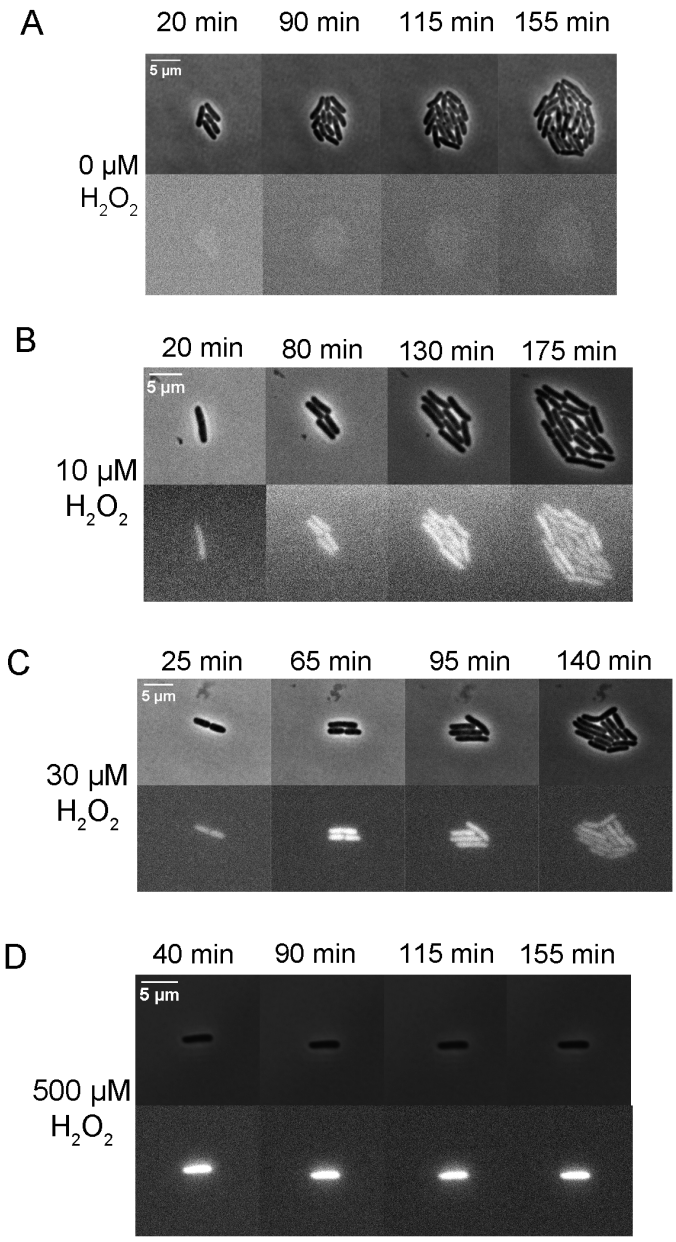

Fig. 5.2 Time-lapse fluorescence of microcolonies exposed to H_2O_2. Individual cells exposed to H_2O_2 concentrations between 0 and 500 µM (A-D) were analyzed using quantitative time-lapse fluorescence microscopy. For each panel, the upper images are phase-contrast images, and the lower images are fluorescence images from a single microcolony over time.

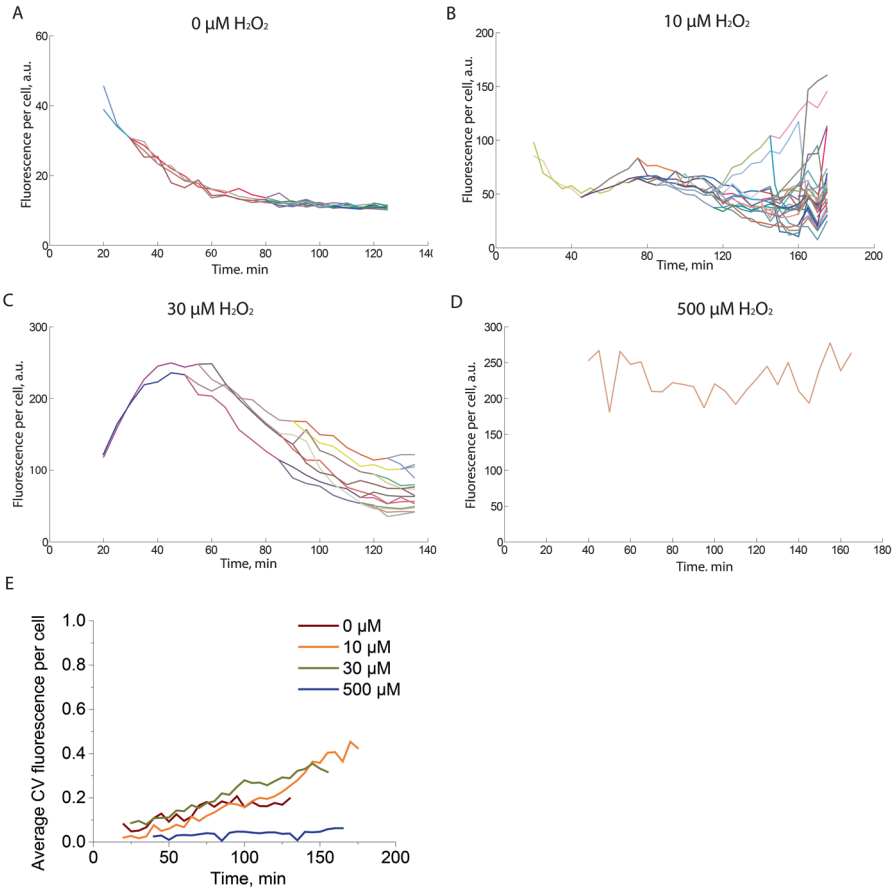

Fig. 5.3 A single pulse of *dps* promoter activity synchronized over each cell with a microcolony is induced upon exposure to H_2O_2. A-D) Examples of fluorescence intensity over time in individual cells in a microcolony exposed to different concentrations of H_2O_2. Each line represents a single cell. E) Average coefficient of variation (CV) over time of the fluorescence intensity among all the cells exposed to the same stress condition.

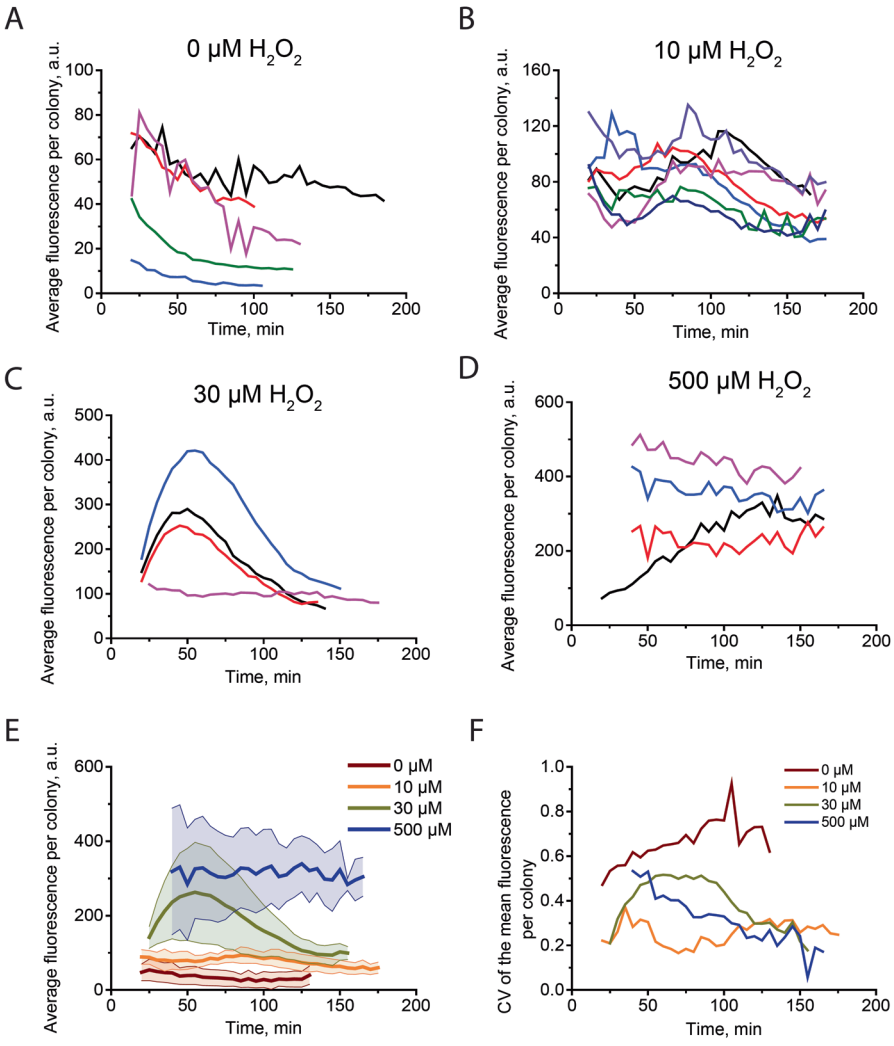

Fig. 5.4 Variation in the intensity and duration of the peak of *dps* response. A-D) The average fluorescence signal over time of microcolonies exposed to different concentrations of H_2O_2. Each line represents the average fluorescence intensity of all cells within one microcolony. E) The average fluorescence signal over time of all the colonies exposed to the same stress condition. The shaded area represents the standard deviation. F) The coefficient of variation (CV) over time of the average fluorescence signals of all the microcolonies exposed to the same stress condition.

5.3.2 Correlations between H_2O_2 concentration and *dps* induction features

The intensity and the duration of the fluorescence peak were quantitatively evaluated for a comparison among colonies. The average fluorescence curves were was fitted with a polynomial function to extract the maximum value of the fluorescence and the time point at which it was reached. The average of the maximum fluorescence values of each colony exposed to the same stress condition was calculated and showed that higher stressor concentrations resulted in a higher fluorescence peak amplitude, from 0 to 30 µM H_2O_2. The maximum fluorescence intensity reached during 500 µM H_2O_2 exposure was not statistically different from 30 µM (Fig. 5.5 A). The coefficient of variation was calculated to evaluate the variability in the maximum fluorescence intensity among different colonies exposed to the same concentration of stressor. These values ranged between 0.19 and 0.48, with the maximum variability observed at 30 µM H_2O_2 (Fig. 5.5 B). No correlation was observed between the CV values and the average maximum fluorescence (Fig. 5.5 C).

Contrary to what was observed with the maximum fluorescence, the average time at which the maximum fluorescence signal was observed for microcolonies in each experimental condition did not vary with the amount of applied stress. The average time to the maximum fluorescence was not statistically different between any of the stress conditions applied (Fig 5.6 A). The coefficient of variation for the time of maximum fluorescence intensity calculated between different microcolonies in the same stress condition revealed a high variability at 10, 30 and 500 µM, with CV values of respectively 0.71, 0.61 and 0.68. A lower variability was observed for 0 µM with a CV value of 0.24 (Fig. 5.6 B). No significant relationship was observed between the coefficient of variation values and the time to the maximum fluorescence, over all the concentrations of H_2O_2 (Fig. 5.6 C). Overall, our observations indicated that an increase in hydrogen peroxide concentration led to an increase of *dps* promoter activity. The duration of the response did not correlate with the amount of stress applied to the bacterial cultures.

In order to detect correlations between the maximum fluorescence intensity and the duration of the increase in fluorescence for individual microcolonies, a correlation analysis was performed. The Pearson correlation coefficient (R) calculated over all the conditions simultaneously was 0.33 (p value > 0.05), showing no correlation between the two parameters analyzed. The data for each individual H_2O_2 concentration considered separately showed a weak positive correlation for 0 and 10 µM (0.29 and -0.07 respectively), whereas the R values at 30 and 500 µM showed a strong correlation (0.97 and -0.95 respectively) (Fig. 5.7 A). Fluorescence peaks with higher amplitude were not correlated with a longer period of *dps* expression.

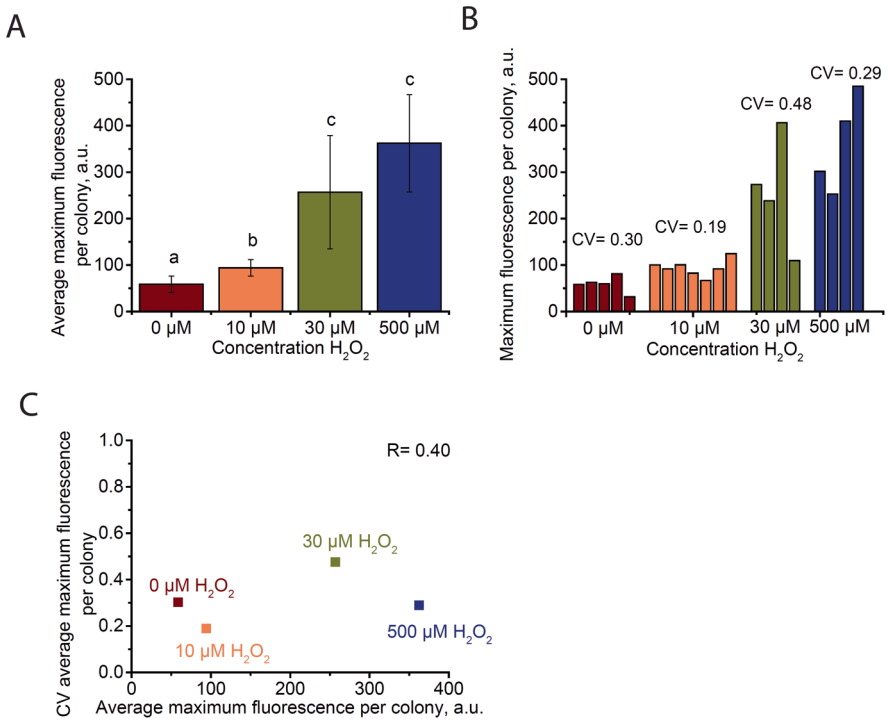

Fig. 5.5. The intensity of the *dps* response increases with higher stressor concentrations. A) The average maximum fluorescence for each microcolony. The error bars represent the standard deviation. The letters represent the statistical significance: samples labeled with different letters are statistically different (ANOVA test, $p < 0.05$). B) The maximum fluorescence values for each microcolony and the coefficient of variation (CV) of the maximum fluorescence intensity among microcolonies. C) Scatter plot of the coefficient of variation vs. the average maximum fluorescence value for each concentration of H_2O_2. R represents the Pearson correlation coefficient.

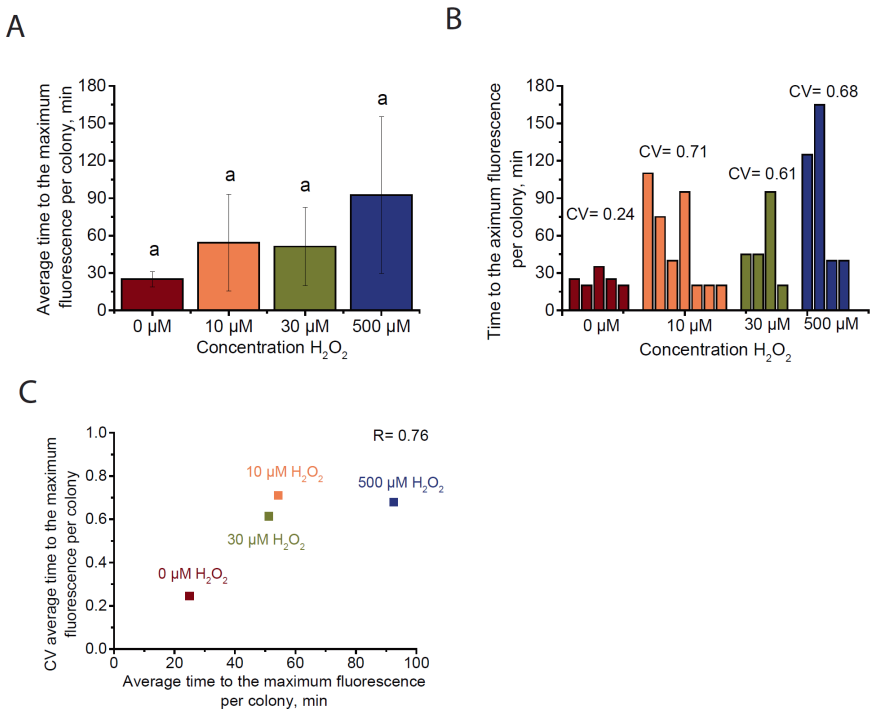

5

Fig. 5.6 The duration of the *dps* induction is not related to the H_2O_2 concentration. A) The average time at which the maximum value of the fluorescence signal was observed for each microcolony. The error bars represent the standard deviation. The letters represent the statistical significance: samples labeled with different letters are statistically different (ANOVA test, $p < 0.05$). B) The time to the maximum value of the fluorescence signal for each microcolony and the coefficient of variation (CV) of the time to the maximum fluorescence intensity among microcolonies. C) Scatter plot of the coefficient of variation vs. the time to the average maximum fluorescence value for each concentration of H_2O_2. R represents the Pearson correlation coefficient.

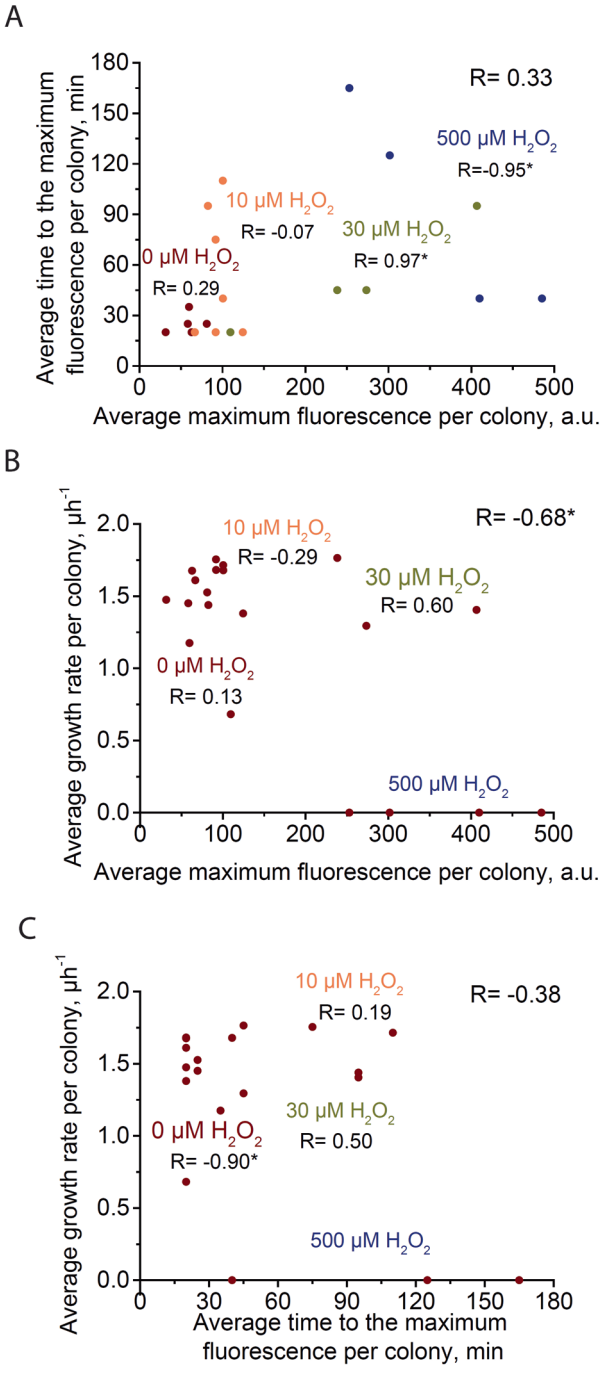

Fig. 5.7. Correlations between growth rate, intensity, and duration of the *dps* induction.

Fig. 5.7. Correlations between growth rate, intensity, and duration of the *dps* induction. A) Scatter plot of the average maximum fluorescence intensity vs. the average time to the maximum fluorescence for individual microcolonies. B) Scatter plot of the average growth rate per colony vs. the average maximum fluorescence intensity for individual microcolonies. C) Scatter plot of the average growth rate per colony vs. the average time to the maximum fluorescence intensity for individual microcolonies. Each dot represents a single microcolony. Microcolonies exposed to the same H_2O_2 concentration are represented in the same color. The R value in the top right corner of each graph represents the Pearson correlation coefficient over all the data. The R below the label for each concentration of H_2O_2 represents the R value calculated over all microcolonies in each stress condition. * = $p<0.05$.

An additional parameter extracted during the data analysis was the cell length, calculated as the length of the axis between the two poles of a cell [18]. Evaluation of the average length of all cells within each microcolony over time indicated that exposure to 0 µM or 10 µM concertation of H_2O_2 lead to a slight decrease in cell length over time (Fig. 5.8 A, B, E, F). When the cells were grown in 30 µM H_2O_2, we observed a minor increase in the average cell length but a higher proportion of elongated cells, reaching a length of up to 9 µm (Fig. 5.8 C, E, F). 500 µM H_2O_2 caused a complete halt of cell growth and division, so that each cell remained at the same length throughout the course of the experiment (Fig. 5.8 D-E-F). The average of the length of all the cells exposed to the same stressor concentration allowed a comparison between the different conditions analyzed. An overlap of the standard deviation could be observed from the analysis of the average of the fluorescence of all the colonies in the same stress conditions, demonstrating that cellular length is not dependent on oxidative stress (Fig. 5.8 E). However a statistical difference could be observed in the distributions of the average lengths of cells exposed to 10 and 30 µM (which were statistically equivalent) and those cells exposed to 0 and 500 µM (which were statistically equivalent) (Fig. 5.8 F).

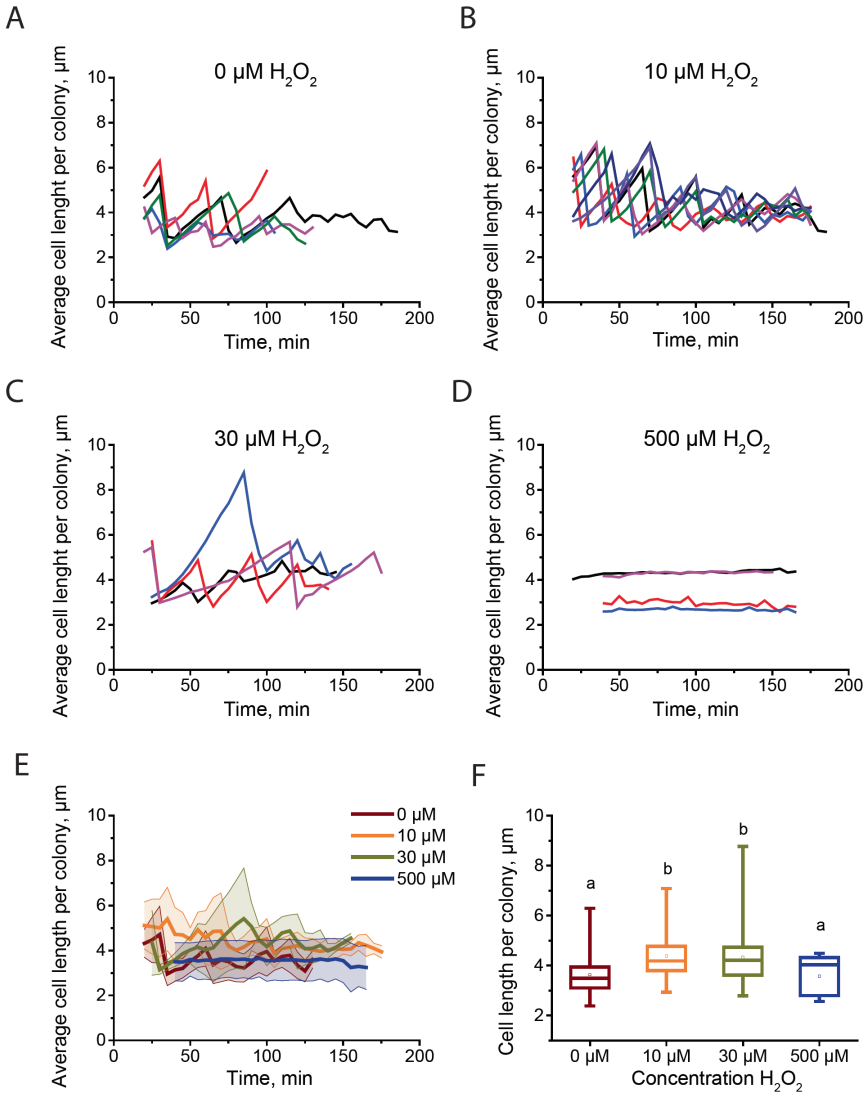

Fig. 5.8. Effects of oxidative stress on cellular length. A-D) The average cellular length over time of microcolonies exposed to different concentrations of H_2O_2. Each line represents the average cellular length of all cells within one microcolony. E) The average length of all cells within the microcolonies over time, for all the concentrations of H_2O_2 analyzed. The shaded areas represent the standard deviation. F) Distribution of the length of all cells in a microcolony, averaged over all timepoints within each experiment, for different H_2O_2 concentrations. The top and bottom of the vertical bars represent the maximum and the minimum length values, respectively; the top and bottom of the rectangular box represent the 75th and the 25th percentile; the horizontal line within the box is the median; and the square in the box is the mean value. The letters represent the statistical significance: samples with different letters are statistically different (ANOVA test, $p < 0.05$).

5.3.3 Cellular growth and oxidative stress

The growth rate was evaluated over time for all the cells present in a microcolony. It allowed evaluation of cellular health during exposure to oxidative stress. The instantaneous growth rate, μ, was calculated by fitting the cell length over time to an exponential function [18]. We calculated the average instantaneous growth rate of all the cells within a microcolony at each point in time (Fig. 5.9). The microcolonies exposed to 0 μM or 10 μM H_2O_2 showed a similar constant growth over time ranging between around 1 and 1.75 μ h^{-1} (Fig. 5.9 A-B). At 30 μM, microcolonies showed a slight increase over time in the growth rate with a minimum of 0.5 and a maximum of 2 μ h^{-1} (Fig. 5.9 C). Exposure to concentration of 500 μM severely affected the growth, with no cell division observed over time (Fig.
5.9 D). An overall analysis of the average growth rate indicated a great overlap of the growth response over time at lower concentrations of stressor. At 0 and 10 μM the average growth rate was constant over time. At 30 μM, after an initial increase, the growth rate reached the values of the lower two concentrations. Increased concentration of stressor led to a complete halt of cellular growth and division (Fig. 5.9 E).

Calculation of the average growth rate per microcolony over the duration of the experiment showed that exposure to concentrations of H_2O_2 up to 30 μM did not significantly affect the growth rate. A complete halt in growth was observed upon exposure to 500 μM (Fig. 5.10 A). The coefficients of variation for the average growth rates were low for 0, 10 and 30 μM concentrations, ranging from 0.09-0.35. For 500 μM H_2O_2 the coefficient of variation could not be calculated because the mean value of the growth rate was zero for all the microcolonies (Fig. 5.10 B). No correlation was observed between the CV and the average growth rate. The R value in fact was not statistically significant. This value could not be analyzed for significance because of the low number of values used for the analysis (Fig. 5.10 C).

A correlation analysis was performed to determine the relationship between the *dps* activation parameters and the cellular growth. Pearson correlation coefficients were calculated between the average growth rate within microcolonies and the intensity and the duration of induction peaks. Between the average growth rate and average maximum fluorescence for all stress conditions compared simultaneously, we observed a strong negative correlation (R= -0.68, p value= 0.001). The correlation coefficients calculated within each stress condition were dramatically weaker, ranging between -0.29 and 0.60 and not significantly correlated. It was not possible to calculate the R value for 500 μM because the average growth rate was equal for all the colonies (Fig. 5.7 B). Interestingly no correlation was observed comparing the growth rate and the time to reach the maximum fluorescence (R= -0.38, p value =0.100). Similarly, no correlation was observed within each individual condition (R value 10 μM = 0.19, R vale 30 μM = 0.50), except for 0 μM that

showed a strong positive correlation (R value -0.90, p value= 0.039). It was not possible to calculate the R value for 500 µM because the average growth rate was equal for all the colonies (Fig. 5.7 C).

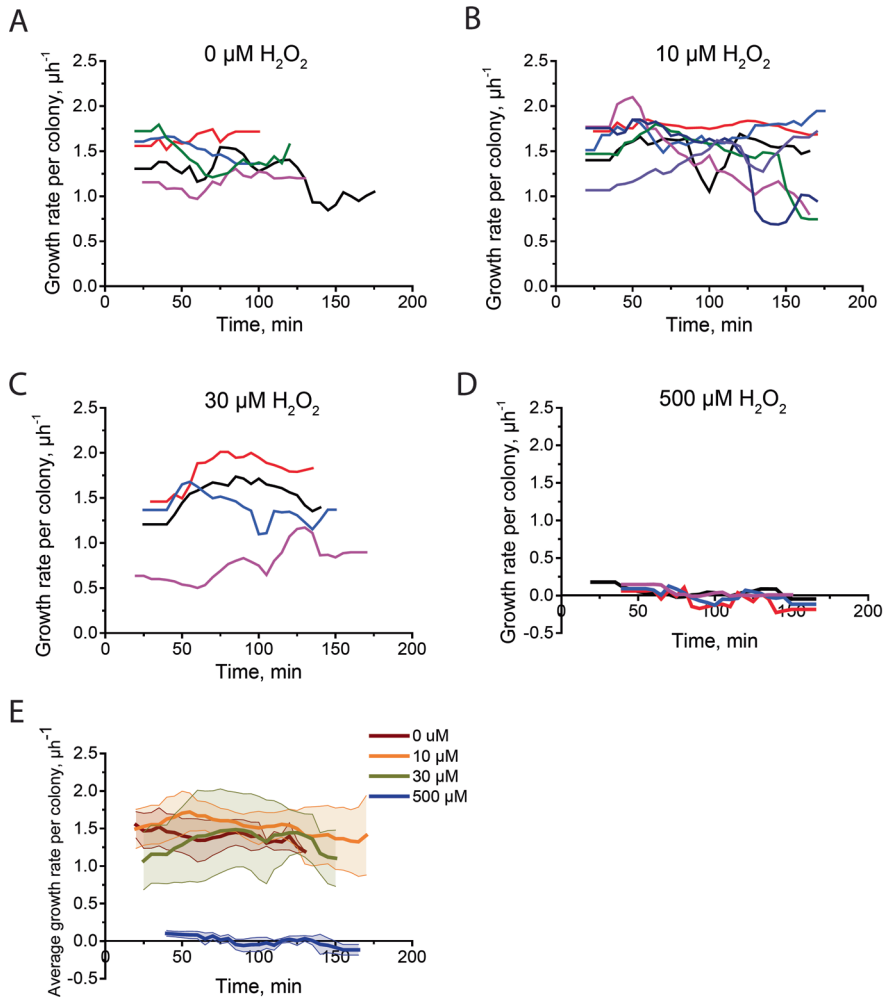

Fig. 5.9 Effect of oxidative stress on the cellular growth rate. A-D) The average instantaneous growth rate of all the cells within a colony over time. Each line represents the average growth rate of all cells within one microcolony. E) The average growth rate over time of all the colonies in the presence of the same concentration of H_2O_2. The shaded areas represent the standard deviation.

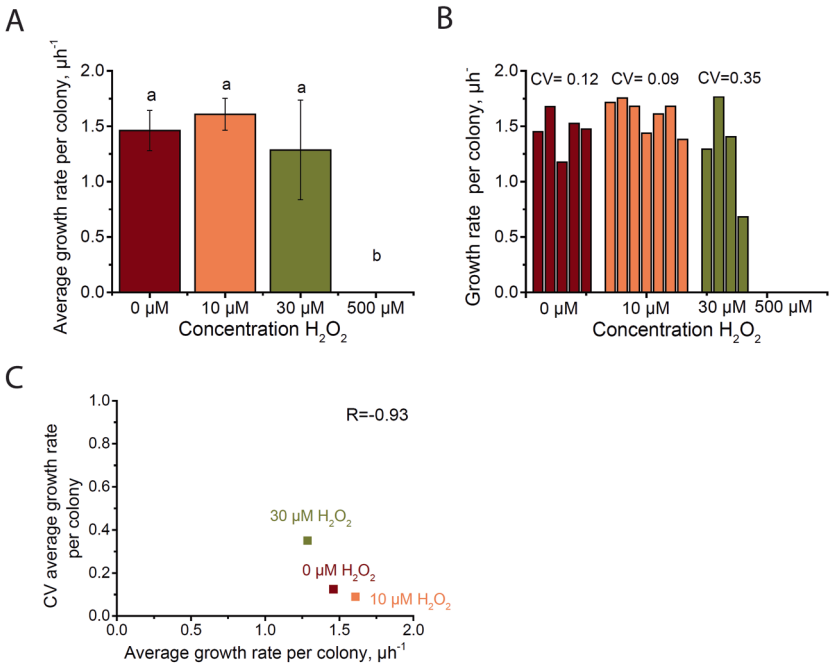

Fig. 5.10. Concentrations of H_2O_2 up to 30 μM did not affect the growth rate. A) The average growth rate per microcolony, averaged over all cells over all timepoints for each microcolony, for each concentration of H_2O_2. The error bars represent the standard deviation. The letters represent the statistical significance: samples labeled with different letters are statistically different (ANOVA test, $p < 0.05$). B) The average growth rate for each microcolony and the coefficient of variation (CV) of growth rate among microcolonies, for each H_2O_2 concentration. The microcolonies exposed to 500 μM H_2O_2 are not visible in the plot because their average growth rate is 0. C) Scatter plot of the coefficient of variation vs. the average growth rate for each concentration of H_2O_2. R represents the correlation coefficient. *= $p < 0.05$.

5.4 Discussion

In this chapter, we have investigated the single-cell Dps response to oxidative stress using a PDMS-based microfluidic device. The microfluidic device differs from the agarose pad described in chapter 3 and 4 because it offers the possibility to precisely control the growth environment of the analyzed cells. To evaluate the effect of stress, the possibility to regulate the timing of the exposure is crucial to have an accurate determination of the bacterial response. The bacteria were able to get accustomed to the growth conditions in this device, before the exposure to the hydrogen peroxide. In fact, during the initial check for possible leakage after the assembly of the device, the cells grew exposed to the rich media for about 20-30 minutes. The delivery of the stress occurred immediately after, with constant flow of fresh H_2O_2 medium. Contrarily, in the agarose pad the H_2O_2 was added during the preparation of the pads with no possibility of stress removal. Another advantage of the microfluidic device is the opportunity to detect and measure the initial moment of the stress delivery. Unfortunately, in our experiments around 20 minutes were necessary for the stabilization of the flow in the growth chamber for the detection of immobile cells. Thus, a time delay is present also in these measurements, as occurred during the experiments with the agarose pads.

Despite the differences of the techniques used, the results described in the chapter 3 were partially similar to the results observed in this work. Exposure to H_2O_2 performed with both agarose pads and the microfluidics device, causes a single pulse of activation of the *dps* promoter. In both cases the intensity of the response increases with the increase of the H_2O_2 concentration (Fig. 5.5 A). However, the duration of the response remains statistically equal for all the amounts of the stressor applied to the cells when the stressor is administered with the microfluidics (Fig. 5.6 A). Contrarily, the agarose pad experiments showed a longer duration of the *dps* response with an increase in the stressor concentration. Different hypotheses could be proposed for the observed behavior of the duration of the Dps response. In the microfluidics device the cells were exposed to the rich growth media for about 30 minutes before the stress exposure. The expression peak is observed around 100 min for 10 µM and 60 min for 30 µM (Fig. 5.4 E). Low concentration of stressor may not trigger an immediate *dps* activation. The transcription initiation may require a certain period of exposure to the H_2O_2. We speculate that other stress responses might operate in the early stage of exposure, such as the alkyl hydroperoxide reductase (Ahp) and catalase G (KatG) whose regulation is OxyR-dependent, along with that of Dps, when bacteria are exposed to low concentrations of exogenous hydrogen peroxide [20]. Exposure to higher concentration of H_2O_2 might determine an immediate activation of the Dps protection mechanism.

The absence of statistical difference in the duration of the *dps* activation between the different stressor concentrations may be caused by the high variability among colonies

exposed to the same amount of stressor (Fig. 5.6 A, B). This variability is likely due to differences between the progenitor cells of each individual colony. Within a clonal population a non-genetic heterogeneity is in fact frequent in many biological processes deriving, for example, from noise in gene expression and biochemical reactions or intracellular protein concentrations [21-23]. However, the low number of colonies analyzed made the statistical analysis not very accurate. A broader experimental investigation with a larger number of colonies and stressor concentrations intermediate between 30 and 500 μM is needed for a deeper understanding of the response with the microfluidics.

The correlation analysis between the maximum fluorescence per colony and the time to reach the maximum fluorescence showed no correlation between the intensity and the duration of the *dps* response (Fig. 5.7 A). The analysis of the individual conditions separately showed that for 10 μM H_2O_2 similar intensities of the induction correspond to variable durations of the induction, while for the highest H_2O_2 concentrations a strong correlation is instead observed. In contrast, during the experiments performed with the agarose pads stronger stresses were associated with both longer and stronger *dps* induction, with a strong correlation between the magnitude of the stress and the duration of the response. The difference may rely in the different method of stress delivery, that resulted in different durations of *dps* induction. Moreover, the lack of intermediate H_2O_2 concentrations and lower number of colonies analyzed may contribute to the differences.

The comparison of the growth rate and the *dps* induction parameters showed that lower average growth rate is strongly correlated with stronger expression but not with longer induction time (Fig 5.7). This observation is similar to what noticed for the agarose-pad-grown colonies where a strong correlation of growth rate and duration and intensity was detected. This result supports our hypothesis that the kinetics of recovery from stress is not governed by the strength of induction of specific stress response enzymes, but on the degree of damage that every cells experience during stress exposure. Cells that endure more damage may have slower growth and induce a more intense Dps response.

Low concentrations of H_2O_2 did not produce a reduction in cellular growth rate although the *dps* gene is already transcribed (Fig. 5.4, 5.9, 5.10). A similar result was observed in chapter 3 where concentrations of stressor up to 30 μM in the agarose pads did not affect the growth rate. In both of these experimental conditions, higher doses of oxidative stress resulted in a reduction and subsequent halt of cell division.

Analysis of the fluorescence intensity of the microcolonies exposed to H_2O_2 in the microfluidic device showed higher fluorescence values compared to the intensity detected in the cells grown on the agarose pads. The data analysis was performed with Schnitzcells software modified to adapt its parameters, such as the background subtraction, to the agarose pad. The corrections could have been specifically adjusted for the analysis of the

cells from the microfluidics device. The increased fluorescence may also arise from the different stress delivery system. The exposure to a constant fresh hydrogen peroxide solution might be responsible for the increased values of fluorescence registered. In the agarose pad, the stressor is applied at once at when the cells are transferred onto it, without the possibility of medium exchange or renewal.

Because the Dps protein is an important factor involved in stress survival [24, 25], a similar profile of response is observed among cells within a microcolony (Fig. 5.3). This observation confirmed the hypothesis formulated in chapter 3 that a large part of *dps* transcription occurs in the single-cell stage, before the founding cell of the microcolony has undergone cell division. Thereafter, the response profile is primarily due to the dilution of the fluorescent proteins following cell division. In both methods, a greater variability is observed in the profile of *dps* activation between different microcolonies exposed to the same amount of stress than among different cells within microcolonies, especially for the colonies not exposed to stress (Fig. 5.3, 5.4). The media supplied to the cells in the microfluidics system is distributed homogeneously within the growth chamber of the device [8], supplying all the cells with constant fresh H_2O_2. This design reduces the possibility of a non-homogenous distribution of the stressor in different positions of the growing chamber. A similar trend in the variability was observed when comparing microcolonies exposed to the same stressor concentration in the agarose pad, despite the relatively moderate amount of site-to-site variability of H_2O_2 concentration observed in the pads. These results strengthen the hypothesis that most of the variability detected in the *dps* responses is likely due to non-genetic cell-to-cell differences between the progenitor cells of each individual colony.

The PDMS-based microfluidic device was demonstrated to be a powerful tool for the investigation of the *dps* response at the single-cell level upon oxidative stress. Despite the requirement of more investigation due to the low number of analyzed colonies that did not allow an accurate statistical analysis and the lack of data for the stressor concentrations intermediate between 30 and 500 µM, this work confirmed some of the important findings described in chapter 3. The exposure to oxidative stress produces a single pulse of *dps* promoter activation. The intensity of the response is proportional to the H_2O_2 concentration. No correlation is observed between cellular growth and stressor concentration. Low H_2O_2 concentrations trigger the Dps response but have no effect on cellular growth. Moreover, cells exposed to the same stressor concentration do not receive a growth advantage in case of higher *dps* induction. These results reinforce the hypothesis that the recovery from stress may rely more on the extent of damage in individual cells than to the strong induction of specific stress proteins. Moreover, The response observed in cells grown in the microfluidic devise appear to be similar to the response observed in the agarose pads containing either H_2O_2 or alkaline medium,

demonstrating that the PDMS-based microfluidic device was accurate instrument for the investigation of the *dps* response at the single-cell level.

5.5 References

1. Whitesides, G.M., *The origins and the future of microfluidics.* Nature, 2006. **442**(7101): p. 368-73.
2. El-Ali, J., P.K. Sorger, and K.F. Jensen, *Cells on chips.* Nature, 2006. **442**(7101): p. 403-11.
3. Huh, D., G.A. Hamilton, and D.E. Ingber, *From 3D cell culture to organs-on-chips.* Trends in Cell Biology, 2011. **21**(12): p. 745-754.
4. Weibel, D.B., W.R. Diluzio, and G.M. Whitesides, *Microfabrication meets microbiology.* Nat Rev Microbiol, 2007. **5**(3): p. 209-18.
5. Breslauer, D.N., P.J. Lee, and L.P. Lee, *Microfluidics-based systems biology.* Mol Biosyst, 2006. **2**(2): p. 97-112.
6. Halldorsson, S., et al., *Advantages and challenges of microfluidic cell culture in polydimethylsiloxane devices.* Biosens Bioelectron, 2015. **63**: p. 218-31.
7. Walker, G.M., H.C. Zeringue, and D.J. Beebe, *Microenvironment design considerations for cellular scale studies.* Lab Chip, 2004. **4**(2): p. 91-7.
8. Nghe, P., et al., *Microfabricated polyacrylamide devices for the controlled culture of growing cells and developing organisms.* PLoS One, 2013. **8**(9): p. e75537.
9. Belanger, M.C. and Y. Marois, *Hemocompatibility, biocompatibility, inflammatory and in vivo studies of primary reference materials low-density polyethylene and polydimethylsiloxane: a review.* J Biomed Mater Res, 2001. **58**(5): p. 467-77.
10. Sia, S.K. and G.M. Whitesides, *Microfluidic devices fabricated in poly(dimethylsiloxane) for biological studies.* Electrophoresis, 2003. **24**(21): p. 3563-76.
11. Piruska, A., et al., *The autofluorescence of plastic materials and chips measured under laser irradiation.* Lab Chip, 2005. **5**(12): p. 1348-54.
12. Bennett, M.R., et al., *Metabolic gene regulation in a dynamically changing environment.* Nature, 2008. **454**(7208): p. 1119-22.
13. Hung, P.J., et al., *Continuous perfusion microfluidic cell culture array for high-throughput cell-based assays.* Biotechnol Bioeng, 2005. **89**(1): p. 1-8.
14. Charati, S.G. and S.A. Stern, *Diffusion of Gases in Silicone Polymers: Molecular Dynamics Simulations.* Macromolecules, 1998. **31**(16): p. 5529-5535.
15. McDonald, J.C. and G.M. Whitesides, *Poly(dimethylsiloxane) as a Material for Fabricating Microfluidic Devices.* Accounts of Chemical Research, 2002. **35**(7): p. 491-499.
16. Pelham, R.J., Jr. and Y. Wang, *Cell locomotion and focal adhesions are regulated by substrate flexibility.* Proc Natl Acad Sci U S A, 1997. **94**(25): p. 13661-5.
17. Tse, J.R. and A.J. Engler, *Preparation of hydrogel substrates with tunable mechanical properties.* Curr Protoc Cell Biol, 2010. **Chapter 10**: p. Unit 10 16.
18. Boulineau, S., et al., *Single-cell dynamics reveals sustained growth during diauxic shifts.* PLoS One, 2013. **8**(4): p. e61686.
19. Young, J.W., et al., *Measuring single-cell gene expression dynamics in bacteria using fluorescence time-lapse microscopy.* Nat Protoc, 2012. **7**(1): p. 80-8.

20. Christman, M.F., G. Storz, and B.N. Ames, *OxyR, a positive regulator of hydrogen peroxide-inducible genes in Escherichia coli and Salmonella typhimurium, is homologous to a family of bacterial regulatory proteins.* Proc Natl Acad Sci U S A, 1989. **86**(10): p. 3484-8.
21. Davey, H.M. and D.B. Kell, *Flow cytometry and cell sorting of heterogeneous microbial populations: the importance of single-cell analyses.* Microbiol Rev, 1996. **60**(4): p. 641-96.
22. Elowitz, M.B., et al., *Stochastic gene expression in a single cell.* Science, 2002. **297**(5584): p. 1183-6.
23. Martins, B.M. and J.C. Locke, *Microbial individuality: how single-cell heterogeneity enables population level strategies.* Curr Opin Microbiol, 2015. **24**: p. 104-12.
24. Martinez, A. and R. Kolter, *Protection of DNA during oxidative stress by the nonspecific DNA-binding protein Dps.* J Bacteriol, 1997. **179**(16): p. 5188-94.
25. Nair, S. and S.E. Finkel, *Dps protects cells against multiple stresses during stationary phase.* Journal of Bacteriology, 2004. **186**(13): p. 4192-4198.

Summary

The life of bacteria is a constant fight for survival in dynamic environmental conditions. Variations in temperature, pH, nutrient availability, and chemical composition are some examples of possible adverse situations that microorganisms encounter during their development. In order to overcome these adverse conditions, bacteria need to perceive these changes and activate an appropriate defense mechanism, called a "stress response". A quick adaptation is the key for survival in a hostile background. The development of a complex network of defense systems is necessary to allow a proper reaction to external stimuli, leading to a coordinated and effective response. The response mechanisms frequently involve specific sets of genes activated to help the cell maintain intracellular stability.

One of the main effectors during exposure to multiple stresses, including oxidation, extreme pH, or nutrient starvation, is the Dps (DNA-binding protein from starved cells) protein. Its intracellular levels are controlled by a complex regulatory network, finely regulated during transcription, translation and post-translationally. Despite the extensive knowledge acquired in recent years, many of the aspects of Dps regulation, in particular the dynamics of its transcriptional regulation in the presence of different stress conditions, are still unknown. In this thesis, our interest was focused on understanding of *dps* transcription at the single-cell level during oxidative and alkaline pH exposure, using time lapse fluorescence microscopy. Two techniques were applied to analyze the *dps* expression: agarose pads and a microfluidic device. Our usage of single-cell technologies was able to overcome the limitations of bulk experiments, allowing the quantification of the cell-to-cell variability in a population and the characterization of the dynamics of transcriptional responses.

In chapter 1 the *E. coli* stress response is introduced. Two main mechanisms are being described: the general stress response and the oxidative stress response, and the interdependency among these mechanisms and other specific stress responses. The main regulatory protein of the general stress response is the sigma factor σ^S, involved in the regulation of more than 70 genes. Microorganisms living in an aerobic environment unavoidably experience also oxidative stress as a byproduct of their aerobic metabolism. The Dps protein is one of the key proteins involved in this response. This chapter includes the description of the structure and regulation of the Dps protein in different stress environments.

To analyze *dps* transcriptional activation, the choice of the most suitable method and the appropriate detection instrument is a key aspect. The chapter 2 describes the optimization of the experimental conditions in order to create a useful reporter strain and identify the appropriate methodology of fluorescence detection of *dps* expression. Several techniques were screened to detect the effect of an individual stressor on the *E. coli dps* promoter activity, including fluorimetry, flow cytometry and fluorescence microscopy. The growth and the Dps protein production of two genetically engineered strains were analyzed, in different growth media and in the presence of oxidative stress. The *dps-mCherry* strain, containing a copy of the *mCherry* gene in the *dps* operon, was shown to be the most appropriate strain. Fluorescence microscopy combined with single-cell analysis was the technique selected to investigate the dynamics of the transcriptional regulation.

The chapter 3 is the core of the thesis. It describes *dps* expression in single cells using time-lapse fluorescence microscopy. Agarose pads were utilized as support for the delivery of the oxidative stress. For the first time we detected and characterized the kinetics of the induction of *dps* expression in individual *E. coli* cells exposed to hydrogen peroxide. A single pulse of promoter activation was observed, with variable intensity and duration correlated with the stressor concentrations applied to the cells. Low H_2O_2 concentrations resulted in robust *dps* induction but had little effect on growth rate. Higher concentrations were associated with a reduced and highly variable cellular growth. Comparison of cells exposed to the same stressor concentration showed that increased levels of *dps* expression did not confer a growth advantage. This observation showed that the recovery from stress may depend predominantly upon the amount of damage experienced by each individual cell, more than to the expression of specific stress enzymes.

During their development, bacteria may encounter alkaline environments, and Dps is one of the proteins involved in cell protection during this exposure. In chapter 4 is described for the first time the *dps* promoter activation during alkaline pH stress in single cells. We use time-lapse fluorescence microscopy to analyze the *dps* promoter activation of cells grown on agarose pads at different pH levels. We observed a single pulse of transcription in all the cells of each microcolony, with an intensity and a duration proportional to the increasing pH value. Analysis of the variability within and between the microcolonies showed a strong homogeneity of the *dps* response. The increase in the alkalinity of the growth media did not correspond to a proportional decrease in the cellular growth. As observed during oxidative stress exposure, increased levels of *dps* expression did not improve cellular growth. The results supported the hypothesis that the healing from the stress is interconnected with the amount of damage experienced by each cell. Taken together, these observations suggested that, during alkaline pH exposure, the *dps* gene is subjected to a transcriptional regulation similar to the one observed during

H_2O_2 stress. Further investigation will help to unravel the common regulatory members involved in both the responses.

Agarose pads represent a valuable platform for single-cell gene expression analysis. However, in recent years the technological progress of research tools has led to the increasing use of microfluidics devices. The possibility of a precise regulation of the timing of the stress exposure and the continuous perfusion of fresh solution allows for a more accurate control of the stressor delivery, compared to the agarose pads. In chapter 5 we investigated the single-cell Dps response to oxidative stress utilizing a PDMS-based microfluidics device. Although a broader investigation could help to deeper understand the response, these experiments confirmed some of the crucial findings described for *dps* expression in cells on agarose pads. A single pulse of promoter activity was identified in cells exposed to variable concentrations of H_2O_2. The intensity of the *dps* induction was correlated to the amount of the applied stress, but no correlation was identified between the duration of the induction and the stress concentration. No correlation is observed between cellular growth and stressor concentration. Cells with a stronger *dps* induction did not receive a growth advantage, as also observed in microcolonies grown on agarose pads. The response observed in cells grown in the microfluidic devise appear to be similar to the response observed in the agarose pads containing either H_2O_2 or alkaline medium, demonstrating that the PDMS-based microfluidic device was a powerful and accurate tool for the investigation of the *dps* response at the single-cell level.

Elucidation of the behavior of specific genes is the first step for a global understanding of the complex regulatory network underlying stress response mechanisms. Single-cell analysis allows the identification of the heterogeneity of a population, in terms of cellular development and fluorescence signal, overcoming the averaging factor of the bulk analysis. By combining fluorescence microscopy and microfluidic devices, the potential of single-cell study expands considerably. The developments presented in this work provide the groundwork for further investigations of the stress response mechanisms, taking advantage of the techniques here described. A large number of genes could be simultaneously analyzed and many other stressors could be applied to the cells in order to fully understand the organization of the response mechanisms.

Samenvatting

Het leven van bacteriën is een constant gevecht voor overleving in dynamische omgevingscondities. Variatie in temperatuur, pH, beschikbaarheid van voedingstoffen en chemische samenstelling zijn een aantal voorbeelden van mogelijk ongunstige situaties die bacteriën tegenkomen tijdens hun ontwikkeling. Om deze ongunstige condities te overleven, moeten bacteriën deze veranderingen waarnemen en een gepast verdedigingsmechanisme, “stress response” genaamd, activeren. Om te overleven in een vijandige omgeving is een snelle aanpassing van vitaal belang. Ontwikkeling van een complex netwerk van afweersystemen, dat een gecoördineerde en effectieve respons teweegbrengt, is nodig voor een gepaste reactie op externe stimuli. Het reactiemechanisme omvat vaak specifieke sets van genen die geactiveerd worden om de cel te ondersteunen bij het behouden van de intracellulaire stabiliteit.

Een van de belangrijkste effectors gedurende blootstelling aan meerdere stressen, waaronder oxidatie, extreme pH of gebrek aan voedingstoffen, is het Dps eiwit (DNA-binding protein from starved cells). Zijn intracellulaire concentratie wordt bestuurd door een complex netwerk en wordt nauwkeurig gereguleerd tijdens transcriptie, translatie en post-translatie. Ondanks de uitgebreide kennis die recentelijk verworven is, zijn veel aspecten van Dps regulatie, in het bijzonder de dynamica van de regulatie van transcriptie in de aanwezigheid van verschillende stress condities, nog onbekend. In deze dissertatie was onze interesse gericht op het leren begrijpen van dps transcriptie op het niveau van de individuele cel gedurende blootstelling aan oxidatieve en alkaline pH stress, met behulp van time-lapse fluorescentie microscopie. Twee technieken zijn toegepast om de dps expressie te analyseren: agarose pads en een microfluidisch apparaat. Door deze single-cell technologie waren wij in staat om de beperkingen van bulk experimenten te omzeilen, wat kwantificatie van cel tot cel variatie in een populatie en karakterisatie van de dynamica van transcriptionele responsen mogelijk maakte.

In hoofdstuk 1 wordt de E. coli stress respons geïntroduceerd. Twee belangrijke mechanismes worden beschreven: de algemene stress responsen de oxidatieve stress respons en de onderlinge afhankelijkheid tussen deze mechanismes en andere specifieke stress responsen. Het belangrijkste regulerende eiwit van de algemene stress respons is de sigma factor σS, welke betrokken is bij de regulatie van meer dan 70 genen. Micro-organismen die in een aerobe omgeving leven ervaren onvermijdelijk ook oxidatieve stress als bijproduct van hun aerobe metabolisme. Dps is een van de belangrijkste eiwitten betrokken bij deze respons. Dit hoofdstuk beschrijft de structuur en regulatie van het Dps eiwit in verschillende stress omgevingen.

Om de transcriptie activatie van dps te analyseren, is de keuze voor de meest geschikte methode en het meest geschikte detectie instrument een essentieel aspect. Hoofdstuk 2 beschrijft de optimalisatie van de experimentele condities ten einde een bruikbare reporter stam te creëren en de geschikte methodologie te identificeren voor fluorescentiedetectie van dps expressie. Verschillende technieken zijn getest om het effect van een individuele stressor op de E. coli dps promotor activiteit te detecteren, waaronder fluorimetrie, flow cytometrie en fluorescentie microscopie. De groei en de productie van Dps eiwit van twee genetisch gemodificeerde stammen zijn geanalyseerd in verschillende kweekmedia en in de aanwezigheid van oxidatieve stress. De dps-mCherry stam, die een kopie van het mCherry gen in het dps operon bevat, bleek de meest geschikte stam. Fluorescentie microscopie gecombineerd met single-cell analyse is de techniek die geselecteerd is om de dynamica van de transcriptie regulatie te onderzoeken.

Hoofdstuk 3 is de kern van de dissertatie. Het beschrijft dps expressie in individuele cellen door middel van time-lapse fluorescentie microscopie. Agarose pads zijn gebruikt als drager voor het toedienen van oxidatieve stress. Voor het eerst detecteerde en karakteriseerde wij de kinetiek van de inductie van dps expressie in individuele E. coli cellen die blootgesteld waren aan waterstofperoxide. Een enkele puls van promotor activiteit werd geobserveerd met variabele intensiteit en duur, die correleerde met de concentratie van de stressor die toegediend was aan de cellen. Lage H2O2 concentraties resulteerden in robuuste inductie van dps , maar hadden weinig effect op de groeisnelheid. Hogere concentraties waren gerelateerd aan een gereduceerde en zeer variabele cellulaire groei. Vergelijking van cellen, blootgesteld aan dezelfde stressorconcentratie, toonde aan dat een toegenomen dps expressie geen groeivoordeel betekende. Deze observatie liet zien dat het herstel van stress waarschijnlijk voornamelijk afhangt van de hoeveelheid schade die elke individuele cel ondervindt en niet zozeer van de expressie van specifieke stress enzymen.

Bacteriën ondervinden soms alkaline omstandigheden tijdens hun ontwikkeling en Dps is een van de eiwitten die betrokken is bij bescherming van de cel tijdens deze blootstelling. In hoofdstuk 4 is voor het eerst de activatie van de dps promotor gedurende alkalische pH stress in individuele cellen beschreven. We hebben time-lapse fluorescentie microscopie gebruikt om de activatie van de dps promotor te analyseren van cellen die gegroeid waren op agarose pads met verschillende pH-waarden. We zagen een enkele puls van transcriptie in alle cellen van elke microkolonie met een intensiteit en een tijdsduur proportioneel aan de toenemende pH-waarde. Analyse van de variabiliteit binnen en tussen de microkolonies toonde een sterke homogeniteit van de dps respons. De toename in alkaliteit van het kweekmedium correspondeerde niet met een proportionele afname van de cellulaire groei. Zoals ook geobserveerd was gedurende oxidatieve stress, verbeterde een verhoogde expressie van dps de groei niet. De resultaten ondersteunen de hypothese dat het herstellen van de stress gerelateerd is met

de hoeveelheid schade die elke cel ondervindt. Samengevat suggereren deze observaties dat gedurende blootstelling aan alkalische pH het dps gen onderworpen is aan een transcriptie regulatie die lijkt op de regulatie die geobserveerd werd gedurende H_2O_2 stress. Verder onderzoek zal helpen de gemeenschappelijke regulators te ontrafelen die betrokken zijn bij beide responsen.

Agarose pads representeren een waardevol platform voor single-cell gen expressie analyse. Echter, in recente jaren heeft de technologische vooruitgang van onderzoeksinstrumenten geleid tot een toename in gebruik van microfluidische apparaten. In vergelijking met agarose pads laat de mogelijkheid van precieze regulatie van de timing van blootstelling aan stress en de continue toevoer van verse oplossing een accuratere controle van de toediening van stressor toe. In hoofdstuk 5 onderzoeken we de Dps respons op oxidatieve stress in individuele cellen met behulp van een op PDMS gebaseerd microfluidisch apparaat. Ook al zou een breder onderzoek kunnen helpen de respons beter te begrijpen, deze experimenten bevestigden een aantal van de cruciale ontdekkingen beschreven voor dps expressie in cellen op agarose pads. Een enkele puls van promotor activiteit was geïdentificeerd in cellen, blootgesteld aan variabele concentraties van H_2O_2. De intensiteit van de dps inductie was gecorreleerd aan de hoeveelheid toegediende stressor, maar er was geen correlatie tussen de duur van de inductie en de stressor concentratie. Er werd geen correlatie gezien tussen cellulaire groei en stressor concentratie. Cellen met een sterkere dps inductie hadden geen groeivoordeel, zoals ook gezien in microkolonies gegroeid op agarose pads. De respons geobserveerd in cellen die in het microfluidisch apparaat waren gegroeid, lijkt gelijk te zijn aan de respons geobserveerd in de H_2O_2 of alkalisch medium bevattende agarose pads, wat aantoont dat het PDMS gebaseerde microfluidisch apparaat een krachtig en accuraat instrument was voor het onderzoek naar de dps respons op het niveau van de individuele cel.

Opheldering van het gedrag van specifieke genen is de eerste stap naar een globaal begrip van het complexe regulerende netwerk dat ten grondslag ligt aan stress respons mechanismen. Single-cell analyse staat identificatie toe van de heterogeniteit van een populatie in termen van cellulaire ontwikkeling en fluorescent signaal, waarmee het de beperking van de middelende factor van massa analyse voorkomt. Door het combineren van fluorescentie microscopie en microfluidische apparaten wordt de potentie van single-cell studies aanzienlijk vergroot. De ontwikkelingen gepresenteerd in dit werk leggen het grondwerk voor verder onderzoek naar de stress respons mechanismes, waarbij de voordelen van de beschreven technieken benut kunnen worden. Een groot aantal genen zou tegelijkertijd geanalyseerd kunnen worden en veel andere stressors zouden aan cellen toegediend kunnen worden om tot een volledig begrip van de organisatie van de respons mechanismes te komen.

Acknowledgements

Per aspera ad astra
(Latin saying)

During these 4 (5) years many times I felt the needs to quit, to find an alternative job, become a backer or having a food track. However, I did not give up and I am here writing the last world of this book, the one that I hated and I will love the most in my life. If I have to summarize these years I can honestly say that they were the best of my life. The Dutch experience, at work and outside, was such an incredible vortex of feelings, emotions, discoveries, and dreams became true. But don't worry, I am not going to describe that.

I would like to write few words to thank all the people that were part of my journey through this roller coaster called Ph.D. I am not a writer and I was never very good with words, so I will keep it short.

My first acknowledgement is for Anne. Thanks for the opportunity that you gave me. I had the possibility to learn so many new things that I never thought I would like. Thanks for your guidance, patience and support. Your door was always open for discussion and advice and I am very grateful for that.

A special thanks is for Dmitry Ershov and Sander Tans, our collaborators. Thanks for the insightful discussions and suggestions, for sharing your knowledge and teaching me the basics of image data analysis. Without your help, the paper would not be possible.

Thanks to my students, Hamideh and Peter. Your work was a nice and important addition to this thesis. It helped to make it a complete story.

Thanks to all the committee members, that find the time to read and evaluate my thesis.

Stanley and Ilja, thanks to be my paranymphs and sit near me ready to support me during the defense. Stan, my great friend. Since the first day in BN I knew that I found a friend. Thanks for teaching me your English, forgetting yours talking with me. Although we are from such different countries, we share the same ideas, values and view of the world. Since the beginning, it was as we knew each other for many years. Thanks for your sincerity, your friendship, your support. I know you will always be there. And thanks for the cover!

Ilja, I will never forget the first period in the lab, with just the two of us, listening to 60s-70s rock music and the Eurovision, unknown to me at that time. And the time that we spent together outside the work, my wedding, the painting party at my house, our trips to USA and Zurich. I was really lucky to work with you. Thanks for always being there when I needed your help and for the nice conversations also outside the lab.

My office mates, Mathia and Jetty. I really enjoy our girl's office (sorry for the guys that were there!). It was pleasant coming to work every day, also when I did not feel like. You were the first persons that I met in the morning, sharing my thoughts, getting advices and spending time talking when the working hours were passing too slowly. Mathia, I was very happy when you decided to join our lab. Since we met, I knew that we were going to have a lot of fun together, not only at work. Thanks for the good time that we spent together during parties (so much fun!), conferences and our trip to USA. Jetty, you perfectly understood the ups and downs of these years. I could always talk to you and get your support. Thanks for being on my side.

Mohammed, Malwina, Luuk, Laura, Stanley, Mathia, Pawel, Viktorija these years would not be the same without you! I am truly happy that I found such lovely group of not only colleagues, but also friends. All our parties, dinner, drinks, clubs were the best part of this period. I will miss you so much! I have so many good memories that I could write a book! Mo, thanks for the long walks and the nice lunches together with Marie, Rayan and Ranya. And the parties with Samantha, memorable! Mal, we were the perfect team for organizing parties and gifts. We have a future! Thanks for always being there to listen to our stories. Luuk, the "baby". I will miss the jelly a looottt! Thanks for your Dutch directness and all the fun. Laura thanks for being always positive. Your Latin groove gave to our group a good energy. Pawel, our favorite chef. Thanks for the dinners, the plan B: the food track, the coffee and the chats in the lazy Rotterdam afternoons. Viktorija, your humor and your beer attitude were a nice surprise. Thanks for all the fun and the 90s music!

Vlad, the student of the thousands questions. I really enjoy working with you. And I will not forget our trips to Germany and to Switzerland. I missed you when you left for Zurich but the ghost was a good company!

Orkide, it was an honor to be such an important part of your big day! Thanks for all the nice chats and the dancing!

Sal, our long conversations about life. I will miss them!

Working in BN was an unforgettable experience and I would like to thank all the BN members (too little space to mention you all) that shared with me this period. Pauline, Zohreh, Fabai, Sriram, Charl, Regis, Marteen, Bojk, Dominik, Natalia, Mahipal, Andrew, David, Jan, Felix, Susanne, Erwin, Serge, Anna, Alicia, Jonas, Esengul, Fabrizio, Mariana, Christophe, Chirlmin, Bertus without you, the department would not be such a nice and

inspiring environment. I would like to thanks you all for the stimulating discussions about science and not, the fun, the Christmas parties, the conferences.

Lasciare il proprio paese non è facile, si lascia un pezzo di cuore. Noi però siamo stati fortunati. Abbiamo incontrato voi, Alessia, Stefano e William. Abbiamo costruito una piccola famiglia. Grazie di esserci sempre e di condividere con noi quest'avventura. Veronica e Fabio, con voi la nostra famiglia italiana si è allargata. Grazie di esserne parte.

Erika, sorella di vita, la lontananza fisica non conta per noi. Grazie essere sempre al mio fianco e sostenermi quando il mondo sembra tutto grigio. Leo, il nostro cuore è sempre vicino, nonostante i chilometri. Siamo sulla pelle. Grazie a tutti i miei amici e amiche lontani, ritornare a casa è come non essere mai partita.

Essere lontana da casa mi ha fatto capire quanto sia importante la mia grande e un po' pazza famiglia. Il sostegno e l'incoraggiamento che ho sempre ricevuto da zii, cugine e cugini, e cognate e cognati, mi ha avvolge mi spinge sempre a migliorare.

Lello e Loredana, siete entrati nella mia e nelle nostre vite e diventati parte integrante di esse. Grazie di essere al mio fianco, pronti a supportarmi nei momenti di necessità.

Annamaria, in questi anni sei diventata una mamma anche per me. Grazie del sostegno che mi hai sempre dimostrato.

Mamma, papa, Fede, mi avete sostenuto e incoraggiato in tutti questi anni, aiutandomi a diventare quello che sono adesso. Non vi ringrazierò mai abbastanza per quello che avete fatto e continuate a fare per me. Senza di voi noi sarei stata in grado di raggiungere questo obiettivo. Vi voglio bene!

Ed infine ci sei tu, Ciro. Grazie per avermi sempre incoraggiata e sostenuta. Mi hai dato la forza spingendomi a non mollare quando avrei voluto. Senza di te questo libro non sarebbe esistito. E forse io non sarei qui.

Michela
Rotterdam, May 2016

Curriculum vitae

14-11-1985	Born in Salerno, Italy
1999-2004	Scientific High school diploma Liceo Scientifico statale “A. Genoino”, Cava De’ Tirreni (Sa), Italy
2004-2007	B.Sc. (*cum laude*) in Agro-food Biotechnology University of Naples “Federico II”, Italy
2007-2010	M.Sc. (*cum laude*) in Biotechnology for Agro-industry University of Naples “Federico II”, Italy
2010-2011	Research Scientist University of Naples “Federico II”, Italy
2011-2016	Ph.D. research Delft University of Technology, Bionanoscience Department , The Netherlands *Supervisor*: Anne S. Meyer

List of publications

1. De Martino M, Ershov D, van den Berg PJ, Tans SJ, Meyer AS. 2016. Single cell analysis of the Dps response to oxidative stress. J Bacteriol 198:000 – 000. doi:10.1128/JB.00239-16.

2. De Martino M, Pourmohammadi fallah H, *et all.*, Single-cell analysis of the Dps response to alkaline pH stress, *in preparation*